Adaptive translational regulation in response to low-dose gamma irradiation in HFL1 lung fibroblasts

Rosette Niloufar Tamaddondoust

Thesis submitted to the University of Ottawa
in partial Fulfillment of the requirements for the

DOCTOR OF PHILOSOPHY

Department of Biochemistry, Microbiology and Immunology

University of Ottawa

Ottawa, Ontario, Canada

Abstract

Understanding the cellular responses to low-dose ionizing radiation (IR; ≤ 0.1 Gy) is essential for developing evidence-based radiation protection policies. While the effects of high-dose IR on gene expression and protein synthesis are well documented, how cells selectively remodel their gene expression under low-dose IR stress remains poorly understood. To address this gap, I performed ribosome profiling on normal human lung fibroblast cells exposed to low (0.1 Gy) and high (1 Gy) doses of ^{60}Cobalt gamma (γ) rays. At 1 and 6 hours post-irradiation, the results demonstrate that while low-dose IR does not significantly change global protein synthesis, subsets of mRNAs show distinct increases or decreases in translation efficiency. These translational changes contrast with minimal alterations observed at the transcriptional level following low-dose exposure. The data suggest that specific biological processes are modulated upon low-dose γ-radiation. The small GTP-binding protein RAB33B was identified as a translationally upregulated target in response to IR. This study emphasizes that conventional transcriptome analyses do not fully capture gene expression dynamics in response to low-dose IR exposure. Moreover, I identify dose-rate as a confounding factor, highlighting the importance of considering both dose-rate and cumulative dose in experimental design. Understanding the features that govern preferential mRNAs translation or repression in response to γ irradiation may offer deeper insights into the subtle adaptive responses to common low-dose radiation exposures from the environment, medical devices, or occupational activities.

Acknowledgements

I would like to express my deepest gratitude to my supervisors, Dr. Tommy Alain and Dr. Yi Wang for their invaluable guidance, support, and encouragement throughout the course of my doctoral research.

I am especially grateful to my thesis committee members, Dmitry Klokov, Dr. Mary-Ellen Harper, and Dr. Soji Sebastian, for their time, insightful feedback, and invaluable contributions to shaping my thesis and academic development.

I would like to sincerely thank Canadian Nuclear Laboratories (CNL) for providing me with the opportunity, resources, and facilities to carry out my research. Working at CNL, in the unique environment of Chalk River, has been both challenging and rewarding. Despite the isolation and logistical difficulties, the experience has significantly contributed to my growth as a researcher.

I am especially grateful to Dr. Eduard Azzam, Dr. Antonella Bertucci, Dr. Martin Roffe and Dr. Marcello Vazquez for their generous mentorship, thoughtful discussions, and unwavering support throughout my academic journey.

I also wish to thank my colleagues and friends at the University of Ottawa and CNL for their camaraderie, encouragement, and shared wisdom along the way.

Finally, I extend my heartfelt appreciation to my family for their unconditional love, patience, and belief in me, without which this journey would not have been possible.

Dedication

To my mom and dad, for planting the seed of curiosity that led me here.

To my grandparents, whose love lives on in every page.

To Judy and John Tracey, for giving me a home away from home.

To Mehrdad, for his endless encouragement.

Table of Contents

List of Figures

List of Tables

List of Abbreviations

Abbreviation	Full Form
2D	Two-dimensional
3D	Three-dimensional
4E-BP	eIF4E-Binding Protein
4E-BP1	eIF4E-Binding Protein 1
5'-UTR	5' Untranslated Region
8-oxo-dG	8-oxo-2'-deoxyguanosine
8-oxoG	8-oxo-7,8-dihydroguanine
80S	Complete eukaryotic ribosome
ABC1	ATP-Binding Cassette Protein 1
AECL	Atomic Energy of Canada Limited
AMPK	AMP-Activated Protein Kinase
ANOVA	Analysis of Variance
APE-1	Apurinic/Apyrimidinic Endonuclease 1
ARE	AU-Rich Element
ARS	Acute Radiation Syndrome
ATCC	American Type Culture Collection
ATF4	Activating Transcription Factor 4
ATM	Ataxia-Telangiectasia Mutated
ATP	Adenosine Triphosphate
BSA	Bovine Serum Albumin
CCU	Consultative Committee for Units
CESR	Core Environmental Stress Response
CHX	Cycloheximide
CNBP/ZNF9	Cellular Nucleic Acid-Binding Protein/Zinc Finger 9
CNL	Canadian Nuclear Laboratories
CT	Computed Tomography
Co-60	Cobalt-60
Ct	Cycle Threshold
Cutadapt	Cutadapt Adapter Trimming Tool
DAPI	4',6-Diamidino-2-Phenylindole
DDB	DNA Damage Binding protein
DDR	DNA Damage Response
DDREF	Dose and Dose-Rate Effectiveness Factor
DNA	Deoxyribonucleic Acid
DNA-PK	DNA-Dependent Protein Kinase
DNase I	Deoxyribonuclease I
DREF	Dose-Rate Effectiveness Factor
DSB	DNA Double-Strand Break
DSBs	DNA Double-Strand Breaks
DTT	Dithiothreitol

ER	Endoplasmic Reticulum
FBS	Fetal Bovine Serum
FDR	False Discovery Rate
FastQC	Fast Quality Control
GAP	GTPase-Activating Protein
GAPDH	Glyceraldehyde-3-Phosphate Dehydrogenase
GCN2	General Control Non-derepressible 2
GDP	Guanosine Diphosphate
GEF	Guanine Nucleotide Exchange Factor
GO	Gene Ontology
GRCh38	Genome Reference Consortium Human Build 38
GTP	Guanosine Triphosphate
Gy	Gray (unit of absorbed radiation dose)
Gy/h	Gray per Hour (unit of dose rate)
Gy/s	Gray per Second
HFL1	Human Fetal Lung Fibroblast 1
HIF-1α	Hypoxia-Inducible Factor 1-alpha
HISAT2	Hierarchical Indexing for Spliced Alignment of Transcripts 2
HR	Homologous Recombination
HRI	Heme-Regulated Inhibitor
HRP	Horseradish Peroxidase
IF	Immunofluorescence
IR	Ionizing Radiation
ISR	Integrated Stress Response
ISRIB	Integrated Stress Response Inhibitor
J/kg	Joules per Kilogram
KCl	Potassium Chloride
LC-MS	Liquid Chromatography-Mass Spectrometry
LDEF	Low-Dose Effectiveness Factor
LDR	Low-Dose Rate
LET	Linear Energy Transfer
LNT	Linear No-Threshold
LSS	Life Span Study
MAPQ	Mapping Quality
MOFA	Multi-Omics Factor Analysis
MS	Mass Spectrometry
Met-tRNAi	Methionyl Initiator Transfer RNA
MgCl2	Magnesium Chloride
NCRP	National Council on Radiation Protection and Measurements
NGD	No-Go Decay
NGS	Next-Generation Sequencing
NHEJ	Non-Homologous End Joining
NMD	Nonsense-Mediated Decay
NaCl	Sodium Chloride
OCM	Organ-on-a-Chip Microfluidic

OXPHOS	Oxidative Phosphorylation
P	p-value
PABP	Poly(A)-Binding Protein
PAGE	Polyacrylamide Gel Electrophoresis
PBS	Phosphate-Buffered Saline
PCR	Polymerase Chain Reaction
PDLs	Population Doubling Levels
PERK	PKR-like Endoplasmic Reticulum Kinase
PET	Positron Emission Tomography
PIC	Pre-Initiation Complex
PKR	Protein Kinase R
PTM	Post-Translational Modification
PVDF	Polyvinylidene Difluoride
RBE	Relative Biological Effectiveness
RIPA	Radioimmunoprecipitation Assay
RNA	Ribonucleic Acid
RNA-seq	RNA sequencing
RNeasy	RNeasy RNA Kit
ROS	Reactive Oxygen Species
RPF	Ribosome-Protected Fragment
RPM	Revolutions Per Minute
RQC	Ribosome-Associated Quality Control
Ribi	Ribosome Biogenesis Regulons
Ribo-seq	Ribosome Profiling Sequencing
SDS	Sodium Dodecyl Sulfate
SDS-PAGE	Sodium Dodecyl Sulfate Polyacrylamide Gel Electrophoresis
SEM	Standard Error of the Mean
SOD	Superoxide Dismutase
SSB	Single-Strand Break
SYBR Gold	SYBR Gold Nucleic Acid Gel Stain
Sv	Sievert (unit of equivalent and effective dose)
TBE	Tris-Borate-EDTA
TBS	Tris-Buffered Saline
TBS-T	Tris-Buffered Saline with Tween-20
TE	Translational Efficiency
TRIzol	TRIzol Reagent
Torin1	Torin1 (mTOR inhibitor)
Tris-HCl	Tris(hydroxymethyl)aminomethane Hydrochloride
Triton X-100	Octylphenol ethoxylate
UMI	Unique Molecular Identifier
UNSCEAR	United Nations Scientific Committee on the Effects of Atomic Radiation
UTR	Untranslated Region
YTHDF	YTH Domain Family Protein
cDNA	Complementary DNA

cGy	Centigray
cIAP1	Cellular Inhibitor of Apoptosis Protein 1
eEF1A	Eukaryotic Elongation Factor 1 Alpha
eEF2	Eukaryotic Elongation Factor 2
eIF	Eukaryotic Initiation Factor
eIF2B	Eukaryotic Initiation Factor 2B
eIF2α	Eukaryotic Initiation Factor 2 alpha subunit
eIF4A	Eukaryotic Initiation Factor 4A
eIF4E	Eukaryotic Initiation Factor 4E
eIF4F	Eukaryotic Initiation Factor 4F complex
eIF4G	Eukaryotic Initiation Factor 4G
eIF5A	Eukaryotic Initiation Factor 5A
eRF1	Eukaryotic Release Factor 1
eRF3	Eukaryotic Release Factor 3
keV/μm	Kiloelectronvolts per Micrometer
limma	Linear Models for Microarray Data
log2 FC	log2 Fold Change
m6A	N6-Methyladenosine
mGpppN	7-methylguanosine cap structure
mGy	Milligray
mRNA	Messenger RNA
mSv	Millisievert
mTORC1	Mechanistic Target of Rapamycin Complex 1
nt	Nucleotides
poly(A) tail	Polyadenylated tail
qPCR	Quantitative Polymerase Chain Reaction
α	Alpha Particle
β	Beta Particle
β-actin	Beta-actin
γ	Gamma Ray
γ-H2AX	Phosphorylated H2AX (at serine 139)

Chapter 1: Introduction

Humans are constantly exposed to ionizing radiation (IR), ranging from low to high doses. Such exposures typically occur through environmental, medical, and occupational sources. Environmental IR can arise from terrestrial sources, airborne particles (such as radon), cosmic rays, and even trace amounts present in food and drinking water. Since Wilhelm C. Roentgen's discovery of X-rays in 1895 [1], humans have also been exposed to artificial sources of IR, particularly through medical imaging technologies such as computed tomography (CT) scans, X-rays, and positron emission tomography (PET) scans for medical diagnosis. In addition, radiotherapy has become an increasingly effective approach to cancer treatment. Occupational radiation exposure, particularly among workers in sectors such as the nuclear industry or mining and flight crews, is also a significant consideration. These exposures are considered physiological stress to which cells usually respond by activating or inhibiting specific stress response pathways. Given the growing use of IR for different purposes, understanding its biological effects on basic cellular functions, particularly gene expression and protein synthesis, is essential to elucidating the molecular mechanisms of radiation-induced cellular stress responses.

Despite decades of research, key questions remain regarding how low-dose IR impacts cellular functions at the molecular level. While high-dose exposures and their biological consequences are well-characterized, low-dose responses are often subtle, context-dependent, and less understood, especially in relation to translational control and stress pathway regulation. Addressing these gaps is important to refining risk models and informing both therapeutic strategies and radiation protection standards.

1.1 IR types, linear energy transfer, dose and dose rate

IR is a form of energy that is released by unstable radionuclides as they transform into more stable states with lower potential energy. This process emits radiation in two main forms:

1) Charged particles such as alpha (α) particles, beta (β) particles, and neutrons.
2) Electromagnetic waves, including gamma (γ) rays and x-rays [2].

Alpha (α) particles: consist of two protons and two neutrons. Due to their large mass and +2 charge, alpha particles show strong ionization potential but low penetration ability. Alpha particles can be stopped by a sheet of paper or the outer layer of human skin. Therefore, external exposure is usually harmless, but internal exposure, via ingestion or inhalation, can lead to significant biological damage.

Beta (β) particles: These are high-speed electrons (β^-) or positrons (β^+). These particles are lighter and carry a single charge, allowing them to travel further than alpha particles, yet with lower ionization density. Therefore, external exposure can cause skin irritation, while internal exposure may result in harmful tissue effects depending on the dose and localization.

Gamma (γ) rays and X-rays: Both are types of electromagnetic waves and are described as pure energy or photons that can produce ions while travelling through materials. However, they differ in origin: X-rays are generated by interactions involving electrons outside the nucleus, whereas gamma rays are emitted from the atomic nucleus during radioactive decay. These rays have high penetration power but low ionization density, allowing them to reach internal organs and deposit energy over a broader area. Cosmic

rays, also composed of high-energy photons, are sometimes referred to as gamma rays due to their similar penetrating properties.

Understanding the different types of IR is essential for characterizing their biological impact, which is largely influenced by physical properties such as linear energy transfer (LET), absorbed dose, and dose rate. These parameters determine the extent and distribution of energy deposition in biological tissues, ultimately shaping the cellular and molecular responses to radiation exposure.

1.1.1 Linear Energy Transfer (LET)

As IR travels through matter, it loses energy through interactions with atoms along its path. This rate of energy loss per unit distance is known as linear energy transfer (LET) and is typically expressed in kiloelectronvolts per micrometer (keV/μm) [2]. The LET varies depending on radiation type and energy.

- High-LET radiation (e.g., alpha particles) are heavy charged particles that deposit energy densely along their tracks due to their greater mass and charge.
- Low-LET (e.g., X-rays and gamma rays) consists of uncharged photons that deposit energy more sparsely, with deeper tissue penetration and lower ionization density.

LET is a key factor in the biological effectiveness of different types of radiation. High LET is more likely to cause severe DNA damage, triggering stronger cellular stress and increased biological impact compared to low-LET.

Table 1) Types of IR in order of increasing energy.

Type of IR	Wave/Particle Nature	Source of Emission	Relative Energy	Effective Shielding
Alpha particle (α)	Two protons and two neutrons	Nuclear decay	Very High	Paper, skin
Beta particle (β)	Electron (β^-) or positron (β^+)	Nuclear decay	High	Clothing, plastic, aluminum (few mm)
X-ray	Photon (electromagnetic wave)	Electron shell interactions (outside nucleus)	Low	Lead, concrete, water
Gamma ray (γ)	Photon (electromagnetic wave)	Nuclear decay	Low	Thick lead, concrete, dense shielding materials

1.1.2 Radiation dose: absorbed and equivalent dose

Absorbed dose is the amount of energy deposited in a material per unit mass, and it is measured in grays (Gy), where 1 Gy equals 1 joule per kilogram (J/kg).

The equivalent dose, expressed in sieverts (Sv), incorporates a radiation weighting factor that reflects the relative biological effectiveness (RBE) of a specific type of radiation. In other words, it quantifies the expected biological damage from the absorbed dose of a specific radiation type, enabling comparison across different radiation types, even when the absorbed dose is the same [3].

The equivalent dose to a given organ or tissue (H_T) is calculated as:

$$\text{Equivalent dose } (H_T) = D_T \times W_R$$

Where:

D_T = Absorbed dose in tissue T

W_R = Radiation weighting factor

The ‘Gy’ and ‘Sv’ are named in honor of two pioneers in radiation science: Dr. Louis Harold Gray, who made foundational contributions to radiobiology, and Rolf Sievert, a physicist known for his work in radiation protection. These units are officially recognized by the Consultative Committee for Units (CCU).

For low-LET radiation (e.g., X-rays, gamma radiation, beta particles), 1 Gy is generally equivalent to 1 Sv. However, high-LET radiation (e.g., alpha particles and neutrons) carries a higher weighting factor (typically 10 to 20), meaning the equivalent dose is larger than the absorbed dose for the same amount of energy deposited.

To express smaller fractions of these measured quantities, the following prefixes are often used:

- Milligray (mGy) = 10^{-3} Gy
- Centigray (cGy) = 10^{-2} Gy
- Millisievert (mSv) = 10^{-3} Sv

1.1.3 Effective dose and risk assessment

The effective dose, also expressed in sieverts (Sv), goes a step further by accounting not only for the type of radiation, but also the sensitivity of the exposed organs or tissues. It is used to estimate the overall risk of stochastic effects (such as cancer) across the entire body.

It is calculated as the sum of the equivalent doses to all exposed tissues and organs, each multiplied by a tissue weighting factor (WT) defined by international guidelines (e.g., International Commission on Radiological Protection (ICRP)):

$$E = \sum_{T} W_T \times H_T$$

Where:

E = effective dose (Sv)

H_T = equivalent dose absorbed by tissue or organ T

W_T = tissue weighting factor for tissue

The effective dose is a key quantity in radiation protection, medical exposure monitoring, and environmental risk assessment, as it provides a standardized measure to estimate population or individual health risks from radiation exposure.

Table 2) IR dose quantities and associated SI units.

Dose Quantity	Description	SI Unit
Absorbed dose (D)	Energy deposited in matter per unit mass (measured in joules per kilogram).	Gray (Gy)
Equivalent dose (H)	Measures the biological effectiveness of the absorbed dose, accounting for radiation type.	Sievert (Sv)
Effective dose (E)	Weighted sum of equivalent doses, considering tissue sensitivity.	Sievert (Sv)

1.1.4 Dose rate and exposure classification

The radiation dose rate is the dose delivered per unit of time, expressed in gray per hour (Gy/h). Human exposure to IR varies in dose, dose rate, and duration of exposure. Depending on the exposure duration, exposures can be classified as:

- Acute: A dose delivered over a short period.
- Chronic: A lower dose received continuously or intermittently over an extended period.

- Fractionated: The total dose divided into smaller doses delivered at regular intervals.

Exposure scenarios can be grouped by both dose and dose rate into categories such as:

- High dose /high dose rate
- Low dose /high dose rate
- Low dose/low dose rate

These classifications are important because the biological effects of radiation depend not only on the total dose but also on the rate and timing of exposure. For example, a low dose delivered over a long period may allow cells time to repair damage, resulting in a different biological outcome than the same dose delivered acutely.

1.1.5 Definition of low-dose and low-dose-rate

According to the United Nations Scientific Committee on the Effects of Atomic Radiation (UNSCEAR) and the ICRP, low-dose exposure is defined as absorbed doses from low-LET radiation (e.g., gamma radiation) below about 100 mGy, in addition to natural background radiation, which averages 2 to 3 mSv per year globally [4, 5]. A moderate dose falls between 100 mGy and about 1 Gy [6].

However, in practice, the terms “low” and “high” are context-dependent [7]. For instance, in radiotherapy, a 2 Gy per fraction may be considered low, whereas in radiation protection, a dose of 10 mGy may be regarded as low dose [8, 9]. Therefore, dose categories must be carefully defined within the context of their specific application field.

Low-dose-rate exposure refers to the delivery of IR at a relatively slow rate over an extended period. In environmental and occupational settings, UNSCEAR and the ICRP

define low dose rate exposure as < 0.1 mGy per minute (equivalent to < 6 mGy per hour) for external X-rays and gamma rays [10, 11].

It is important to note that in medical applications, particularly in low-dose-rate brachytherapy, the term "low-dose-rate" refers to much higher dose rates (i.e. 0.5 to 2 Gy per hour), which are significantly higher than environmental low-dose definitions [12]. Therefore, as with the dose magnitude, the interpretation of dose-rate terminology is relative to the specific field of application.

Dose rate plays an important role in modulating the biological effectiveness of radiation. When delivered at low dose rates (mGy/week or mGy/year), cells have more time to repair DNA damage, resulting in lower biological effectiveness compared to the same dose at a high-dose-rate (Gy/min or Gy/sec) [13].

To account for these differences, the dose and dose-rate effectiveness factor (DDREF) was introduced to adjust risk models when extrapolating from high-dose/high-rate exposure studies to low-dose scenarios. More recent literature, however, suggests using separate factors, low-dose effectiveness factor (LDEF) and dose-rate effectiveness factor (DREF), to enable more accurate risk estimation [14].

In conclusion, understanding how dose magnitude and dose rate influence biological responses provides the foundation for distinguishing between the two main categories of radiation effects: deterministic effects and stochastic effects.

Table 3) Dose and dose rate classification across contexts

Category	Definition	Typical Thresholds / Examples	Context
Low dose	Absorbed dose considered biologically minimal	< 100 mGy	UNSCEAR / ICRP, Radiation Protection
Moderate dose	Transitional range between low and high biological impact	~100 mGy to ~1 Gy	General dosimetry
High dose	Likely to cause deterministic effects	> 1 Gy	Radiotherapy, Accidental Exposure
Low dose rate	Slowly delivered dose over time	< 0.1 mGy/min (≈6 mGy/h)	Environmental / Occupational
Moderate dose rate	Dose delivered over hours	~0.5–2 Gy/h	Low-dose-rate Brachytherapy
High dose rate	Rapid delivery of dose	> 0.1 Gy/min (up to several Gy/sec)	External Beam Radiotherapy
Fractionated dose	Divided into smaller doses over intervals	e.g., 2 Gy per fraction over multiple sessions	Clinical Radiotherapy
Chronic exposure	Long-term, continuous or repeated exposure	Months to years (e.g., radon, occupational)	Environmental / Occupational
Acute exposure	Single exposure or short-duration high dose	Seconds to hours (e.g., nuclear accident, therapy)	Clinical / Emergency

1.2 Types of radiation-induced biological effects: deterministic and stochastic effects

Radiation risk assessments conducted by advisory bodies such as (the National Council on Radiation Protection and Measurements) NCRP and ICRP traditionally classify the biological effects of IR as either deterministic or stochastic.

Deterministic effects, known as tissue reactions, are characterized by the outcomes that occur only after a certain threshold is exceeded [15]. The severity of these effects increases with dose. These outcomes depend on factors such as dose magnitude, exposure duration, and radiation type. Common deterministic effects include acute radiation syndromes (ARS) and chronic radiation injuries.

- Acute radiation syndromes (ARS) can develop shortly after high-dose exposure and may involve symptoms such as headache, vomiting, nausea, fever, and skin or tissue burns. Such symptoms are often easy to cure with medical intervention.
- Chronic radiation effects, in contrast, may appear long after and include cataracts, hair depigmentation, organ damage, and in some cases, cancer and genetic mutation [16].

The threshold dose for deterministic effect varies depending on the biological endpoint and is influenced by individual sensitivity, age, health status, and detection method sensitivity [17]. For instance, the eye lens has been shown to be more radiosensitive than previously thought. The ICRP now recommends a threshold dose of 0.5 Gy for radiation-induced cataract formation, defined at the 1% incidence level, regardless of the dose rate [18].

In contrast, stochastic effects describe biological outcomes where the probability of occurrence increases with dose, but severity is independent of dose [19]. The outcomes

include radiation-induced mutations, genomic instability, and the development of cancer [20, 21].

The 2020 UNSCEAR report consolidates epidemiological data from studies of atomic bomb survivors (Life Span Study), Chornobyl cleanup workers, and patients exposed to medical radiation, confirming that radiation-induced cancers are stochastic in nature [22, 23].

However, the major unanswered question in radiation epidemiology is not whether radiation causes cancer, but rather what level of risk is associated with low-dose (<100 mGy) or low-dose-rate exposure to IR [24].

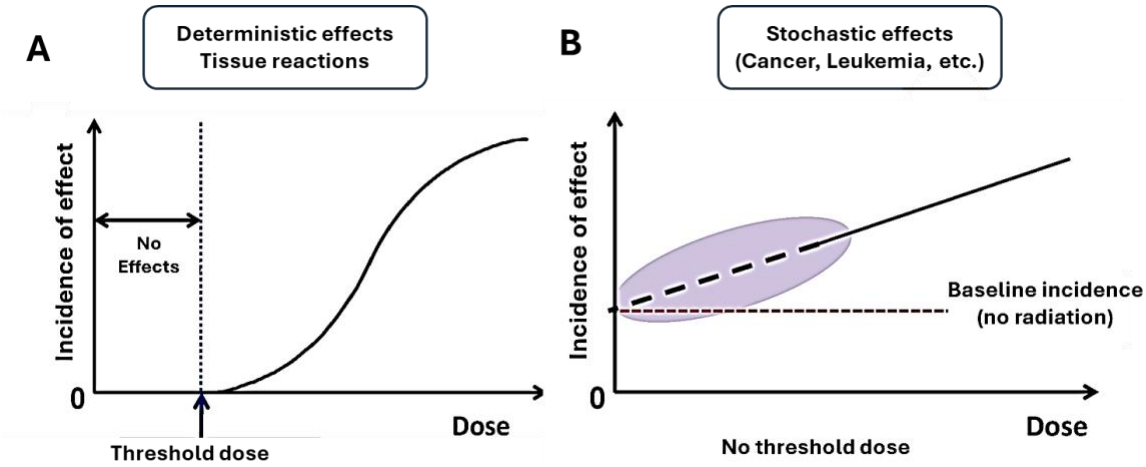

Figure 1) Deterministic versus stochastic effects of IR:

A) the graph illustrates deterministic effects (also referred to as tissue reactions), which occur only above a threshold dose and increase in severity with higher doses. The graph reflects the ICRP's (2007) definition, where the threshold dose is the level at which 1% of individuals exhibit symptoms.

B) The graph shows stochastic effects, such as radiation-induced cancer or hereditary changes, which are probabilistic and do not have a known threshold. In this model, the incidence of effects increases with dose, and even very low doses may carry some risk. This reflects the ICRP's assumption used in radiological protection, particularly at low-dose exposures.

1.3 Radiation risk models:

1.3.1 Linear no-threshold (LNT) model

Direct measurement of stochastic effects at low doses is challenging due to their probabilistic nature and low incidence. Therefore, most risk assessments for low-dose IR are extrapolated from high-dose data using the Linear No-Threshold (LNT) model [25, 26]. According to the LNT model, the probability of biological damage increases linearly with the absorbed dose. This implies that any exposure to IR, no matter how small, is assumed to carry some level of risk, particularly for stochastic effects such as cancer [25-27].

The foundation for the LNT model was laid by Hermann Mulle'r 1928 genetic experiments on *Drosophila melanogaster*, which showed that radiation-induced mutation frequency increased in a linear dose-dependent fashion [28]. These findings were later supported by human epidemiological data, especially from the Life Span Study (LSS) of atomic bomb survivors [29].

Additional evidence comes from clinical data, such as the UK pediatric CT cohort study, which reported a linear increase in the risk of leukemia and brain tumors in children exposed to cumulative doses as low as ~30-60 mGy. This supported the absence of a threshold in radiation-induced carcinogenesis. This study concluded that CT scans ought to be minimized, and when appropriate, non-ionizing imaging alternatives should be considered [30].

Together, these findings have led radiation protection bodies such as the ICRP and NCRP to adopt the LNT model as a conservative framework in formulating radiation protection guidelines, especially to safeguard vulnerable populations.

Nevertheless, the LNT model remains a subject of ongoing debate. Advances in molecular and cellular biology have raised concerns that the model may overestimate risk in the low-dose range and may oversimplify the complex biological responses induced by low-level IR exposure [31-34].

1.3.2 Non-linear threshold model

As an alternative to the LNT paradigm, several researchers have proposed a competing model based on the non-linear threshold response curve [35-37]. This model suggests that there is a level of radiation dose below which no harmful biological effects occur. In other words, biological damage becomes detectable only when exposure exceeds a defined threshold, beyond the capacity of cellular repair and defense mechanisms to compensate [38].

The biological plausibility of this model is supported by observations of deterministic effects, or tissue reactions, such as cataract formation and radiation-induced fibrosis, where a minimum dose is required to induce a biological response [39].

Mechanistic evidence in favor of the threshold model includes:

- Non-linear dose-response relationships for DNA double-strand breaks (DSBs) at very low doses and dose rates [40]: At very low doses, DNA double-strand breaks (DSBs), a form of severe DNA damage, may not increase in a straight line with dose, suggesting the cell's repair systems might keep up better at low doses than at high ones.

- Apoptosis elimination of severely damaged cells, which may prevent long-term damage [33, 41]: The body can actively remove damaged cells before they turn into cancer cells, a natural protective mechanism called programmed cell death.
- Adaptive responses, in which low-dose exposures stimulate protective biological functions [42]: Small amounts of radiation may trigger the body's natural defenses, such as DNA repair enzymes or antioxidants, making the cells more resistant to future damage.

Furthermore, individuals' radiosensitivity may vary based on factors such as genetic background, sex, age, lifestyle, and co-exposures to other environmental agents. These variables cannot be ignored when assessing cancer risk associated with low-dose radiation exposure [43].

Nevertheless, the threshold model remains highly debated, particularly regarding stochastic effects such as carcinogenesis. Unlike deterministic effects, stochastic events lack a clearly defined dose threshold, and epidemiological evidence for low-dose thresholds in cancer risk remains limited and inconclusive [29, 44-46].

1.3.3 Adaptive responses/ Hormesis effects

The radiation-induced adaptive response, also referred to as radiation hormesis, is an intriguing biological phenomenon in which exposure to a low-dose of IR induces increased resistance to damage from a subsequent higher dose. This effect was first reported in the early 1980s by Olivieri et al. in human lymphocytes [47] and has since been

documented and confirmed in various cell types and organisms, both *in vitro* and *in vivo* [48-54].

For instance, Youngblom et al. demonstrated that preconditioning human lymphocytes with an acute dose of 10 mGy significantly reduced chromatid aberrations and increased protein synthesis following a subsequent 1500 mGy dose administered 4-6 hours later [48]. Similarly, low-dose X-ray exposure appears to prime human lymphocytes with protective mechanisms that mitigate DNA damage from subsequent high-LET alpha particles [55].

In animal studies, pre-treatment of mouse splenocytes, including T and B lymphocytes, dendritic cells, and macrophages, with 10 mGy of γ-radiation prior to an acute high-dose exposure led to significantly greater proliferation relative to non-treated controls [56]. Cchronic low-dose-rate γ-irradiation (0.5 Gy at 1.2 mGy/h) in mice also induced an adaptive response, reducing DNA damage in spleen cells following a high-dose-rate challenge. This radiation-induced protective effect was linked with increased expression and activity of antioxidative enzymes [57].

A metabolic shift from oxidative phosphorylation to aerobic glycolysis has also been observed following low-dose radiation, contributing to increased radiation resistance in both normal human cells and murine models [49].

Furthermore, clinical case studies also support the potential therapeutic benefits of low-dose radiation. Repeated low-dose X-ray or radon-based exposures have been associated with favorable clinical outcomes in patients with prostate cancer and ulcerative colitis, indicating the potential for radio-adaptation as a potential non-traditional therapeutic approach [50].

Despite its broad biological relevance, the molecular mechanisms underlying radiation-induced adaptive responses remain an area of active investigation. Emerging evidence points to a coordinated program involving:

- Enhanced DNA repair
- Upregulated antioxidant defenses
- Altered metabolism

These conserved cellular responses, evolved to maintain genomic stability and tissue function, are further explored in the following sections.

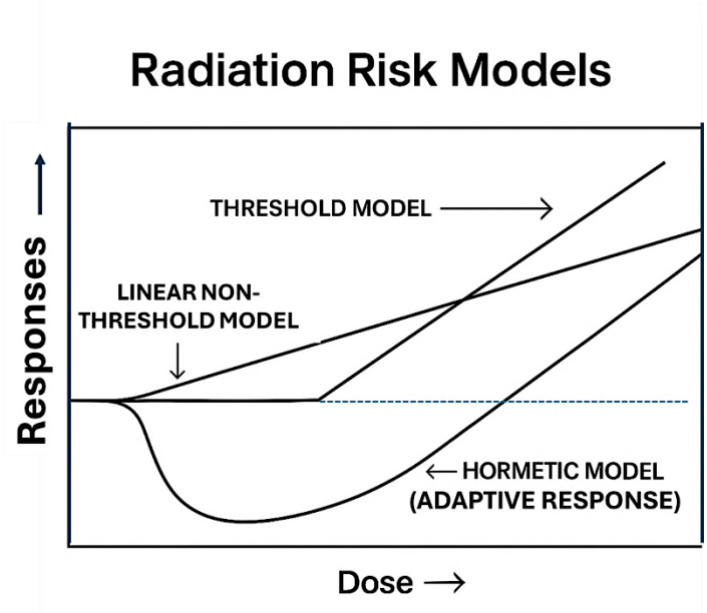

Figure 2) Comparison of radiation risk models: linear non-threshold, threshold, and adaptive response (hormetic) models

This diagram illustrates three conceptual models describing the biological response to ionizing radiation. The Linear Non-Threshold (LNT) model assumes that any dose, no matter how small, increases biological risk proportionally. The Threshold model suggests that no adverse biological effects occur below a certain dose threshold, beyond which damage increases with dose. The Adaptive response model, also known as Hormetic model, proposes that low doses may trigger beneficial cellular responses before becoming detrimental at higher exposures. These models guide regulatory frameworks and ongoing scientific debate surrounding low-dose radiation exposure.

1.4 Molecular mechanisms underlying adaptive responses

1.4.1 The DNA damage response (DDR)

IR can damage various cellular components, but DNA damage is the most important mechanism of radiation-induced injury and initiation event in carcinogenesis. IR generates DNA lesions either directly, by ionizing DNA molecules, or indirectly through the formation of reactive oxygen species (ROS). These lesions range from oxidative base modifications (e.g., 8-oxo-dG and thymine glycol) to more severe forms such as single-strand breaks (SSBs) and double-strand breaks (DSBs) [58].

Among these, DSBs are the most dangerous type of DNA damage because of their repair complexity and high potential to compromise genomic integrity. Inaccurate disrepair of DSBs is a hallmark of genomic instability and cancer development, making DSBs a central endpoint in the biological evaluation of radiation exposure [59].

The cellular response to DSBs activates a network of signaling pathways, known as DNA damage response (DDR). It functions to detect DNA lesions, arrest the cell cycle, and initiate repair. DDR initiation involves phosphorylation of the histone variant H2AX at serine 139 by ATM or DNA-PK, producing γH2AX, which serves as a platform for the recruitment of repair proteins. These proteins accumulate at DNA damage sites, forming nuclear foci detectable by immunofluorescence microscopy [60]. The efficacy of the DDR greatly influences cell survival and genomic stability [61].

In mammals, non-homologous DNA end joining (NHEJ) is the main DSB repair pathway that functions throughout the cell cycle [62]. In the NHEJ pathway, the Ku protein binds to each broken DNA end, and recruits processing enzymes including the DNA ligase

IV complex for DNA ligation [63]. In contrast, homologous recombination (HR) employs a sister chromatid as a repair template and only happens during the S and G2 phases, providing more accurate repair than the error-prone NHEJ [64].

While DNA damage is a reliable biomarker of radiation exposure, the efficiency of DSB repair following low-dose IR remains inconsistently reported. Several studies have demonstrated that low-dose IR can enhance repair factors activity, increase end-joining fidelity, or promote pro-survival signaling, suggesting that DDR capacity may be modulated in a dose-dependent manner [47, 65-69]. These findings support the adaptive response model, proposing that low-dose IR may stimulate cellular defense systems and reduce both radiation-induced and background DNA damage [38]. However, others report no considerable improvement in DSB repair under low-dose radiation [70-74]. These differences may be due to difficulty in distinguishing between exogenous and endogenous DNA damage, inter-individual variation in repair capacity, and limitation of extrapolation from high-dose data. Therefore, there is an urgent need for specific and sensitive biomarkers that can accurately assess cellular responses to low-dose and low-dose-rate IR [75-79].

1.4.2 Oxidative stress and antioxidant systems

IR affects not only DNA but also a wide range of cellular macromolecules, such as nucleic acids, proteins, and complex lipids, by generating reactive oxygen species (ROS). These ROS are produced via radiolysis of water and through disruption of mitochondrial function [80]. ROS include a variety of highly reactive species such as hydroxyl radicals

(•OH), hydrogen radicals (H•), hydrated electrons (eaq^-) and hydronium ions (H_3O^+). Although ROS are endogenously generated as byproducts of normal cellular metabolism, they also play essential roles in cell signaling, proliferation, and immune responses [81, 82].

Under physiological conditions, ROS levels are tightly regulated by a network of enzymatic and non-enzymatic antioxidant defense systems, including superoxide dismutase (SOD), catalase, glutathione peroxidase, and vitamin C/E systems. These systems work together to neutralize excess ROS and maintain redox homeostasis. When ROS concentration exceeds the buffering capacity of the antioxidants, oxidative stress proceeds, leading to damage to cellular components, including oxidative modifications of DNA bases such as 8-oxo-guanine [83].

The association between low-dose IR and ROS has been investigated. Emerging evidence suggests that the effects of low-dose IR on cellular ROS production may not be entirely detrimental. Interestingly, at sublethal levels, IR-induced ROS regulates enzyme activity including the human APE (APE-1) gene and thymidine kinase, that promotes DNA repair and preserves genome stability [84-86]. Moreover, it is demonstrated that low-dose, low-LET exposure is associated with antioxidant enzyme overexpression and inhibition of superoxide production that leads to enhanced resistance to DNA damage [81, 87].

These findings highlight a complex and context-dependent relationship between low-dose IR, ROS, and cellular adaptive responses wherein a transient, moderate increase in ROS may act as a trigger for protective signaling cascades and radiation-induced stress adaptation mechanisms rather than simply causing oxidative injury. Nevertheless, the

effect of low-dose IR on oxidative damage and antioxidant responses appears to vary among species, age classes, biological systems, and even between sexes [88].

1.4.3 Metabolic reprogramming

While the high-throughput data genomics, transcriptomics, and proteomics analyses offer indirect information into cellular phenotypes, metabolomics provides a more direct and dynamic snapshot of the cell or tissue's physiological state [89]. Unlike transcripts or proteins, metabolites are not significantly influenced by post-translational modifications, making them closer proxies to actual cellular function and phenotypic status. As such high-resolution mass spectrometry (LC-MC)-based metabolomic profiling has emerged as a powerful strategy to identify biomarkers of radiation-induced toxicity across multiple tissues and contexts [90].

The metabolic response to low-dose IR is, multifactorial and context-dependent. Evidence suggests that cells exposed to low-dose IR undergo adaptive metabolic reprogramming to maintain viability and genomic integrity. An interesting observation in both *in vitro* fibroblast cultures and *in vivo* animal models is a metabolic shift in response to low-dose IR. This shift involves switching from mitochondrial oxidative phosphorylation (OXPHOS) to aerobic glycolysis, mediated by hypoxia-inducible factor 1-alpha (HIF-1α). This adaptation, similar to the Warburg effect, helps sustain ATP production and preserve redox balance under oxidative stress conditions [49]. Such metabolic plasticity challenges the LNT model of radiation exposure risk, which assumes a proportional relationship between dose and biological adverse effects.

Recent metabolite fingerprinting studies using LC-MS have shown distinct metabolic signatures in individuals with varying degrees of radiation-induced chromosomal aberration [91]. Differentially expressed metabolites, such as 3-hydroxy-propanoate and glycolaldehyde, as well as altered taurine metabolism, show potential as early biomarkers of radiation-induced cellular stress and genomic damage. Nevertheless, mechanistic investigations are needed to clarify whether these metabolic changes are causal contributors or merely reactive markers of cellular stress.

Despite these advances, the acute and chronic effects of low-dose IR are often subtle and difficult to detect, and they cannot be predicted solely based on observation gained from high-dose short-term radiation studies. Furthermore, in a real-world setting, interindividual variability, including differences in genomic background, diet, environment, and lifestyle can significantly confound the metabolite expression in responses to low-dose IR in healthy populations [92]. In addition, ethical and logistical constraints limit sample availability from human cohorts, hindering the comprehensive characterization of systemic metabolic responses to low-dose radiation [93].

1.5 Gene expression in eukaryotic cells and the importance of post-transcriptional control

The classical view of gene expression, often summarized by the central dogma of molecular biology DNA to RNA to protein presents a linear and deterministic pathway for the flow of genetic information. However, this model has been significantly revised over the past few decades. Advances in molecular biology have revealed that gene expression is highly regulated at multiple levels and that post-transcriptional events play a critical role

in shaping the final protein output of a cell, particularly in response to cellular stress and environmental stimuli.

The discrepancies between mRNA abundance and protein levels underscore the influence of regulatory mechanisms such as RNA splicing, transport, stability, localization, and translation efficiency. These mechanisms introduce significant variability between the genetic blueprint encoded in DNA and the actual proteins synthesized within the cell.

A comprehensive understanding of these layers of regulation is essential for interpreting cellular responses to external challenges such as IR, where transcriptional and translational controls can diverge distinctly.

1.5.1 The post-transcriptional regulation under stress and its time scale

Environmental stressors such as oxidative stress, radiation, and heat shock require cells to initiate rapid and coordinated responses to ensure survival. These responses generally occur in distinct phases: initial damage control and repair, energy conservation and adaptation, and, finally, recovery and growth once homeostasis is restored [94, 95].

Eukaryotic cellular responses to stress operate at different time scales. Posttranslational modifications (PTM), that can occur within seconds, enable immediate cellular reactions and offer functional changes in proteins that cannot be pre-encoded in gene sequences on evolutionary timescales [96].

Post-transcriptional events, including messenger RNAs (mRNAs) turnover, translational activity, covalent modifications, and subcellular localization of RNA, are well suited for minute-scale responses. These processes allow rapid reprogramming of gene

expression in response to transient stress and facilitate dynamic recovery upon restoration of normal conditions. These responses are tightly regulated through multiple signaling pathways to ensure appropriate intensity, avoid unnecessary activation under mild stress, and prevent prolonged or excessive responses [97].

In contrast, transcriptional induction and repression are slower and more long-lasting. On average, eukaryotic cells transcribe only two mRNA molecules per gene per hour, whereas translation can yield 180 to 1000 protein molecules per mRNA per hour [98]. This contrast emphasizes the unique advantage of post-transcriptional regulation: it acts as an intermediate layer between the fast-acting PTMs and the slower transcriptional programs, enabling efficient cellular adaptation during transient stress.

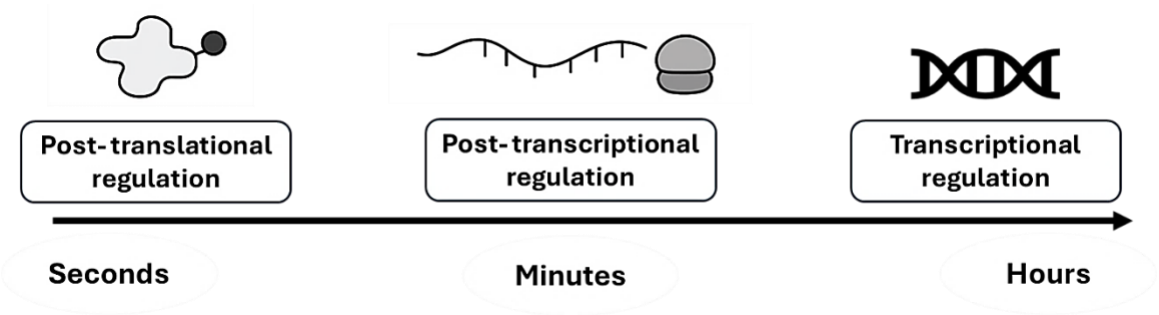

Figure 3) Time-scale hierarchy of cellular stress responses: post-translational, post-transcriptional, and transcriptional regulation.

A schematic illustration of how cells respond to stress across different time domains. Post-translational modifications (PTMs) act within seconds, enabling immediate functional changes. Post-transcriptional regulation (e.g., mRNA turnover, translation control) operates over minutes, adjusting gene expression programs dynamically. Transcriptional responses occur over hours, establishing long-term adaptation. This tiered response enables cells to balance urgency with sustained recovery.

1.5.2 Lack of correlation between transcript and gene products necessary for the survival of stress

Upon sudden environmental stress, cells activate a conserved transcriptional program known as the core environmental stress response (CESR) [99, 100]. This response includes two broad gene sets: one commonly upregulated across stressors, usually genes involved in carbohydrate metabolism, protein folding, and oxidative defense [95, 99, 100], and another consistently downregulated, including genes encoding ribosomal proteins, translation factors, and ribosome biogenesis (Ribi) regulons [101, 102]. As the stress signal is further processed, CESR evolves into a stressor-specific response. This cross-regulatory flexibility also underlies cross-adaptation, where prior exposure to mild stress increases resistance to subsequent or even unrelated stressors [103].

However, transcriptional induction does not always correlate with functional relevance. For example, in response to DNA-damaging agents, many upregulated genes do not overlap with those proven essential for DNA repair [104]. Similarly, no significant correlation was found between oxidative stress-induced genes and those required for oxidative stress resistance in *S. cerevisiae* [105].

This discrepancy is further emphasized by the well-documented lack of correlation between mRNA and protein abundance in eukaryotic cells [98]. Following high-dose radiation, transcriptomic data often show limited overlap with proteomic changes, suggesting a disconnect between gene expression and protein output [106, 107].

One possible explanation is that many stress-induced transcripts belong to a generic CESR program, which may not be directly involved in immediate stress survival. Instead, early survival may depend on pre-existing proteins or those rapidly mobilized post-transcriptionally, such as DNA repair enzymes or chaperones [104]. Moreover, transcriptional changes may mostly help long-term recovery, rather than acute stress tolerance.

Together, these observations emphasize the limitations of transcriptomic analyses in isolation and highlight the important role of post-transcriptional and translational regulation in determining cell fate during environmental stress.

1.5.3 mRNAs modification, establishment and quality control mechanism under stress

Chemical modification of mRNAs plays a large role in regulating cellular responses to stress [108]. In eukaryotic cells, N^6-methyladenosine (m^6A), generally located within the 5′ untranslated region (5′-UTR), is the most abundant internal mRNA modification [109]. m^6A influences mRNA stability, nuclear export, splicing, and translation efficiency [110]. Interestingly, stress-response mRNAs are often enriched in m^6A compared to average transcripts.

Under normal conditions, m^6A acts as a “disposal tag”, targeting the mRNA for degradation via the YTHDF enzyme, thereby maintaining stress-response proteins at low levels [111]. However, under stress conditions, m^6A enables cap-independent translation,

allowing transcripts to bypass global translational repression and be preferentially translated [112].

In addition to chemical modification, mRNA secondary structures also influence translation during stress. RNA rich in guanine can form guanine quadruplexes (G-quadruplexes or G4), a stable secondary structure that is usually more seen in single-stranded RNAs. Intriguingly, while *in vitro* studies suggest that G4 structure in the 5′-UTR of an mRNA inhibits translation [113], *in vivo* data reveal that RNA-binding proteins (RBPs) like CNBP (also known as ZNF9) actively unwind these structures to maintain translational readiness [114, 115].

Guanine residues are particularly susceptible to oxidation by ROS due to their low redox potential, leading to the formation of 8-oxo-7,8-dihydroguanine (8-oxoG) [116]. RNA is particularly vulnerable to guanine oxidation because of its single-stranded nature and proximity to ROS-generating organelles such as mitochondria and peroxisomes. 8-oxoG lesions can disrupt RNA structure and interfere with RBP binding, thereby impairing translation [117, 118].

To safeguard translational fidelity, damaged RNAs are rapidly identified and degraded via RNA quality control pathways, including:

- Nonsense-mediated decay (NMD)
- No-go decay (NGD)
- Ribosome-associated quality control (RQC)

These mechanisms ensure that defective mRNAs do not persist or produce dysfunctional proteins [119]. Additionally, the high redundancy in mRNA copies in cells provides a

buffering effect, ensuring that only functional transcripts stay available even when some are damaged. Such surveillance activity reduces the likelihood of significant adverse effects on cellular physiology. [120]

In summary, post-transcriptional regulation offers an intermediate and efficient mechanism to fine-tune gene expression during stress. It bridges the rapid responsiveness of post-translational modifications with the slower adaptation afforded by transcriptional changes, ensuring cells conserve resources while maintaining essential protein synthesis. Given its central role in stress resilience and recovery, understanding how mRNA stability, structure, and translation are modulated under stress, particularly IR, is critical. The next section delves into the fundamentals of eukaryotic mRNA translation, laying the groundwork for exploring its modulation under stress conditions.

1.6 Eukaryotic mRNA translation: A central mechanism of post-transcriptional control of gene expression

A key mechanism of post-transcriptional control of gene expression is translational regulation because it directly determines the rate and specificity at which proteins are synthesized from available messenger RNAs (mRNAs). Unlike transcription, which alters mRNA abundance, translational regulation provides cells with the ability to rapidly and reversibly modulate protein production without needing to generate new transcripts. This is particularly advantageous during environmental stress, where a swift cellular response is critical for survival [121, 122].

Protein synthesis is a fundamental yet energetically expensive and tightly regulated cellular process [123]. Under stress conditions, cells must efficiently reprogram mRNA

translation to conserve energy, prevent the production of faulty proteins, and prioritize the synthesis of stress-response proteins. Thus, translation control modulates both global protein output and the selective translation of specific mRNAs [124].

Moreover, since the correlation between mRNA levels and protein abundance is often weak, translational regulation serves as a more accurate determinant of functional protein output.

Translation is regulated through a four-stage cyclic process: initiation, elongation, termination, and ribosome recycling. While modulation of mRNA translation can happen at any stage, most regulatory events occur at the initiation phase.

1.6.1 Cap-Dependent translation initiation

Most eukaryotic mRNAs are marked by a 7-methylguanosine cap structure (m7GpppN, where N is any nucleotide) at their 5′ ends and a polyadenylated (polyA) tail at their 3′ ends [125]. These elements serve as molecular docks for multi-protein complexes that regulate translation. During the initiation phase of cap-dependent translation, the eukaryotic initiation factor 4F (eIF4F) complex, comprising the cap-binding protein eIF4E, scaffold protein eIF4G, and the ATP-dependent helicase eIF4A, accelerates this process [126].

The poly(A)-binding protein (PABP) connects to poly(A) tails, increasing mRNA stability and interacting with eIF4G to circularize the mRNA. The 43S pre-initiation complex (PIC) forms independently of mRNA and consists of the 40S ribosomal subunit, the ternary complex (eIF2-GTP-Met-tRNAi), eIF3, eIF1, eIF1A, and eIF5 [127, 128].

Through interaction with eIF3, the PIC binds to eIF4F and scans the 5′ untranslated region (5′ UTR) for the start codon, usually the AUG codon [129].

When the start codon is recognized, the GTP bound to eIF2 is hydrolyzed by the GTPase activating protein (GAP), eIF5. The inactive eIF2-GDP is recycled back to its active form, eIF2-GTP, by the guanine nucleotide exchange factor (GEF), eIF2B [130]. eIF4G functions as a scaffold that enables the interaction of the eIF4F complex with PIC [131]. 4E-binding proteins (4E-BPs) regulate eIF4E availability by competing with eIF4G for binding to eIF4E [132]. eIF4E is the least abundant translation initiation factor, and therefore, its expression can be a rate-limiting factor in the eIF4F complex assembly [133]. This competition is modulated by the phosphorylation status of 4E-BPs, controlled by the mechanistic target of rapamycin complex 1 (mTORC1) [134].

The final step in initiation is mediated by eIF5B-GTP, which promotes joining of the 60S ribosomal subunit to the 40S-PIC, forming the complete 80S ribosome, and marking the transition to the elongation phase [135].

1.6.2 Translation Elongation and Termination

Elongation is the stage during which the polypeptide chain is synthesized. It begins with the delivery of aminoacyl-tRNAs to the A-site of the ribosome by elongation factor eEF1A, which binds GTP and ensures codon-anticodon accuracy. Once the correct tRNA is in place, a peptide bond forms between the amino acid in the A-site and the growing polypeptide chain in the P-site, catalyzed by the ribosomal peptidyl transferase activity. The ribosome then translocates along the mRNA, a process facilitated by elongation factor eEF2, which also requires hydrolysis of GTP [136, 137].

Termination occurs when one of the three stop codons (UAG, UAA, or UGA) is positioned in the A-site. Release factor eRF1 recognizes the stop codon, while eRF3, a GTP-binding protein, promotes polypeptide release and hydrolysis of the ester bond linking the polypeptide to the tRNA. GTP hydrolysis by eRF3 triggers conformational changes that enable disassembly of the translation complex. Ribosome recycling is facilitated by eIF5A and ATP-binding cassette protein 1 (ABC1), which help dismantle and reset ribosomal subunits for another round of translation [138-140].

1.6.3 Reprogramming of protein synthesis under stress

When exposed to stress, cells must shift their translational priorities: global protein production is downregulated to conserve energy and prevent the accumulation of misfolded proteins, while the selective translation of specific mRNAs, often encoding protective or repair proteins, is enhanced. Rather than shutting down the translation process entirely, the cell engages in adaptive programs that rewire the translational landscape to favor survival. Two key signaling networks orchestrate this shift:

1) Integrated stress response pathway (ISR) and

2) The pathways of the mechanistic target of rapamycin complex 1 (mTOR1) and its downstream effectors.

These pathways enable a fine-tuned and context-dependent translational output, allowing cells to balance stress resistance with recovery and growth once favorable conditions return.

1.6.3.1 ISR pathway

Integrated Stress Response (ISR) regulates mRNA translation in response to various cellular stressors, including endoplasmic reticulum (ER) stress, oxidative stress, and nutrient deprivation. Key to this response is the phosphorylation of eIF2α by one of four kinases: heme-regulated inhibitor (HRI), general control non-derepressible-2 (GCN2), PKR-like endoplasmic reticulum kinase (PERK), or protein kinase R (PKR) [141, 142]. Phosphorylated eIF2α inhibits eIF2B activity, decreasing the availability of eIF2-GTP and consequently reducing the global cap-dependent translation [143, 144].

Interestingly, while ISR suppresses bulk protein synthesis, it selectively enhances the translation of specific transcripts, such as activating transcription factor 4 (ATF4) and cellular inhibitor of apoptosis protein 1 (cIAP1), via cap-independent mechanisms. For instance, the ATF4 mRNA contains upstream open reading frames (uORFs) in its 5′ untranslated region, which normally prevent efficient translation. However, under ISR-induced conditions where eIF2α is phosphorylated, ribosomes bypass these uORFs and initiate translation at the ATF4 coding region, allowing for selective upregulation during stress. These selectively translated proteins play critical roles in promoting stress adaptation and cell survival [145, 146]. Hence, ISR acts as a dual regulator, reducing global translation while selectively increasing stress-adaptive protein synthesis.

1.6.3.2 mTORC1 pathway

In mammals, mTORC1 maintains cellular homeostasis by integrating upstream signals such as growth factors and amino acid availability into downstream signals that maintain cellular homeostasis [147, 148]. Under stress conditions such as DNA damage, low ATP levels, or low oxygen levels (hypoxia), AMP-activated protein kinase (AMPK)

phosphorylates and inhibits mTORC1 activity and its downstream effectors' signaling. This suppression of signaling leads to cell cycle arrest, conserving cellular energy and enhancing survival during stress [149].

The two key downstream targets of mTORC1 are the ribosomal S6 protein and the 4E-BP1 [150]. mTORC1 activation leads to the phosphorylation of both targets, activating the S6 protein while deactivating 4E-BP1, which in turn allows the assembling of an active protein translation machinery [151]. Phosphorylated S6 protein is commonly used as a readout of the mTORC1 activity [152, 153]. While S6 supports ribosomal biogenesis, phosphorylated 4E-BP1 releases eIF4E to form the eIF4F complex, enabling cap-dependent translation initiation [154-159].

Together, the ISR and mTORC1 pathways provide a coordinated regulatory framework between translational suppression and selective protein synthesis, enabling cells to adapt and survive under stressful conditions.

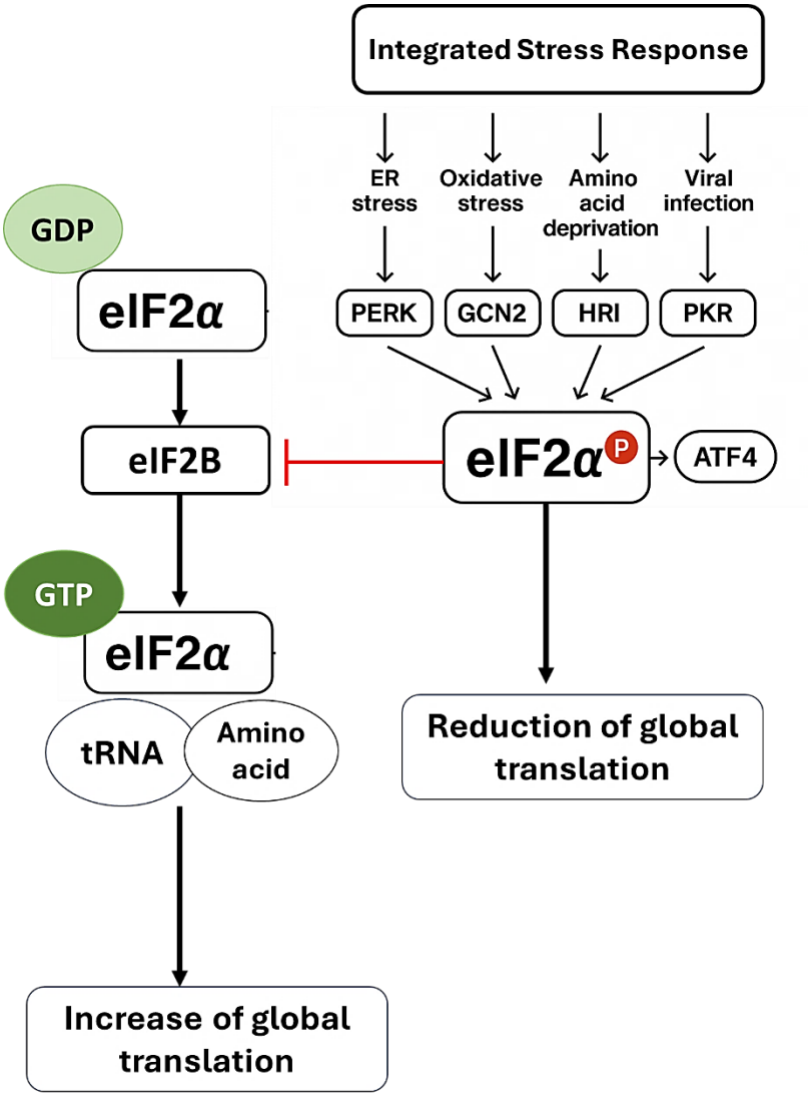

Figure 4) Regulation of eIF2α in the Integrated Stress Response (ISR) pathway and its role in translational control.

This schematic illustrates the modulation of global protein translation by the eIF2α under stress conditions. Various cellular stressors, including ER stress, oxidative stress, amino acid deprivation, and viral infection, activate one of four specific kinases: PERK, GCN2, HRI, or PKR. These kinases phosphorylate eIF2α (p-eIF2α), which inhibits its guanine nucleotide exchange factor (eIF2B), blocking the recycling of GDP-bound eIF2α to its active GTP-bound form. This leads to a reduction in the formation of the eIF2-GTP-tRNA^Met ternary complex, thereby suppressing global cap-dependent translation. However, selective translation of stress-responsive transcripts such as ATF4 is enhanced. In contrast, when stress is resolved and eIF2α is dephosphorylated, active eIF2-GTP-tRNA-Met complexes are regenerated, restoring global protein synthesis. This dynamic control allows cells to conserve resources during stress and quickly resume growth and repair upon recovery.

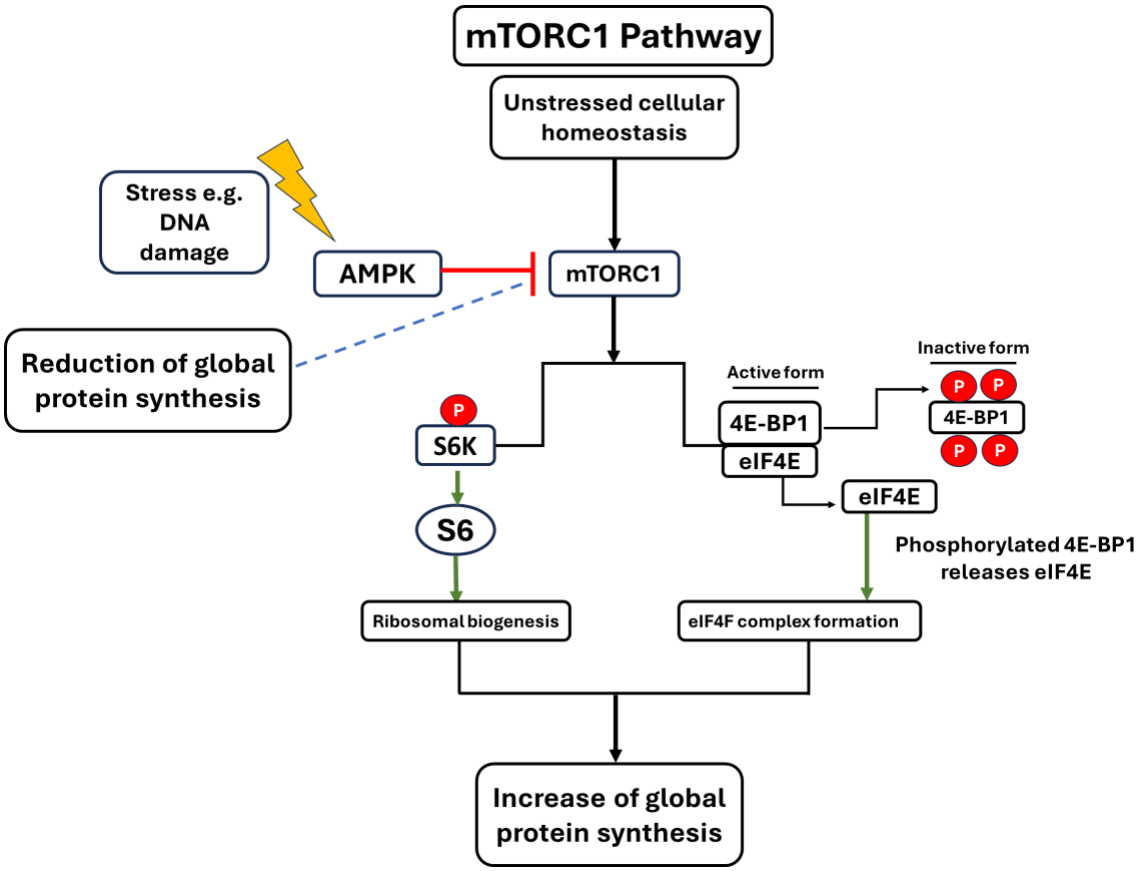

Figure 5) mTORC1 signaling pathway

The mTORC1 signaling pathway in the regulation of protein synthesis. Under normal conditions, mTORC1 promotes protein synthesis through phosphorylation of S6K (leading to ribosomal biogenesis) and 4E-BP1 (which releases eIF4E for eIF4F complex formation). Under stress (e.g., DNA damage), AMPK inhibits mTORC1 activity, suppressing global protein synthesis to conserve energy and support survival.

1.7 Translatome analysis and translation efficiency quantification via ribosome profiling

The central role played by translation in gene expression has motivated the development of advanced techniques to elucidate translational control mechanisms. Ribosome-profiling (Ribo-seq) strategy is a powerful, high-throughput sequencing method that enables genome-wide analysis of the translatome, the full set of actively translated mRNAs, by sequencing ribosome-protected mRNA fragments (RPFs) also known as ribosome footprints. These fragments are typically ~28 nucleotides in length and resistant to nuclease digestion [160, 161].

These footprints are isolated and converted into DNA libraries using next-generation sequencing (NGS) platforms. By in-parallel comparison of RPF and total mRNA levels, translation efficiency (TE) can be calculated for each transcript as the ratio of RPFs to total mRNA (RPF/RNA), offering a direct, transcript-specific measure of translational activity.

In addition to TE quantification, Ribo-seq provides high-resolution information into ribosome distribution along transcripts, initiation sites, elongation dynamics, and even non-canonical translation events in both in *vitro* and *in vivo* models [160, 162].

Therefore, in the context of cellular stress responses, especially under low-dose IR, Ribo-seq can be used as a powerful lens into how translational reprogramming contributes to cellular adaptation. It allows the identification of stress-responsive translational signatures and the discovery of potential biomarkers of radiation exposure and resistance.

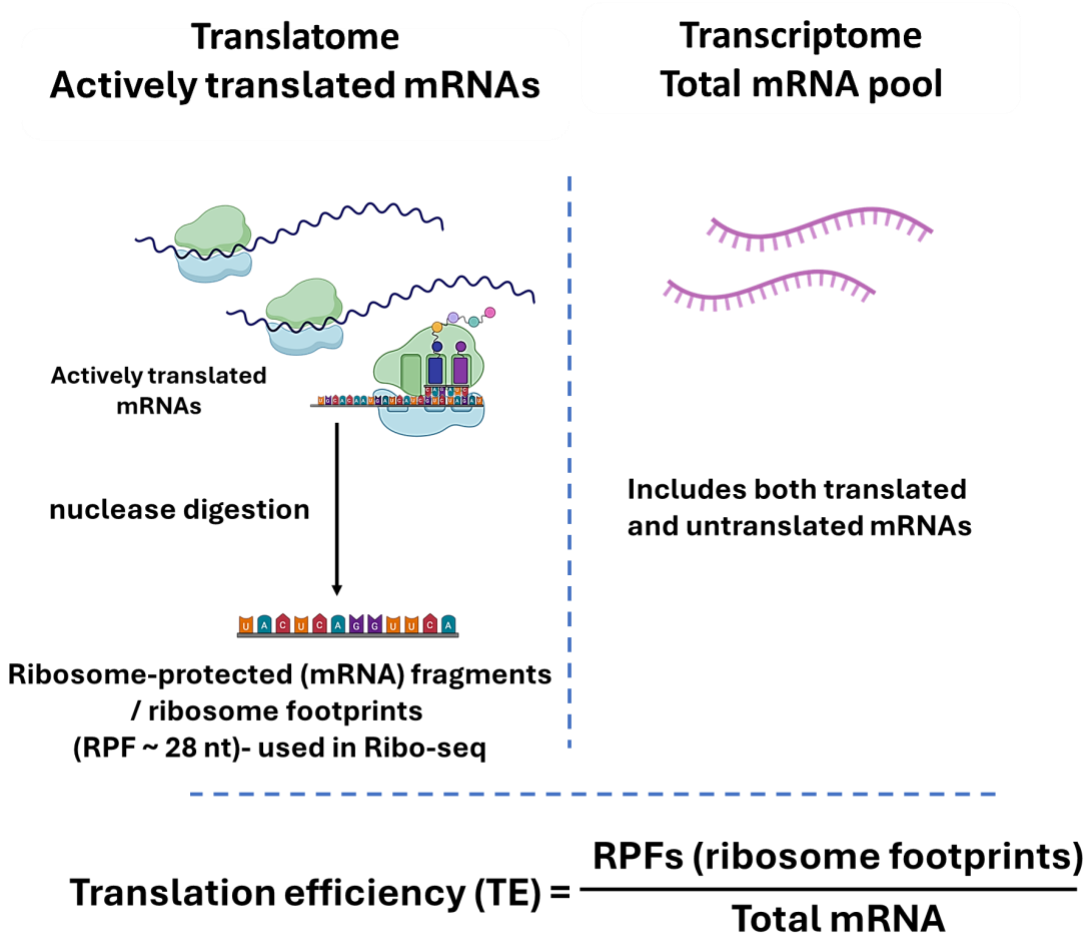

Figure 6) Comparison of translatome and transcriptome as revealed by ribosome profiling.

The translatome represents mRNAs actively engaged with ribosomes and being translated into proteins, as detected by ribosome-protected fragments (RPFs). In contrast, the transcriptome includes the entire mRNA pool within a cell, including both translated and untranslated transcripts. Ribosome profiling (Ribo-seq) isolates RPFs (~28 nucleotides) to quantify translation efficiency and assess the spatial distribution of ribosomes on mRNAs.

1.8 Study rationale and objectives

Low-LET radiation, including γ-rays, is characterized by high penetration ability through biological tissues, making them widely used in both medical diagnostics and biological research [163]. While the biological effects of high doses of IR, including both deterministic effects such as skin burns and hair loss as well as stochastic outcomes like genotoxicity and carcinogenesis, are well studied [164-168], the cellular impact of low-dose IR (≤ 0.1 Gy) remains less understood.

Changes in gene expression represent one of the initial biological responses to IR. At the molecular level, transcriptomic studies have profiled gene expression in response to different doses and dose rates of γ-radiation [13, 169-172], revealing complex, dose-specific transcriptional changes that distinguish low-dose from high-dose responses [173, 174]. However, as discussed above, gene expression regulation extends beyond transcription. Post-transcriptional control, especially at the level of mRNA translation, plays a critical role in stress responses.

In response to stress factors, such as radiation, oxidative stress, and nutrition deficiency, global protein synthesis, which is highly energy-consuming, can be rapidly downregulated, while the translation of stress-response mRNAs can be selectively enhanced. This coordinated regulation can enable a rapid and efficient cellular adaptation to environmental stressors and physiological changes [175]. In the context of high doses of IR, studies have shown that gene expression can be dramatically repressed through mRNA translation, suggesting that cells selectively regulate protein synthesis to manage radiation-induced stress [106, 176, 177]. However, how cells remodel gene expression through the translation machinery under low-dose IR has not been properly addressed [178].

Given the uncertainties surrounding the biological effects of low-dose IR, I hypothesize that exposure to low-dose γ-radiation induces specific changes in protein synthesis regulation, leading to adaptive responses in the cellular proteome. These changes may mirror high-dose responses or involve unique, subtler mechanisms tailored to low-level stress.

To address this hypothesis, I employed a multi-layered approach to evaluate translational control under low-dose IR. This included the assessment of:

- Quantify global protein synthesis activity using puromycin incorporation assays to assess overall translational output.
- Evaluate the activity of key translation regulatory pathways, including eIF2α and mTORC1, by analyzing phosphorylation status via Western blotting.
- Perform genome-wide ribosome profiling (Ribo-seq) to assess ribosome occupancy and calculate translational efficiency (TE) at the transcript level.
- Validate selected mRNAs and proteins identified by Ribo-seq using qPCR and immunoblotting, to confirm translational changes and assess functional relevance.

Hypothesis: Exposure to low-dose γ-rays induces specific changes in the regulation of protein synthesis, facilitating cellular adaptation to stress. These changes may involve both conserved and low-dose-specific translational mechanisms that differ from those observed under high-dose IR.

Research objectives

Aim 1: Evaluate global protein synthesis in response to IR:

Determine whether low-dose IR alters overall translational activity by quantifying nascent protein synthesis via puromycin incorporation. In parallel, assess phosphorylation status of translation regulators (eIF2α, S6, and 4E-BP1) as indicators of ISR and mTORC1 pathway activity.

Aim 2: Characterize the translational reprogramming dynamics under low-dose γ-radiation:

Perform genome-wide translatome profiling using Ribo-seq to identify mRNAs with altered TE. This analysis will reveal ribosome distribution, changes in translation initiation, and selective ribosome engagement across transcripts following γ-radiation.

Aim 3: Validate and characterize candidate mRNAs as translational biomarkers of low-dose radiation exposure:

Confirm changes in TE of selected candidate transcripts identified by Ribo-seq using quantitative PCR (qPCR) for mRNA levels and western blotting for protein expression. This aim will assess whether altered TE corresponds to changes in protein abundance and help identify robust translational biomarkers indicative of cellular response to low-dose γ-radiation.

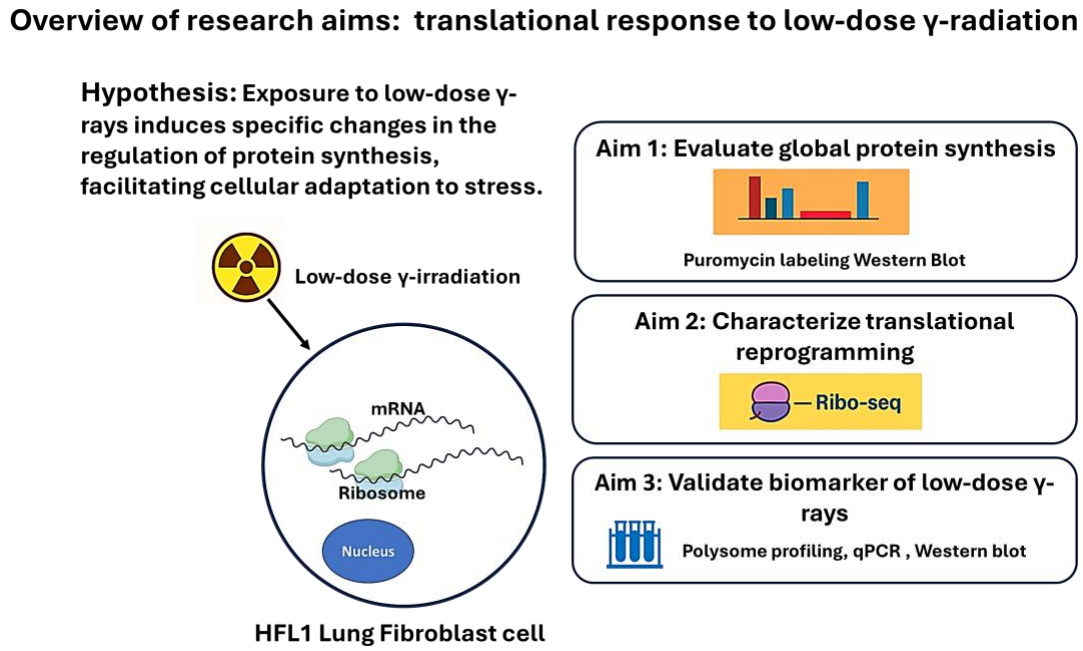

Figure 7) Graphical abstract summarizing the hypothesis and experimental design

This figure illustrates the central hypothesis that exposure to low-dose γ-radiation induces specific changes in protein synthesis regulation. Upon γ-radiation exposure, cellular translation responses are examined through three experimental aims. Aim 1 evaluates global protein synthesis by assessing translation rates and phosphorylation of key signaling molecules. Aim 2 characterizes transcript-specific translational reprogramming using ribosome profiling (Ribo-seq). Aim 3 validates candidate mRNAs identified from Ribo-seq as potential biomarkers through quantitative PCR and protein-level analysis. This integrative approach provides insight into how low-dose γ-radiation modulates the translational landscape to mediate cellular adaptation.

Chapter 2: Methods & Materials:

2.1 Cell culture

The human fetal lung fibroblast cell line HFL1 (ATCC® CCL-153™) was cultured in Ham's F-12K medium (Gibco™, Cat# 21127030) supplemented with 10% fetal bovine serum (FBS; Gibco™, Cat# A3840302). Cells were maintained at 37°C in a humidified incubator with 5% CO_2. The culture medium was replaced every 2–3 days, and cells were subcultured at approximately 80% confluency using TrypLE™ Express Enzyme (Gibco™, Cat# 12605028). Population doubling levels (PDLs) were tracked across passages to ensure experimental consistency. Cell viability and total counts were measured using Trypan Blue exclusion (Bio-Rad, Cat# 1450021) and the TC20™ Automated Cell Counter (Bio-Rad).

2.2 Radiation treatment

Cell cultures were irradiated when 80% confluent in Ham's F-12K medium supplemented with 10% fetal bovine serum (FBS). Low-dose rate exposures were performed using ^{60}Cobalt Gammacell 200 irradiator (AECL, Ottawa, Canada) at a dose rate of 0.0005 Gy/s (1.8 Gy/h). High-dose-rate exposures were conducted using a Gammacell 220 irradiator (AECL, Ottawa, Canada) at a dose rate of 0.0157 Gy/s (56.52 Gy/h), **(Figure 8).** A dose of 0.1 Gy was selected as the upper threshold of low-dose radiation, while 1 Gy served as a positive control for comparison with 0.1 Gy.

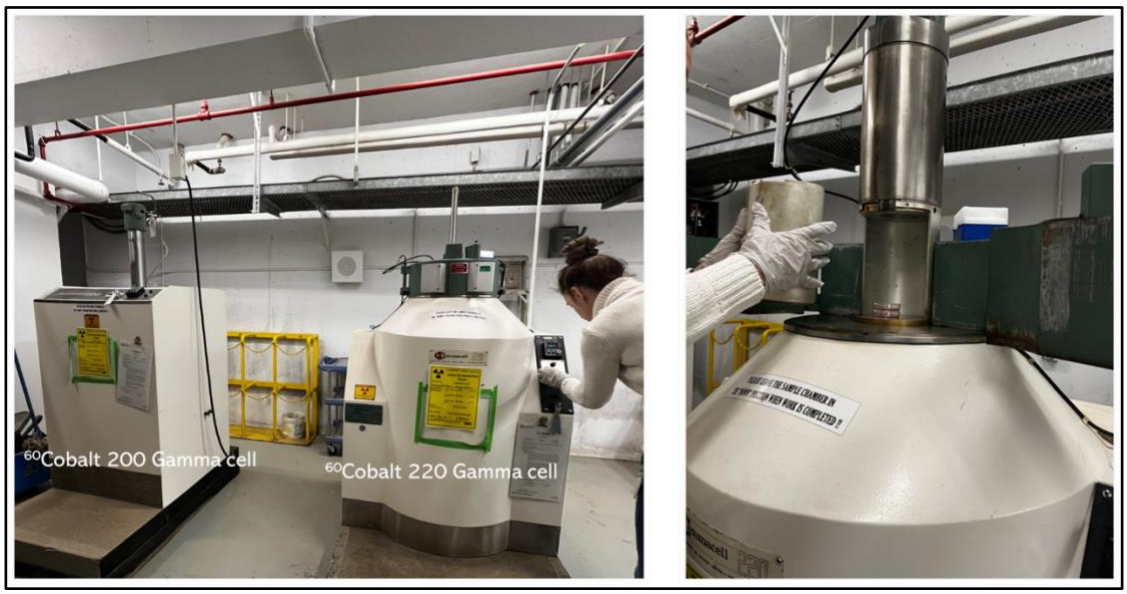

Figure 8) Irradiation setup using 60Cobalt gamma irradiators

(Left) Two ^{60}Cobalt gamma irradiators used for cell culture exposure: Gammacell 200 (low-dose rate, 0.0005 Gy/s) and Gammacell 220 (high-dose rate, 0.0157 Gy/s), both located at Canadian Nuclear Laboratories (CNL), Chalk River, ON, Canada. **(Right)** Close-up of the Gammacell 220 sample chamber during placement of cell culture flasks for high-dose rate γ-radiation exposure.

2.3 γH2AX Immunofluorescence staining and quantification

To assess DNA double-strand break formation following ionizing radiation, γH2AX foci were visualized using immunofluorescence microscopy. HFL1 cells were seeded onto sterile 18 mm round glass coverslips placed in 35 mm culture dishes at a density of 1×10^5 cells per dish. Cells were cultured overnight in Ham's F-12K medium (Gibco™, Cat# 21127030) supplemented with 10% fetal bovine serum (FBS; Gibco™, Cat# A3840302) at 37°C in a humidified incubator containing 5% CO_2.

The next day, cells were irradiated either at low-dose rate (0.0005 Gy/s) or high-dose rate (0.0157 Gy/s) using a Cobalt-60 (^{60}Co) Gammacell irradiator (AECL, Ottawa, Canada). Following exposure, cells were allowed to recover for 30 minutes at 37°C to permit γH2AX focus formation.

Cells were then fixed by immersion in cold 100% methanol at –20°C for 10 minutes. Permeabilization and blocking were performed using BD Perm/Wash Buffer (BD Biosciences, Cat# 560445) for 30 minutes at room temperature. γH2AX foci were stained using Alexa Fluor® 488-conjugated mouse anti-H2AX (phospho-Ser139) monoclonal antibody (clone JBW301; Millipore, Cat# 05-636-AF488) at a dilution of 1:20 in Perm/Wash Buffer for 1 hour in a humidified chamber. After three washes with PBS (5 minutes each), nuclei were counterstained with 300 nM DAPI (4′,6-diamidino-2-phenylindole; Cell Biolabs, Cat# 112002) for 10 minutes at room temperature.

Coverslips were mounted onto glass microscope slides. Images were captured using a Zeiss Axioscope fluorescence microscope equipped with a 40× oil-immersion objective and appropriate filters for DAPI and FITC (Alexa Fluor 488). Exposure time and gain settings

were kept constant across all samples. For each condition, a minimum of 50 randomly selected nuclei were analyzed from at least three independent experiments.

γH2AX foci were quantified using *Fiji* (ImageJ v2.9.0, NIH) with the "Find Maxima" function or the "Analyze Particles" plugin following background subtraction and thresholding. Foci counts per nucleus were averaged, and values were normalized to the non-irradiated control group. Statistical analyses were performed using GraphPad Prism (v10.0.2). One-way ANOVA with Dunnett's multiple comparisons test was used for comparing multiple irradiated conditions to control, while unpaired two-tailed Student's *t*-tests were used for pairwise comparisons. A p-value of < 0.05 was considered statistically significant.

2.4 Western blot analysis

Western blotting was used to assess protein expression levels and phosphorylation status of translational regulators following irradiation. HFL1 cells were first washed twice with cold phosphate-buffered saline (PBS; pH 7.4) and lysed in ice-cold RIPA buffer [50 mM Tris-HCl (pH 7.4), 150 mM NaCl, 1% NP-40, 0.5% sodium deoxycholate, 0.1% SDS], supplemented with protease and phosphatase inhibitor cocktails (Roche, Cat# 11836170001 and 4906837001, respectively). Cell lysates were incubated on ice for 30 minutes with intermittent vortexing, followed by clarification via centrifugation at 16,000 × *g* for 15 minutes at 4 °C. The supernatant was collected, and total protein concentration was determined using the DC™ Protein Assay (Bio-Rad, Cat# 5000112), based on a modified Lowry method. BSA standards were used to generate a standard curve, and absorbance was measured at 750 nm using a microplate reader.

Equal amounts of total protein (20 µg per sample) were mixed with 4× Laemmli sample buffer (Bio-Rad, Cat# 1610747) and heated at 95 °C for 5 minutes. Samples were then loaded onto 4–20% Mini-PROTEAN® TGX™ precast gradient SDS-PAGE gels (Bio-Rad, Cat# 4568083 / 4568085) and electrophoresed at 120 V for approximately 60–90 minutes in 1× Tris-Glycine-SDS running buffer.

Following electrophoresis, proteins were transferred onto 0.2 µm PVDF membranes (Bio-Rad, Cat# 1704156), pre-activated in methanol, using the Trans-Blot® Turbo™ Transfer System (Bio-Rad) with the high molecular weight protocol (25 V, 1.0 A, 3 minutes). Membranes were blocked at room temperature for 1 hour in 5% non-fat dry milk (BioShop, Cat# NON005) dissolved in Tris-buffered saline with 0.1% Tween-20 (TBS-T; MilliporeSigma™, Cat# 524750). Membranes were then incubated overnight at 4 °C with primary antibodies diluted in either 5% BSA or milk/TBS-T according to the manufacturer's recommendations.

The following day, membranes were washed three times with TBS-T (5 minutes each) and incubated with species-appropriate HRP-conjugated secondary antibodies (Bio-Rad or Cell Signaling Technology) diluted 1:5,000 in 5% milk/TBS-T for 1 hour at room temperature. After a second round of three washes with TBS-T, protein bands were detected using Clarity Max™ Enhanced Chemiluminescence (ECL) substrate (Bio-Rad, Cat# 1705062) according to the manufacturer's instructions.

Chemiluminescent signals were captured using the ChemiDoc™ MP Imaging System (Bio-Rad), ensuring non-saturating exposure settings to allow for linear quantification. Band intensities were quantified using Image Lab™ software (Bio-Rad, v6.1) and normalized to housekeeping proteins such as α-tubulin. All antibody details, including

target, host species, dilution, and supplier, are listed in Table 4. Where necessary, membranes were stripped using Restore™ Western Blot Stripping Buffer (Thermo Fisher Scientific, Cat# 21059) and reprobed for additional targets.

Table 4) Antibodies

Antibody	Provider	Catalog #
eIF2α	Cell Signalling	9722
Phospho- eIF2α (Ser 51)	Cell Signalling	9721
4EBP1	Cell Signalling	9452
Phospho-4EBP1(Thr37/46)	Cell Signalling	9459
Phospho-S6 Ribosomal Protein (Ser240/244)	Cell Signalling	2215
S6 Ribosomal Protein	Santa Cruz	Sc-74459
Anti-mouse IgG, HRP-linked Antibody	Cell Signalling	7076P2
Anti-rabbit IgG, HRP-linked Antibody	Cell Signalling	7074P2
Alpha-Tubulin	Santa Cruz	Sc-23948
Alexa Fluor® 488 Mouse anti-H2AX (pS139)	BD Pharmingen™	560445
anti-Puromycin primary antibody clone 12D10	MilliporeSigma™	MABE343

2.5 Puromycin labeling assay:

To assess nascent protein synthesis following ionizing radiation, the puromycin incorporation assay was employed. This method allows for the detection of translation by exploiting the ability of puromycin, a structural analogue of aminoacyl-tRNA, to incorporate into elongating polypeptide chains and terminate translation. The incorporated puromycin can then be detected by an anti-puromycin antibody via Western blotting.

HFL1 cells were seeded into 60-mm culture dishes at a density of approximately 2×10^5 cells per dish and allowed to adhere and proliferate until reaching ~80% confluency. Cells were maintained in Ham's F-12K medium supplemented with 10% fetal bovine serum (FBS) and incubated at 37°C in a humidified atmosphere containing 5% CO_2. Upon reaching the desired confluency, cultures were exposed to ionizing radiation at either low-dose or high-dose rates using a Cobalt-60 (^{60}Co) irradiator as described previously. After irradiation, dishes were returned to the incubator to allow for recovery.

At designated post-irradiation time points (1 hour, 6 hours, and 24 hours), puromycin (MilliporeSigma™, Cat# P8833) was added directly to the culture medium at a final concentration of 10 µg/mL. Cells were incubated at 37°C for 10 minutes to allow incorporation of puromycin into newly synthesized polypeptides. Immediately following incubation, cells were placed on ice to halt metabolic activity, washed twice with cold phosphate-buffered saline (PBS, pH 7.4), and lysed using ice-cold RIPA buffer [50 mM Tris-HCl (pH 7.4), 150 mM NaCl, 1% NP-40, 0.5% sodium deoxycholate, 0.1% SDS], supplemented with protease (Roche, Cat# 04693116001) and phosphatase (Roche, Cat# 04906837001) inhibitor cocktails.

Lysates were clarified by centrifugation at 16,000 × *g* for 15 minutes at 4°C, and the supernatant was collected for Western blot analysis. Total protein concentration was measured using the DC™ Protein Assay (Bio-Rad), and 20 µg of protein per sample was loaded onto 4–20% SDS-PAGE gels (Bio-Rad). The presence of puromycin-labeled polypeptides was detected using a monoclonal anti-puromycin antibody (clone 12D10; Millipore, Cat# MABE343), which specifically recognizes puromycin-conjugated peptides.

To validate assay specificity and provide a positive control for translation inhibition, a subset of cells was pretreated with Torin1 (MilliporeSigma™, Cat# 475991), a selective ATP-competitive inhibitor of mTORC1 kinase activity. Torin1 was added to the culture medium at a final concentration of 250 nM for 3 hours prior to cell harvesting. This treatment inhibits cap-dependent translation and is expected to suppress global puromycin incorporation. In addition, HFL1 cell lysates from samples not treated with puromycin served as negative controls to confirm antibody specificity and rule out non-specific signal. Band intensities representing global puromycin incorporation were quantified using Image Lab™ Software (Bio-Rad), normalized to a loading control (α-tubulin), and compared between irradiated and control conditions. This assay was repeated across at least three independent biological replicates.

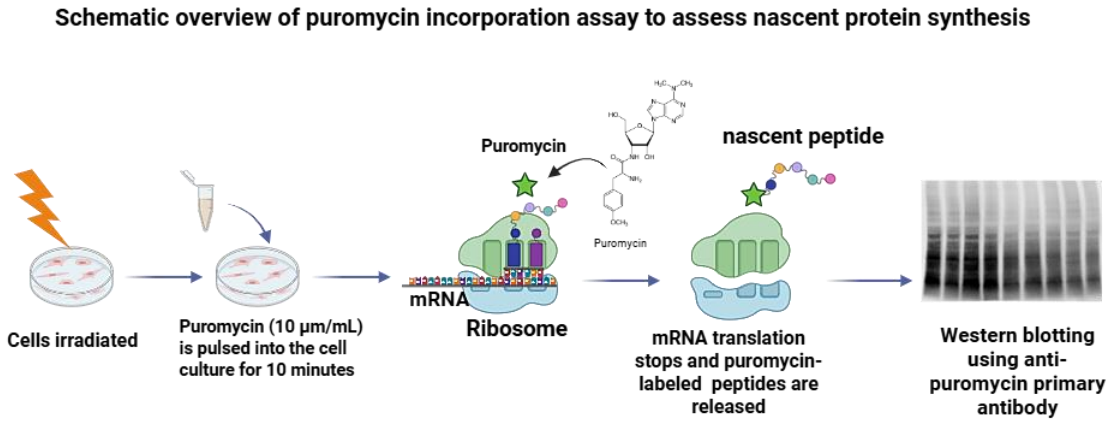

Figure 9) Schematic of the puromycin labeling assay used to assess global protein synthesis.

HFL1 cells are irradiated and allowed to recover, followed by a 10-minute pulse with puromycin (10 µg/mL). Puromycin is incorporated into nascent polypeptides by the ribosome, leading to premature termination of translation. These puromycin-labeled peptides are then released and detected via Western blotting using a monoclonal anti-puromycin antibody.

2.6 Ribosome profiling

Ribosome profiling (Ribo-seq) was used to quantify genome-wide translation by capturing ribosome-protected mRNA fragments (RPFs)/ ribosome footprints, allowing inference of ribosome occupancy across transcripts. The method was adapted from previously published protocols (McGlincy, 2017 [162]; Mito, 2020 [179]) with minor modifications and performed as follows.

2.6.1 Step 1: Ribosome stalling and cell harvest

- HFL1 cells were treated with 100 µg/mL cycloheximide (CHX) directly in culture medium for 1 minute at 37 °C to stall elongating ribosomes on mRNA.

- Following treatment, cells were washed twice with ice-cold PBS supplemented with 100 µg/mL CHX to preserve ribosome-mRNA complexes.
- Cells were harvested by scraping in 1 mL of PBS/CHX and pelleted by brief centrifugation.

2.6.2 Step 2: Cell lysis and clarification

Cell pellets were lysed in a specialized ribosome lysis buffer formulated to preserve ribosome-mRNA interactions and allow efficient release of ribosome-protected fragments. The buffer consisted of the following components:

- 20 mM Tris-HCl (pH 7.4): Maintains physiological pH and provides buffering capacity to stabilize proteins and RNA during lysis.
- 150 mM NaCl: Ensures isotonic conditions, mimicking intracellular ionic strength to preserve native protein-RNA interactions, including those between ribosomes and mRNA.
- 5 mM $MgCl_2$: Magnesium ions are essential for maintaining ribosome structural integrity and stabilizing ribosome-mRNA complexes during and after cell lysis.
- 1 mM DTT: A reducing agent that prevents the formation of disulfide bonds and preserves protein function by maintaining thiol groups in their reduced state.
- 100 µg/mL CHX: Freezes elongating ribosomes on mRNA by inhibiting translocation, thus preserving ribosome positioning and preventing ribosome runoff during the lysis procedure.
- 1% Triton X-100: A non-ionic detergent that solubilizes cell membranes gently without disrupting ribosomes or protein-RNA complexes.

- 25 U/mL Turbo DNase I (Invitrogen): Degrades genomic DNA released during lysis to reduce viscosity and facilitate downstream RNA purification and handling.

Cell lysis was carried out by mechanical shearing: suspensions were passed through a 25-gauge needle attached to a 1 mL syringe ten times on ice. This method ensures thorough disruption of cellular membranes and efficient homogenization while minimizing heat and mechanical stress, which could otherwise destabilize ribosome-mRNA complexes.

Lysates were then clarified by centrifugation at 20,000 × g for 10 minutes at 4 °C to remove insoluble cellular debris, organelles, and nuclei. The resulting supernatant, enriched in intact ribosomes and associated RNA, was used for downstream RNA extraction and ribosome footprinting.

2.6.3 Step 3: Total RNA isolation

A portion of the clarified lysate was reserved for total mRNA extraction, which was carried out using the RNA Clean & Concentrator Kit (Zymo Research, Cat# R1017), following the manufacturer's protocol. The quality of purified total RNA were assessed using the Agilent Bioanalyzer and then submitted for bulk RNA sequencing to determine transcript abundance. These transcriptome data were later integrated with RPF data to calculate translational efficiency (TE).

2.6.4 Step 4: RNA quantification using RiboGreen assay

Following RNA purification (either total RNA or RPFs), RNA concentration was quantified using the Quant-iT™ RiboGreen RNA Assay Kit (Thermo Fisher Scientific, Cat# R11490). This fluorescence-based assay is highly sensitive and selective for RNA over DNA, making it suitable for accurate quantification of low-input RNA such as RPFs. Briefly, RNA samples were diluted in TE buffer (10 mM Tris-HCl, 1 mM EDTA, pH 7.5).

A standard curve was generated using RNA standards provided with the kit, typically in the range of 1-200 ng/mL. 100 µL of each sample or standard was mixed with 100 µL of RiboGreen working solution (diluted 1:200 from stock) in black, flat-bottom 96-well plates. Fluorescence was measured using a microplate reader (excitation: 480 nm, emission: 520 nm). Sample concentrations were calculated from the standard curve and used to normalize RNA input for RNase I digestion and downstream sequencing library preparation. This step was necessary for ensuring accurate and consistent RNA input (e.g., 30 µg for RPF digestion) across all samples and conditions.

2.6.5 Step 5: RNase I digestion for RPF generation (extended with polysome profiling optimization)

To RPFs, 30 µg of RNA from the clarified lysate was diluted in ribonuclease digestion buffer containing 20 mM Tris-HCl (pH 7.4), 150 mM NaCl, 5 mM $MgCl_2$, 1 mM DTT, and 100 µg/mL CHX. Digestion was performed by adding RNase I (0.5 U/µg RNA) (Gibco™, Cat# AM2295), followed by incubation at room temperature for 45 minutes with gentle shaking to ensure uniform enzymatic activity.

To stop the reaction, 10 µL of SUPERase•In RNase inhibitor (20 U/µL) (Gibco™, Cat# AM2696) was added.

2.6.5.1 Optimization of RNase I digestion conditions:

Optimization of RNase I digestion conditions was first performed using polysome profiling. Specifically, I assessed polysome integrity and ribosome dissociation across a gradient of RNase I concentrations to determine the optimal digestion conditions that yielded monosome-enriched fractions without over-digesting ribosomes or degrading protected mRNA fragments. This step ensured that subsequent ribosome profiling

experiments captured high-quality, monosome-associated RPFs while minimizing artifacts from incomplete digestion or ribosome disassembly. These optimized conditions were then applied to all ribosome profiling samples to generate consistent and reproducible RPF libraries.

2.6.5.2 Monosome peak interpretation for RNase I Optimization (Figure 10)

Pre-digestion (Untreated) Profile:

In untreated lysates, the polysome profile showed multiple distinct peaks corresponding to 80S monosomes, disomes, and polysomes (3 or more ribosomes per mRNA). The polysome region is broader and of higher absorbance, indicating active translation with multiple ribosomes engaged per mRNA.

Post-digestion (RNase I-treated) Profile:

Following RNase I treatment, it was expected ribosomes to be released from polysomes and protect only the short mRNA segments they occupy (~28–30 nt).

A successful digestion was indicated by the collapse of polysome peaks and sharp enrichment of the monosome (80S) peak with a corresponding reduction in polysomes.

If the monosome peak was weak or polysomes remained, it indicated under-digestion.

If the monosome peak decreased or shifted significantly, or total absorbance dropped, it suggested over-digestion or ribosome disassembly.

Final conditions selected:

The RNase I concentration of 0.5 U/μg RNA and a digestion time for 45 minutes were selected because they produced:

- A clear, sharp monosome peak
- A marked reduction in polysomes

- Minimal loss of total signal, indicating ribosome integrity was preserved

These optimized digestion conditions ensured that RPFs could be reliably isolated while avoiding artifacts from partial or excessive digestion.

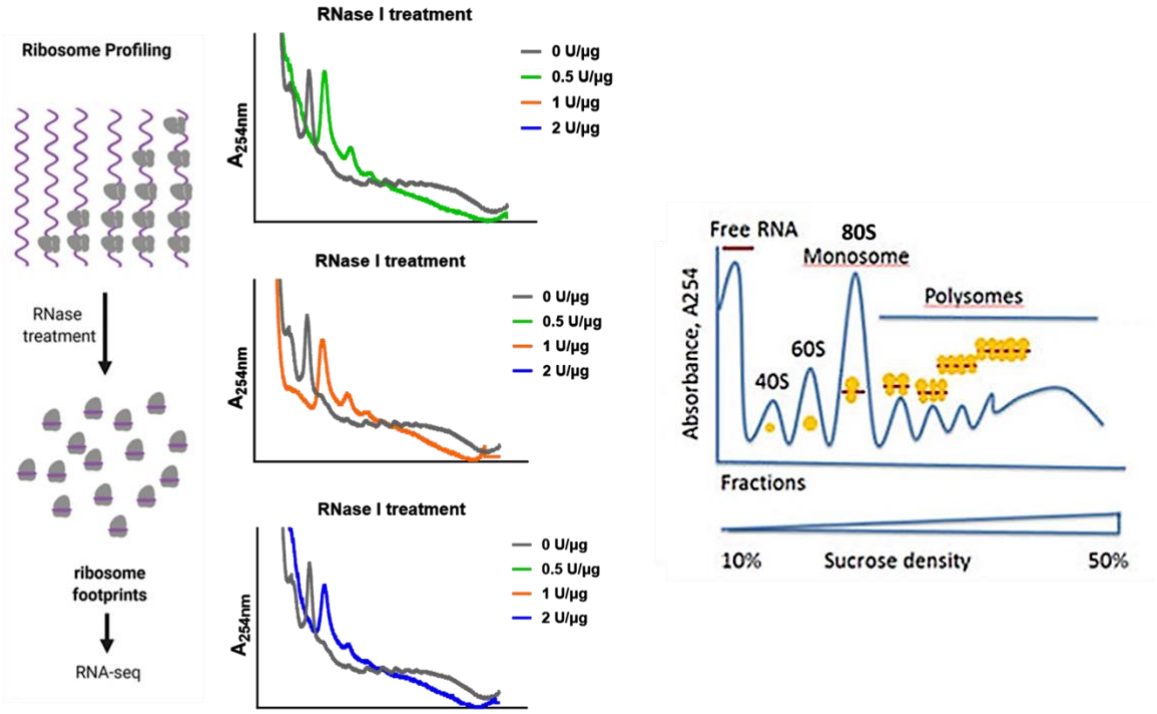

Figure 10) Optimization of RNase I Digestion for Ribosome Profiling Using Polysome Profiling

Polysome profiling was used to empirically optimize RNase I digestion conditions prior to ribosome profiling. (Left) Schematic representation of the ribosome profiling workflow. (Middle) Polysome profiles show the effect of increasing RNase I digestion, with optimal conditions yielding a sharp 80S monosome peak and reduced polysome signal, indicating successful conversion of polysomes into monosomes. (Right) Reference sucrose gradient profile illustrates the typical position of ribosomal subunits, monosomes (80S), and polysomes. This approach ensured efficient footprint generation and minimized over-digestion or ribosome disassembly artifacts.

2.6.6 Step 6: Ribosome footprint purification

The digested lysate was passed through S-400 spin columns (GE Healthcare, Cat# 27514001) to enrich for ribosome-protected mRNA fragments. RNA was further purified using the Zymo RNA Clean & Concentrator-5 Kit (Cat# R1015).

2.6.7 Step 7: Size selection of RPFs

To isolate RPFs, purified RNA was separated by electrophoresis on a 15% TBE-Urea denaturing polyacrylamide gel (Gibco™, Cat# EC68852BOX). This gel type provides high resolution for short RNA fragments, which corresponds to the expected size of RPFs generated by RNase I digestion.

Urea acts as a strong denaturant, disrupting secondary structures in RNA. This ensures that RNA migrates strictly according to size, not shape or structure. It allows for precise resolution and reproducible recovery of small RNA fragments, which is important when working with highly size-specific products like RPFs. To accurately isolate RPFs, synthetic RNA oligonucleotides were used as size markers in **Table 5**. Gel slices corresponding to the 17-34 nt region were carefully excised using a sterile scalpel under low-intensity UV illumination or SYBR® Gold staining. RNA was extracted from the gel using the Zymo Small-RNA PAGE Recovery Kit (Cat# R1070), which enables efficient recovery of short RNA fragments from polyacrylamide matrices. Purified RPFs were eluted in RNase-free water and quantified using the Agilent Bioanalyzer.

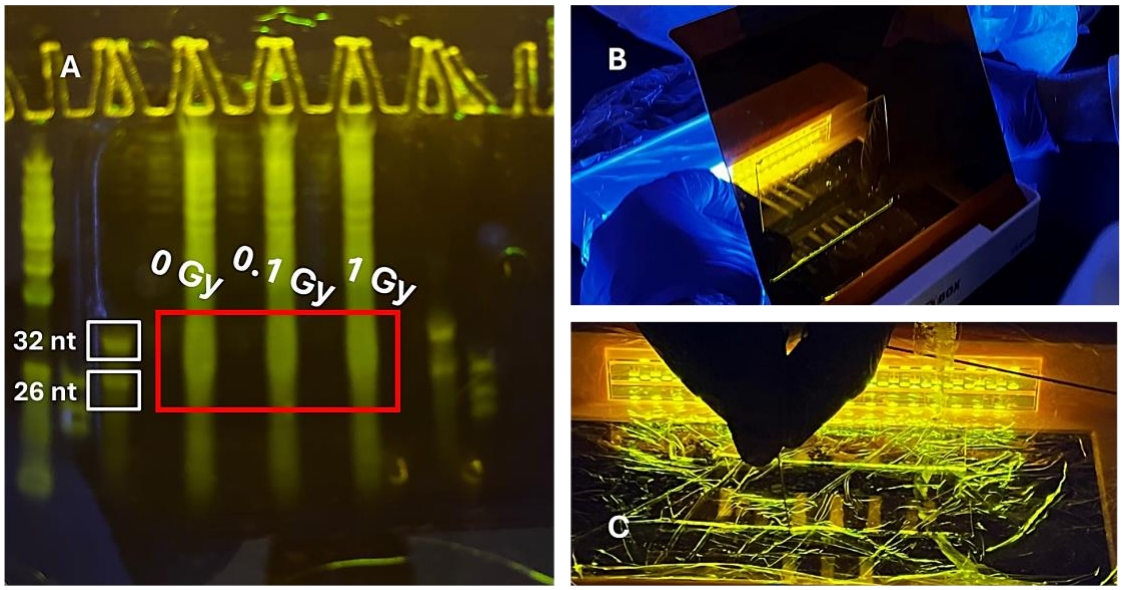

Figure 11) Gel-based size selection of RPFs

A) Representative 15% TBE-Urea polyacrylamide gel showing RPFs extracted from HFL1 cells exposed to 0, 0.1, or 1 Gy γ-radiation. RNA samples were separated based on size, and footprints between 26-32 nucleotides (nt) were visualized using SYBR® Gold staining. The red box indicates the excised region containing the desired RPFs. **B)** UV transillumination of the gel during visualization using a protective shielded viewer and personal protective equipment. **C)** Manual excision of the footprint band using a sterile scalpel under low-intensity UV illumination. Bands in the 26–32 nt range were excised for downstream RNA extraction and ribosome profiling library preparation.

Table 5) Oligonucleotide size markers used for RPF size selection

Primer	Oligo sequence
Upper size marker, NI-800	5-AUGUACACUAGGGAUAACAGGGUAAUCAACGCGA/3Phos/
Lower size marker, NI-801	5-AUGUUAGGGAUAACAGGGUAAUGCGA/3Phos/

2.6.8 Step 8: Sequencing and analysis

Final RPF were submitted for small RNA sequencing, following ribosomal RNA (rRNA) depletion.

- It was noted that RNase I digestion yielded RPFs slightly longer than the canonical ~28-nt footprints commonly observed, consistent with previous reports [180]. Due to this length variability, codon-level resolution and P-site inference were not feasible.

Nevertheless, transcript-level ribosome occupancy was reliably quantified by mapping reads to transcripts using HTSeq-count to generate count matrices for downstream analysis of translation efficiency (TE).

2.7 Computational analysis of ribosome profiling and RNA-seq data

Pre-processing and quality control: Raw RPF reads (single-end, 75 bp) were first assessed with FastQC v0.12.1. Adapter sequences were trimmed, and low-quality bases ($Q < 20$) were removed using Cutadapt v4.5.

rRNA/tRNA depletion in silico: To reduce contamination and eliminate abundant non-coding contaminants, trimmed reads were aligned to a custom Bowtie2 index containing human rRNA and tRNA sequences (GenBank release 260) using Bowtie2 v2.5.2. Unaligned reads, representing mRNA footprints, were retained for downstream mapping.

Genome and transcriptome alignment: Remaining reads were aligned to the human reference genome GRCh38 (hg38) with HISAT2 v2.2.1. Alignments with mapping quality <10 were discarded with SAMtools v1.17.

PCR duplicate removal: Unique molecular identifiers (UMIs, 8 bp) embedded at the 5′ end of each read were extracted, and PCR duplicates were collapsed using UMI-tools v1.1.4. This step prevents artificial inflation of ribosome occupancy estimates.

Quantification of ribosome occupancy and mRNA abundance: Transcript-level read counts were generated using HTSeq-count v2.0.2 in intersection-strict mode with GENCODE v43 gene annotations. These count matrices served as input for translational efficiency (TE) and differential expression analyses (Section 2.8).

Table 6) Computational pipeline for ribosome profiling and RNA-seq data analysis

Tool	Version	Purpose
FastQC	v0.12.1	Quality control of raw FASTQ reads (base quality, GC content, adapter content)
Cutadapt	v4.5	Adapter trimming and quality filtering (Q < 20)
Bowtie2	v2.5.2	Alignment to custom rRNA/tRNA index for contamination removal
HISAT2	v2.2.1	Spliced alignment to human genome (GRCh38/hg38)
SAMtools	v1.17	Filtering alignments with low mapping quality (<10)
UMI-tools	v1.1.4	PCR duplicate removal using 5′-end UMIs
HTSeq-count	v2.0.2	Gene-level quantification using intersection-strict mode
GENCODE	v43	Reference annotation for human transcripts

2.8 Gene expression and translational efficiency analysis (Bioinformatic)

Differential gene-expression analysis:

To identify transcripts that changed at the mRNA or RPF level after irradiation (0 Gy, 0.1 Gy, 1 Gy), normalized counts were analyzed with the limma package in R. Two significance criteria were used:

- Moderate cutoff: $|\log_2 FC| \geq 1.2$ and $p < 0.05$
- Stringent cutoff: $|\log_2 FC| \geq 1.5$ and $p < 0.02$

These thresholds allow to balance sensitivity and specificity, as the subtle transcriptional responses to low-dose IR would likely be missed under stricter corrections.

Translational-efficiency (TE) analysis:

Changes in TE were further evaluated with anota2seq v1.2.2, which jointly models RPF and mRNA counts to distinguish translational regulation from transcriptional changes and buffering effects. The anota2seq function was run with the following filtering parameters:

MinEff = $\log_2$ (1.2)

MaxSlopeTranslation = 2

MinSlopeTranslation = -1

MaxSlopeBuffering = 1

MinSlopeBuffering = -2

DeltaPT = log2(1.2)

DeltaTP = log2(1.2)

DeltaP = log2(1.2)

DeltaT = log2(1.2)

MaxP = 0.05.

Given the mild nature of the treatment and the correspondingly small expression changes observed, false discovery rate (FDR) correction was not applied, as it would have been overly stringent and likely excluded biologically relevant but subtle effects.

Table 7) Bioinformatic pipeline

Tool / Package	Version	Purpose
DESeq2	v1.40.2	Normalization of RPF and mRNA count data using size factors
limma	Latest stable CRAN version (e.g., v3.56.2)	Differential expression analysis of mRNA and RPFs
anota2seq	v1.2.2	Joint modeling of RPF and mRNA to detect changes in translational efficiency, buffering, or transcription
R	≥ v4.3.0	Statistical environment for all analyses
GENCODE	v43	Reference gene annotation used for count assignment

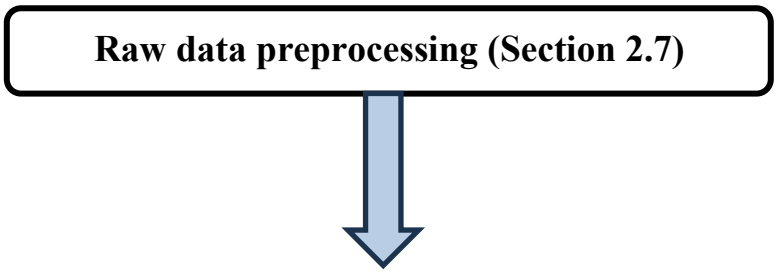

Steps	Tool	Purpose
1. Quality check	FastQC	Make sure reads aren't garbage (check quality scores, GC content, etc.)
2. Adapter trimming	Cutadapt	Remove adapter contamination and low-quality bases
3. Remove junk reads	Bowtie2	Align to rRNA and tRNA — discard anything that matches
4. Map to human genome	HISAT2	Map remaining reads to genome/transcriptome
5. Remove PCR duplicates	UMI-tools	Use UMIs to collapse artificially duplicated reads
6. Quantify gene expression	HTSeq-count	Count how many reads map to each gene (for RPF and mRNA samples separately)

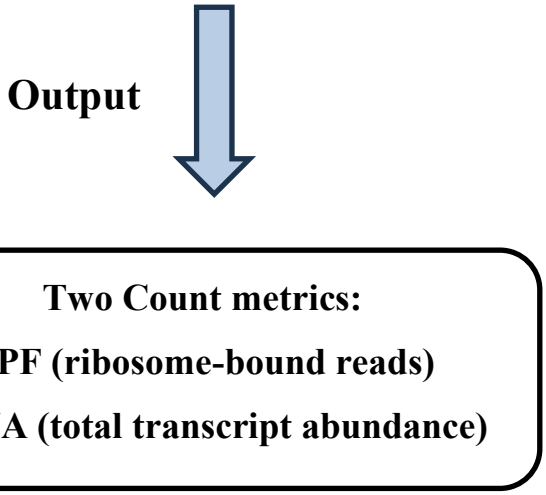

Figure 12) Computational pipeline for ribosome profiling and RNA-seq data analysis flowchart

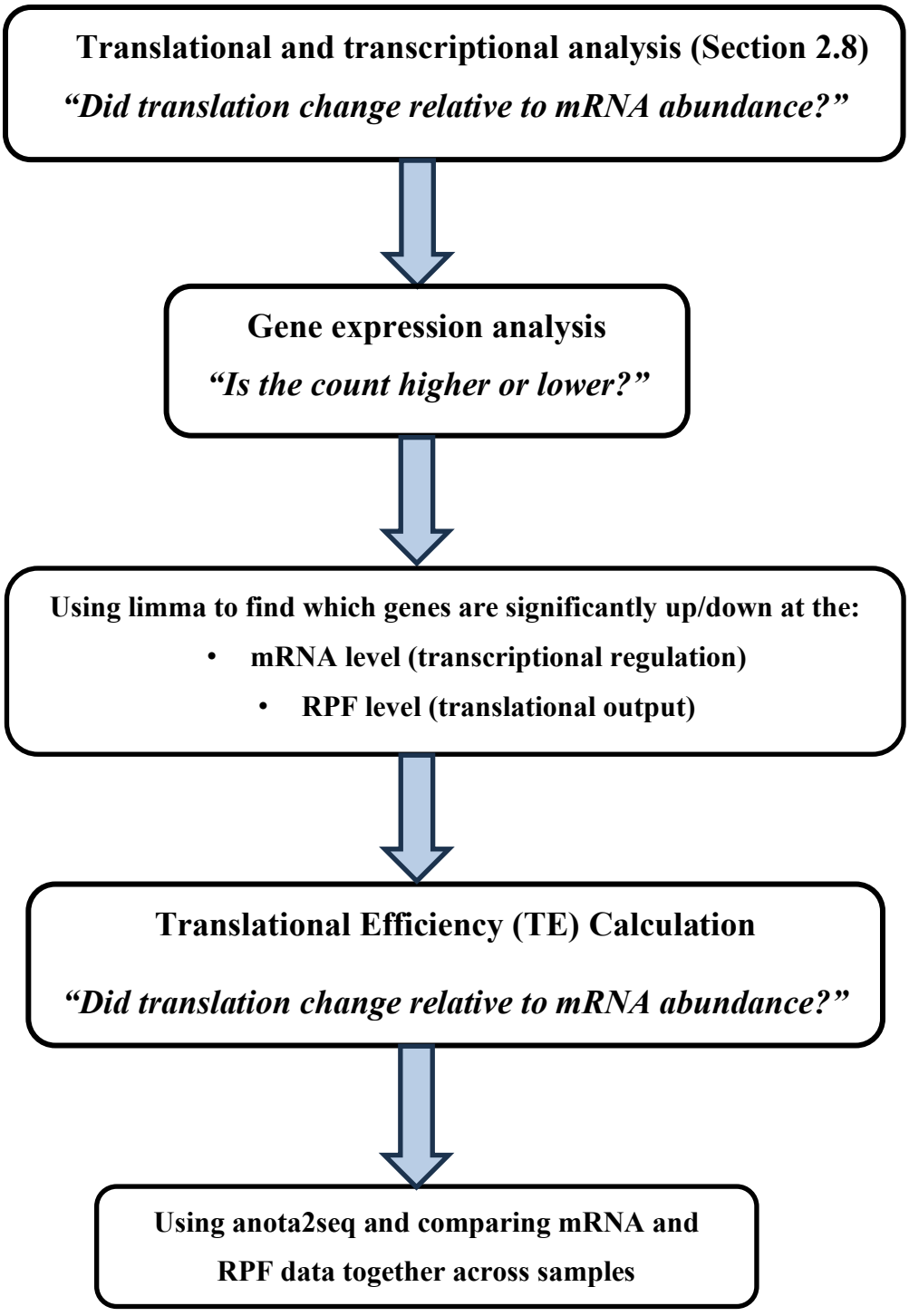

Figure 13) Bioinformatic pipeline flowchart

2.9 Polysome Profiling

Polysome profiling was performed to assess ribosome occupancy and global translational activity, following the protocol described by Gandin et al., 2014 [180], with some optimization.

Linear 10–50% (w/v) sucrose gradients were prepared in advance by sequentially layering increasing concentrations of sucrose in Beckman ultracentrifuge tubes, followed by diffusion overnight at 4 °C to ensure the formation of a smooth, continuous gradient. These gradients provide a medium for separating ribosomal subunits, monosomes, and polysomes based on their sedimentation properties under ultracentrifugation.

Prior to cell lysis, cells at ~80–90% confluency in 15 cm petri dishes were treated with cycloheximide (CHX; 100 µg/mL) for 7 minutes at 37 °C to arrest translation elongation and stabilize ribosome-mRNA complexes on transcripts. Following treatment, cells were rapidly washed with ice-cold PBS containing CHX to prevent ribosome runoff and then scraped into ice-cold PBS with CHX for collection.

Cells were pelleted by centrifugation at 300 × g for 5 minutes at 4 °C, and the resulting cell pellets were resuspended in 162 µL of hypotonic lysis buffer (5 mM Tris-HCl, pH 7.5; 2.5 mM $MgCl_2$; 1.5 mM KCl) supplemented with RNase inhibitor (Promega, Cat# N2511), protease inhibitor cocktail (Roche or equivalent), 1 mM DTT, and 100 µg/mL CHX. The hypotonic buffer gently disrupts the plasma membrane while preserving ribosome integrity.

Lysis was performed by incubating the suspension on ice for 10 minutes, followed by centrifugation at 10,000 × g for 10 minutes at 4 °C to remove nuclei and cellular debris. The concentration and quality of RNAs were measured by nanodrop.

The same amount of supernatant, containing RNA material, was carefully layered onto the pre-formed sucrose gradients and subjected to ultracentrifugation at 36,000 rpm for 2 hours at 4 °C using an SW41Ti rotor (Beckman Coulter). This step separates ribosomal subunits, monosomes (80S), and actively translating polysomes.

After centrifugation, gradients were placed into a Brandel Fraction Collector System equipped with an A254 UV detector, which records the absorbance of each gradient fraction, enabling visualization of the ribosome profile. Fractions were collected manually or automatically for further RNA or protein analysis, allowing investigation of translational changes and ribosome distribution under different treatment conditions.

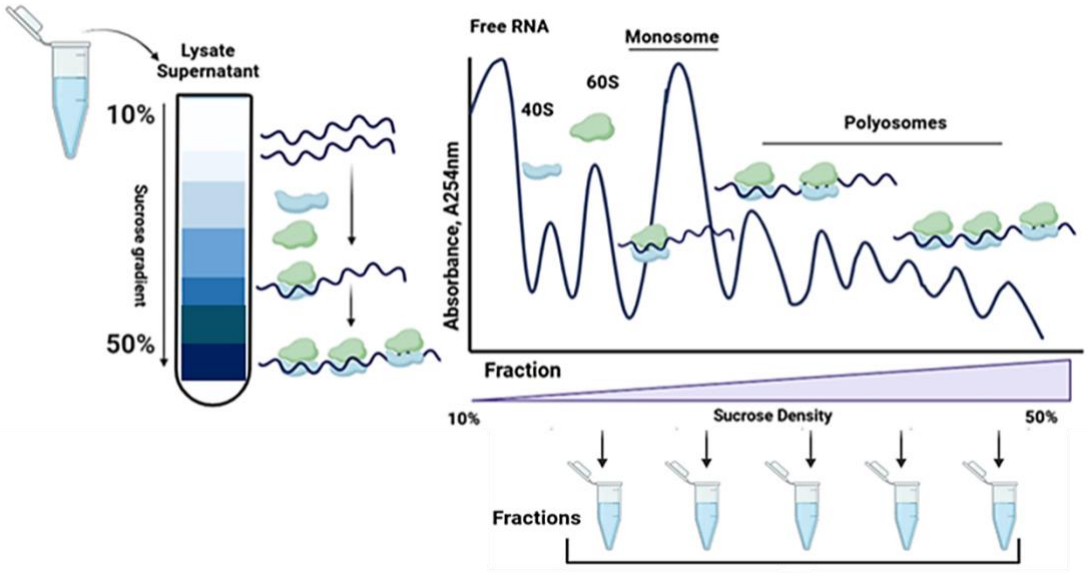

Figure 14) Polysome profiling using sucrose density gradient centrifugation.

Cell lysates are layered onto pre-formed 10–50% sucrose gradients and subjected to ultracentrifugation. During centrifugation, ribosome-associated complexes sediment according to size and mass, separating into distinct fractions: free RNA, ribosomal subunits (40S, 60S), monosomes (80S), and polysomes (multiple ribosomes bound to mRNA). Following centrifugation, the gradient is fractionated and absorbance at 254 nm is recorded to visualize the distribution of ribosomes across the gradient. Heavier complexes, such as polysomes, migrate further into the gradient. Collected fractions can be used for downstream RNA or protein analysis.

2.10 RNA purification and qPCR

RNA was isolated from individual sucrose gradient fractions immediately after fractionation to preserve RNA integrity. For each fraction, TRIzol reagent (Invitrogen) was added at a ratio of 3:1 (TRIzol: sample volume), and total RNA was extracted according to the manufacturer's protocol. Briefly, fractions were mixed thoroughly with TRIzol, followed by phase separation with chloroform. The aqueous phase was transferred to a new tube, and RNA was precipitated using isopropanol, washed with 75% ethanol, and resuspended in nuclease-free water.

For total RNA extracted from unfractionated samples, the RNeasy Mini Kit (QIAGEN, Cat# 74104) was used following the manufacturer's spin column protocol, including on-column DNase digestion to remove any contaminating genomic DNA. The concentration and purity of all RNA samples were assessed using a Nanodrop spectrophotometer (Thermo Scientific). Complementary DNA (cDNA) was synthesized from 500 ng to 1 µg of total RNA using the iScript™ Advanced cDNA Synthesis Kit (Bio-Rad) in a 20 µL reaction volume. The reverse transcription reaction was carried out according to the manufacturer's instructions, which includes a genomic DNA removal step and a mix of oligo(dT) and random hexamer primers to ensure efficient and unbiased reverse transcription. Equal volumes of synthesized cDNA were used for quantitative PCR (qPCR) reactions using SsoAdvanced™ Universal SYBR® Green Supermix (Bio-Rad, Cat#1725271) on a CFX96 Real-Time PCR Detection System (Bio-Rad).

The PCR conditions were as follows:

- Initial denaturation at 95 °C for 5 minutes,

- Followed by 40 cycles of:
    - 95 °C for 10 seconds
    - 60 °C for 30 seconds
    - 65 °C for 5 seconds

Cycle threshold (Ct) values were calculated using CFX Maestro. Relative mRNA abundance was calculated using the ΔΔCt method. For normalization of gradient-fractionated RNA, exogenous luciferase mRNA was spiked into each fraction prior to extraction and used as an internal control to account for variability in RNA recovery and reverse transcription efficiency. For non-fractionated total RNA samples, GAPDH was used as a reference housekeeping gene.

Primer sequences used for qPCR amplification are listed in **Table 8.**

Table 8) PCR primers

Primers for RT-qPCR	**Forward**	**Reverse**
RAB33B	CGA TAG GGG TGG ATT TCC GAG	TGTCCCATAGCTGGATCTTGA
Luciferase RNA	GCCAGTCAAGTAACAACCGC	TTGGACTTTCCGCCCTTCTT
GAPDH	AGCCGCATCTTCTTTTGCGT	CCCAATACGACCAAATCCGTTG

2.11 Statistical analysis

All statistical analyses and data visualizations were conducted using GraphPad Prism version 10.0.2 (GraphPad Software) and RStudio (R version 4.2.1). Data are presented as mean ± standard error of the mean (SEM), unless otherwise indicated in figure legends. For comparisons involving more than two groups, a one-way analysis of variance (ANOVA) was performed, followed by Dunnett's multiple comparisons test to compare each experimental group to the designated control. For direct pairwise comparisons between two groups, a two-tailed unpaired Student's *t*-test was used.

Prior to conducting parametric tests, normality and variance homogeneity were assessed to ensure test assumptions were met. A P-value < 0.05 was considered statistically significant and denoted as follows: $P < 0.05$ (*), $P < 0.01$ (**), $P < 0.001$ (***), and $P < 0.0001$ (****). Unless otherwise specified, all experiments were independently repeated at least three times ($n \geq 3$) using biological replicates.

Table 9) Material/ Reagent list

Material / Reagents	Source/ Vendor	Catalog #
Ham's F-12K (Keigan's) medium	Gibco™	21127030
Fetal Bovine Serum	Gibco™	A3840302
TrypLE™ Express Enzyme	Gibco™	12605028
Trypan Blue Stain	Bio-Rad	1450021
Cover glass	Corning™	285018, #1.5 thickness
Perm/Wash Buffer	BD Biosciences	560445
4′,6-diamidino-2-phenylindole (DAPI)	Cell biolabs	112002
puromycin	Gibco™	A1113803
cOmplete™ Protease Inhibitor Cocktail	Roch	04693116001
RIPA	Abcam	ab288006
phosphatase inhibitors (PhosSTOP™)	Roch	04906837001
Torin1	MilliporeSigma™	47599
4–20% Mini-PROTEAN TGX Stain-Free Gels	Bio-Rad	4568083 / 4568085
Trans-Blot Turbo Mini 0.2 µm PVDF Membranes	Bio-Rad	1704156
TBST (Tris-buffered saline with Tween-20)	MilliporeSigma™	524750
Clarity Max Western ECL Substrate	Bio-Rad	1705062
PBS (Phosphate-buffered saline)	Gibco™	10010049
DC Protein Assay Package	Bio-Rad	5000116
RNase inhibitor (RNasin 40 units/µl)	Promega	N2511
MgCl2 (1 M)	Gibco™	AM9530G
NaCl (5 M), RNase-free	Gibco™	AM9760G
Tris (1 M), pH 8.0, RNase-free	Gibco™	AM9855G
TURBO™ DNase (2 U/µL)	Gibco™	AM2238
UltraPure™ 1 M Tris-HCI Buffer, pH 7.5	Gibco™	15567027
TRITON® X-100 Detergent, Molecular Biology Grade	Sigma	CAS 9002-93-1
Cycloheximide solution	Sigma	C4859-1ML
Cycloheximide powder	Gibco™	AAJ6690103
DL-Dithiothreitol solution	Sigma	43816-10ML
Dimethyl sulfoxide	Sigma	D2650-5X5ML
SUPERase•In™ RNase Inhibitor (20 U/µL)	Gibco™	AM2696
Amersham MicroSpin S-400 HR Columns (50 columns)	Cytiva	27514001
Ambion™ RNase I, cloned, 100 U/µL	Gibco™	AM2271
RNase T1 (1000 U/µL)	Gibco™	EN0542
Novex TBE-Urea Gels, 15%, 12-well	Gibco™	EC68852BOX
Ultra Low Range DNA Ladder	Gibco™	10597012
SYBR™ Gold Nucleic Acid Gel Stain (10,000X Concentrate in DMSO)	Gibco™	S11494
Novex™ TBE-Urea Sample Buffer (2X)	Gibco™	LC6876
RNase-free Microfuge Tubes	Gibco™	AM12450
microRNA Marker	New England Biolabs	N2102S
ZR small-RNA PAGE Recovery Kit	Zymo Research	R1070
RNA Clean & Concentrator-5 (DNase not Included)	Zymo Research	R1015
RNA Clean & Concentrator-25	Zymo Research	R1017
Quant-it™ RiboGreen RNA Assay Kit	Gibco™	R11490
SDS Solution, Molecular Biology Grade (10% w/v)	Gibco™	V6551
Nuclease-Free Water (not DEPC-Treated)	Gibco™	AM9930
SsoAdavanced Universal Sybro green Supermix	Bio-Rad	1725271
iScript Adv cDNA kit for RT-qPCR	Bio-Rad	1725037
GlycoBlue™ Coprecipitant	Invitrogen	AM9516
TRIzol™ Reagent	Invitrogen	15596018
Luciferase Control RNA	Promega	L4561
RNeasy kits for RNA purification	QIAGEN	74104
10x Tris/Glycine/SDS Running buffer	Bio-Rad	1610732
Precision Plus Protein Dual Color Standards	Bio-Rad	1610374

Chapter 3: Results

3.1 Low-dose IR induces measurable DNA damage responses in HFL1 cells

The cellular responses of cells exposed to low-dose IR can be subtle. To confirm that the HFL1 cell model used in this study showed measurable effects from ^{60}Cobalt γ-irradiation performed at the Canadian Nuclear Laboratories, its sensitivity was quantified by measuring phosphorylation of histone protein H2AX at serine 139 residue (also known as γH2AX) [60]. γH2AX acts as a signaling hub for DNA repair machinery, recruiting repair proteins to form *foci* in the regions of double-stranded breaks [61]. These phosphorylated *foci* can be visualized and quantified using the γH2AX immunofluorescent assay.

To determine the extent of radiation-induced DNA damage, γH2AX foci formation was examined 30 minutes post-irradiation, a time point corresponding to the reported peak of foci formation [181]. A clear dose-dependent increase in *foci* was observed under both low and high-dose rate exposure **(Fig. 15 A-E)**, confirming the responsiveness of the cell model.

Based on these results, and to ensure consistency across all subsequent experiments, 0.1 Gy as the representative low-dose and 1 Gy as the high-dose condition was selected. Both doses were delivered at a high dose rate of 0.0157 Gy/s.

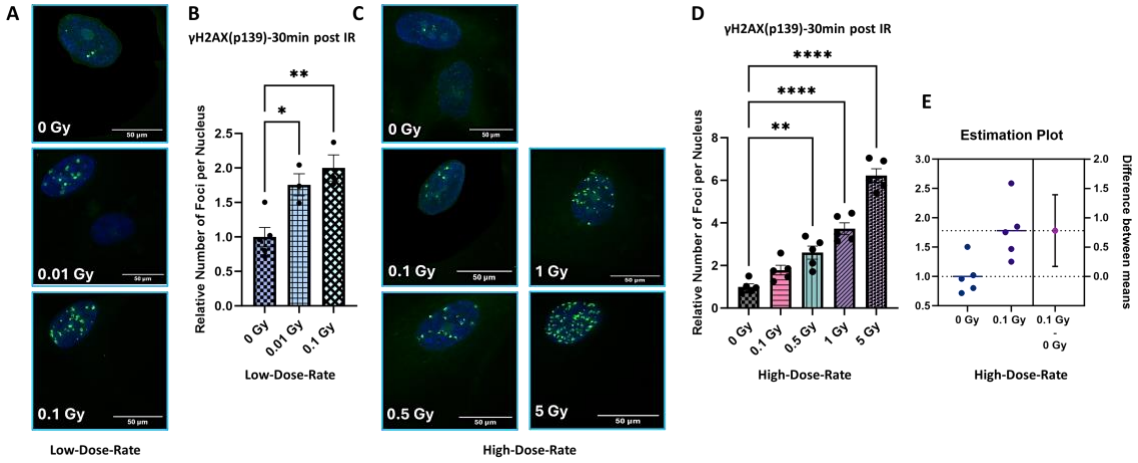

Figure 15) Detection and quantification of stress after exposure to γ-rays

A, B) Representative immunofluorescence images showing γH2AX *foci* (green) in HFL1 cells exposed to (A) low-dose-rate γ-rays (dose rate: 0.0005Gy/s) with accumulated absorbed doses of 0.01 Gy and 0.1 Gy and (B) high-dose-rate γ-rays (dose rate: 0.0157Gy/s) with cumulative absorbed doses of 0.1, 0.5, 1, and 5 Gy. Nuclei are counterstained with DAPI (blue). C, D) Quantification of γH2AX *foci* per nucleus following IR exposure. Results were normalized against non-irradiated controls. Bar graphs represent the mean ± standard error of the mean (SEM) from at least three independent experiments (n≥3), scoring a minimum of 50 nuclei per dose. Statistical significance was determined using one-way ANOVA with Dunnett's multiple comparisons test. Significance levels: *p <0.05, ***p < 0.001, ****p < 0.0001. E) Estimation plot was used to show the statistical significance comparing γH2AX *foci* formation between untreated cells (0 Gy) and cells expos 0.1 Gy of high-dose-rate IR. Statistical significance was assessed using an unpaired two-tailed t-test.

3.2 Low-dose IR exposure does not significantly alter global protein synthesis

Protein synthesis is a fundamental yet energetically expensive and tightly regulated cellular process [123]. Under stress conditions, cells must efficiently reprogram mRNA translation to conserve energy, prevent the accumulation of faulty proteins, and promote the repair of stress-induced damage. These stress responses impact global protein synthesis whilst adjusting the selective translation of specific mRNAs [124].

3.2.1 Protein synthesis rate

To measure the global protein synthesis, puromycin incorporation assay (puromycin labeling method), originally developed by Schmidt *et al*. was used [182]. Puromycin is an antibiotic produced by *Streptomyces alboniger* that mimics the structure of aminoacyl tRNAs [183-185]. At low concentrations, puromycin incorporation serves as a direct proxy for measuring ongoing translation [182].

In this assay, cell cultures were pulsed with puromycin (10 μg/mL) for 10 minutes at short-term (1 hour), transient (6 hours), and longer-term (24 hours) time points post-irradiation. Puromycin-labeled polypeptides were detected by immunoblotting using the monoclonal anti-puromycin antibody (clone 12D10). Torin1, a known inhibitor of mTORC1 activity and mRNA translation, served as a positive control for translation shutdown and validated the assay's sensitivity. To confirm the specificity of puromycin detection, HFL1 cell lysate samples without puromycin treatment and radiation exposure were used as negative controls. The intensity of each lane was compared to the control (0 Gy). No substantial changes in puromycin signal intensity at any post-irradiation time point compared to the 0 Gy control, suggesting that low-dose γ-radiation does not significantly impact global translation rates **(Fig. 16 A, B).**

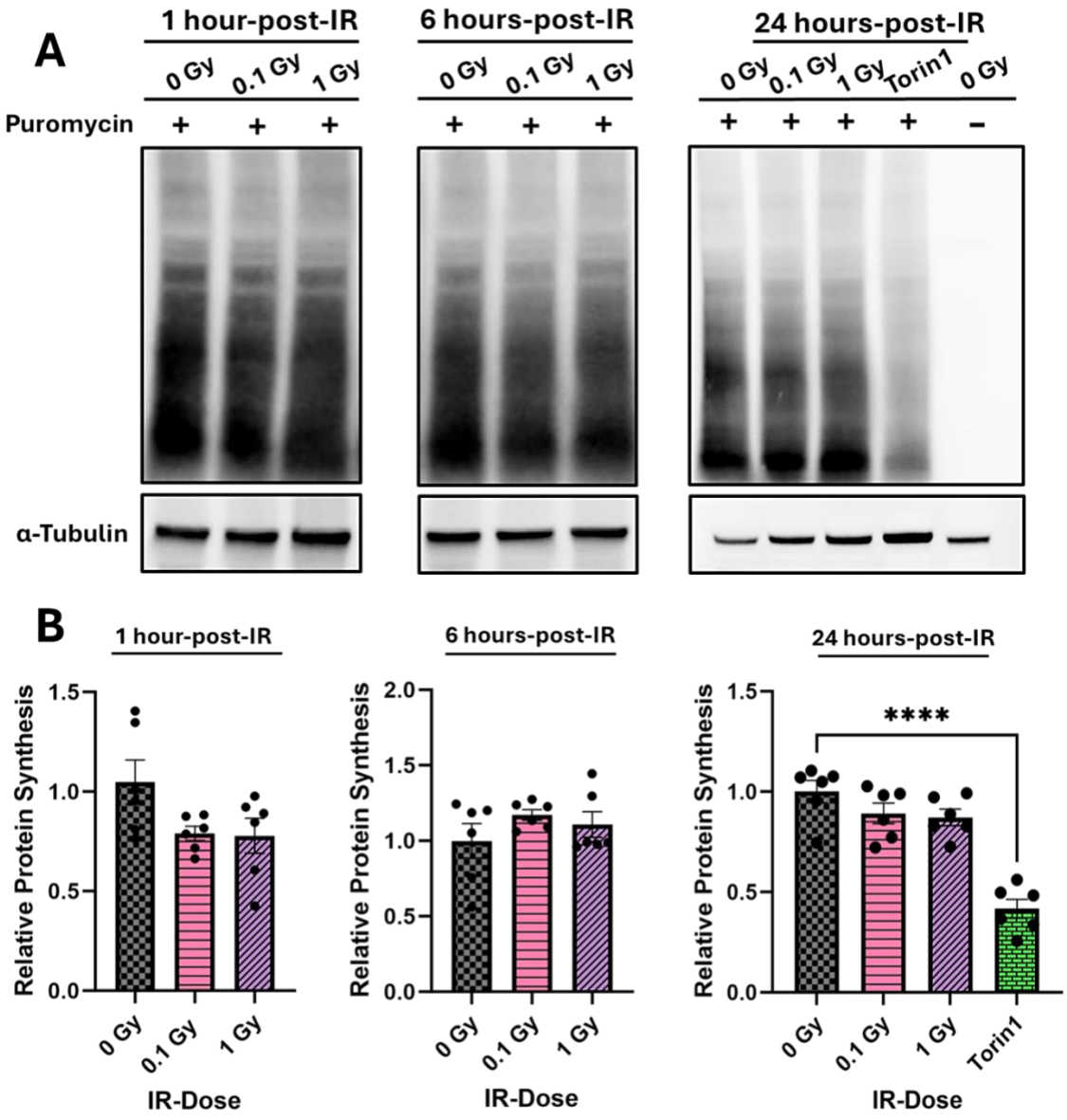

Figure 16) Low dose γ-rays does not significantly change global protein synthesis rate in HFL1 cells

A) Representative Western blot showing puromycin-labeled peptides at 1 hour, 6 hours, and 24 hours post-irradiation in HFL1 cells. α-Tubulin was used as a loading control, confirming similar protein loading. Torin1 treated samples were used as a positive control to validate the assay's sensitivity. HFL1 cell lysate samples with no puromycin treatment nor radiation exposure were used as a negative control, confirming the specificity of puromycin detection. **B)** Quantification of puromycin incorporation was normalized to loading controls and expressed relative to the untreated control sample (0 Gy). Bar graphs

represent the mean ± SEM from at least three independent experiments ($n \geq 3$) conducted at 1-, 6-, and 24-hours post-irradiation. Statistical analysis was performed using one-way ANOVA followed by Dunnett's multiple comparisons test, with p-values assessed relative to the untreated control. Significance is indicated as *$p < 0.05$, ****$p < 0.0001$; all other comparisons were not statistically significant unless otherwise noted.

3.2.2 Canonical Protein Synthesis Pathways; ISR & mTORC1:

To assess whether low-dose γ-irradiation activates canonical stress-responsive translation pathways, I examined the integrated stress response (ISR) and mTORC1 signaling cascades.

First, phosphorylated eIF2α (p-eIF2α) level across all tested conditions was quantified in the conditions tested. Consistent with the puromycin incorporation assay, no visible induction of eIF2α phosphorylation was observed following γ-radiation at any dose tested. As a positive control, Thapsigargin, a known inducer of endoplasmic reticulum (ER) stress, was used as a positive control and robustly induced p-eIF2α, confirming the assay's sensitivity **(Fig. 17 A, B)**.

Next, I also investigated the status of mTORC1 signaling following γ-irradiation by examining the phosphorylation of two key downstream effectors: 4E-BP1 (Thr37/46) and S6 (Ser240/244); the latter being a phosphorylated substrate of S6K, another direct target of mTORC1[151]. Western blotting with phospho-specific antibodies showed no dose-dependent changes for all tested IR doses across the time points, suggesting that mTORC1 is likely unaffected in these conditions. As expected, treatment with Torin1, a potent mTORC1 inhibitor, led to reduced phosphorylation of both 4E-BP1 and S6, validating the responsiveness of the assay **(Fig. 18 A-D)**. These data suggest that low-dose

γ-irradiation does not robustly activate ISR or mTORC1 pathways and has limited impact on global translation under the conditions tested.

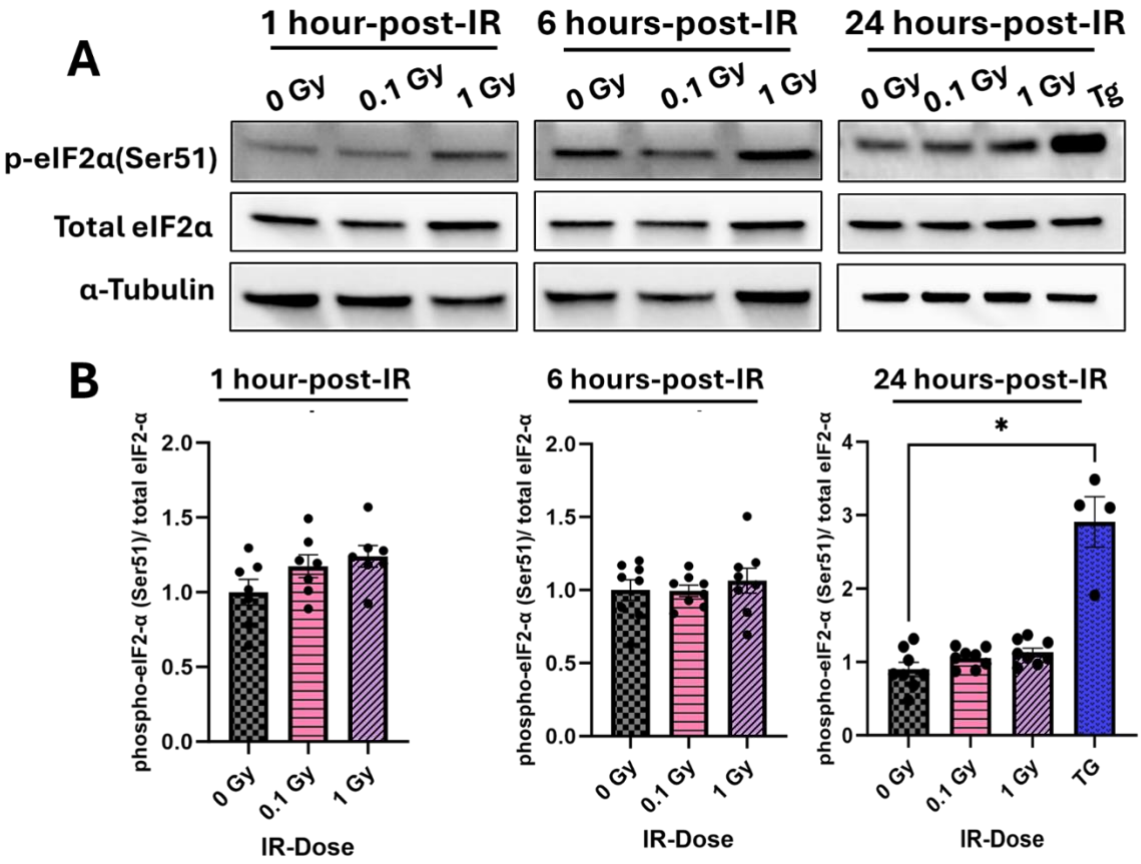

Figure 17) Low-dose ionizing radiation does not significantly activate the ISR pathways

A) Western blot analysis of phosphorylated eIF2α (p-eIF2α) at Ser51 in HFL1 cells exposed to 0, 0.1, or 1 Gy of γ-ray and harvested at 1-, 6-, or 24 hours post-irradiation. Thapsigargin (Tg), a known ER stress inducer, was used as a positive control to validate p-eIF2α induction. Total eIF2α and α-Tubulin served as loading controls. **B)** Quantification of p-eIF2α levels normalized to total eIF2α and expressed relative to the untreated control (0 Gy). Bar graphs represent mean ± SEM from at least three independent experiments (n ≥ 3). Statistical analysis was performed using one-way ANOVA followed by Dunnett's multiple comparisons test. *p < 0.05; **p < 0.01; **** p < 0.0001.

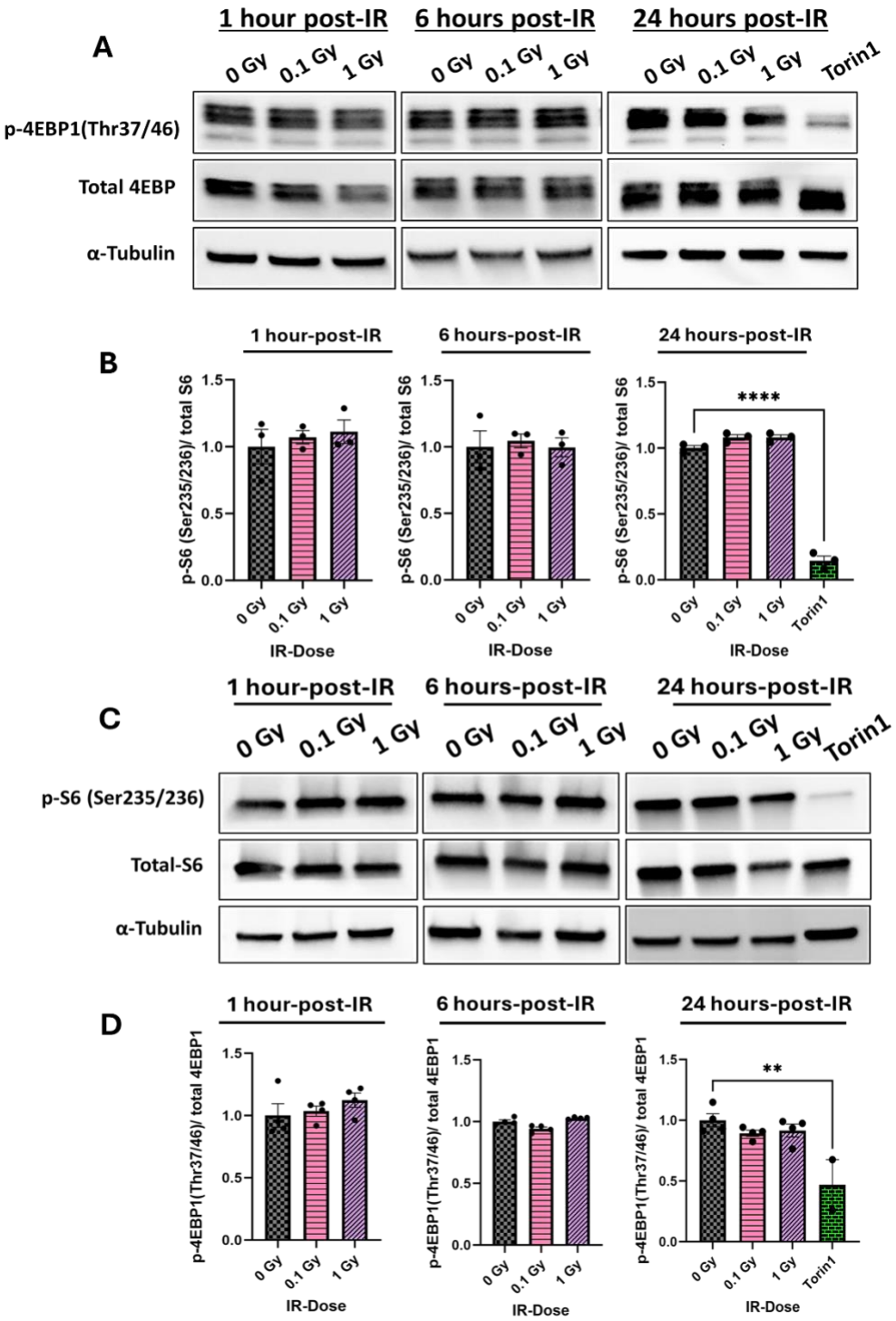

Figure 18) Low-dose ionizing radiation does not significantly change mTORC1 signaling

A, C) Western blot analysis of phosphorylated 4E-BP1 (Thr37/46) and phosphorylated S6 ribosomal protein (Ser240/244), key downstream targets of mTORC1 signaling. IR-

exposed HFL1 cells were analyzed at the indicated time points. Torin1, an mTORC1 inhibitor, was included as a positive control. Total 4E-BP1, total S6, and α-Tubulin were used as loading controls. B, **D)** Quantification of phospho-4E-BP1 and phospho-S6 levels, normalized to their respective total protein levels and expressed relative to untreated controls. Bar graphs display mean ± SEM from at least three independent experiments. One-way ANOVA with Dunnett's multiple comparisons test was used to assess statistical significance. *$p < 0.05$; **$p < 0.01$; **** $p < 0.0001$.

.

3.3 Translation reprogramming in response to γ-irradiation assessed by ribosome profiling

While no clear changes in global protein synthesis, or phosphorylation status of eIF2α and mTORC1effectors were observed at 1-, 6- or 24-hours post-irradiation, it is possible that transient changes and/or alternative translation control mechanisms could mediate subtle and/or selective alterations in mRNA translation and thus more sensitive approaches are warranted. To identify such potential changes in the translatome, I employed the ribosome-profiling (Ribo-seq) strategy.

Changes in both total RNA and ribosome-protected RNA fragments (RPFs) were analyzed in cells exposed to 0, 0.1 Gy and 1 Gy after both 1- and 6-hours post-exposure and plotted as different gene expression categories based on changes in total mRNA levels (x-axis, transcriptome) and translated mRNA level (y-axis, translatome) (**Fig. 19 A**). A modest threshold of 1.2-fold (log_2FC ±0.263) was applied to enable the detection of biologically meaningful but subtle expression shifts that could be overlooked with stricter cutoffs.

At 1 hour post-0.1 Gy exposure, a pronounced shifts in translational efficiency (TE) was observed with minimal changes at the transcriptional level: 121 genes showed increased translation ("Translation up") and 107 genes were translationally downregulated, while only 2 transcripts were upregulated ("Abundance up") and 2 downregulated at the mRNA level. This translation-centric response persisted at 6 hours, with 119 transcripts upregulated and 234 downregulated at the translation level, but again there was a minimal change in transcript abundance) (**Fig. 19 B, C**). These findings support the hypothesis that

low-dose IR induces a significant translational response that does not strongly change mRNA levels.

In contrast, 1 Gy exposure triggered a broader and more conventional response. At 1 hour post-irradiation, a significant number of transcripts fell into both translation and abundance categories, and by 6 hours, transcript-level regulation (i.e., "Abundance up/down") became dominant. This pattern is consistent with a more classical stress response to higher-dose IR, involving transcriptional activation and repression of gene networks (**Fig. 19 D, E**).

Furthermore, buffered RNAs represent transcripts in which changes in mRNA abundance are opposite the changes in their translation (e.g., increased mRNA but decreased translation). This buffering effect suggests a regulatory mechanism to stabilize protein output and maintain proteome homeostasis under radiation-induced stress.

Overall, these results demonstrate that, under this study experimental conditions, low-dose γ-ray modulates gene expression at the translation level rather than transcription, highlighting the importance of integrating translatome data to uncover nuanced radiation responses that may not be apparent from transcriptomic analysis alone.

The following sections will explore specific transcriptome, translatome, and TE changes in detail.

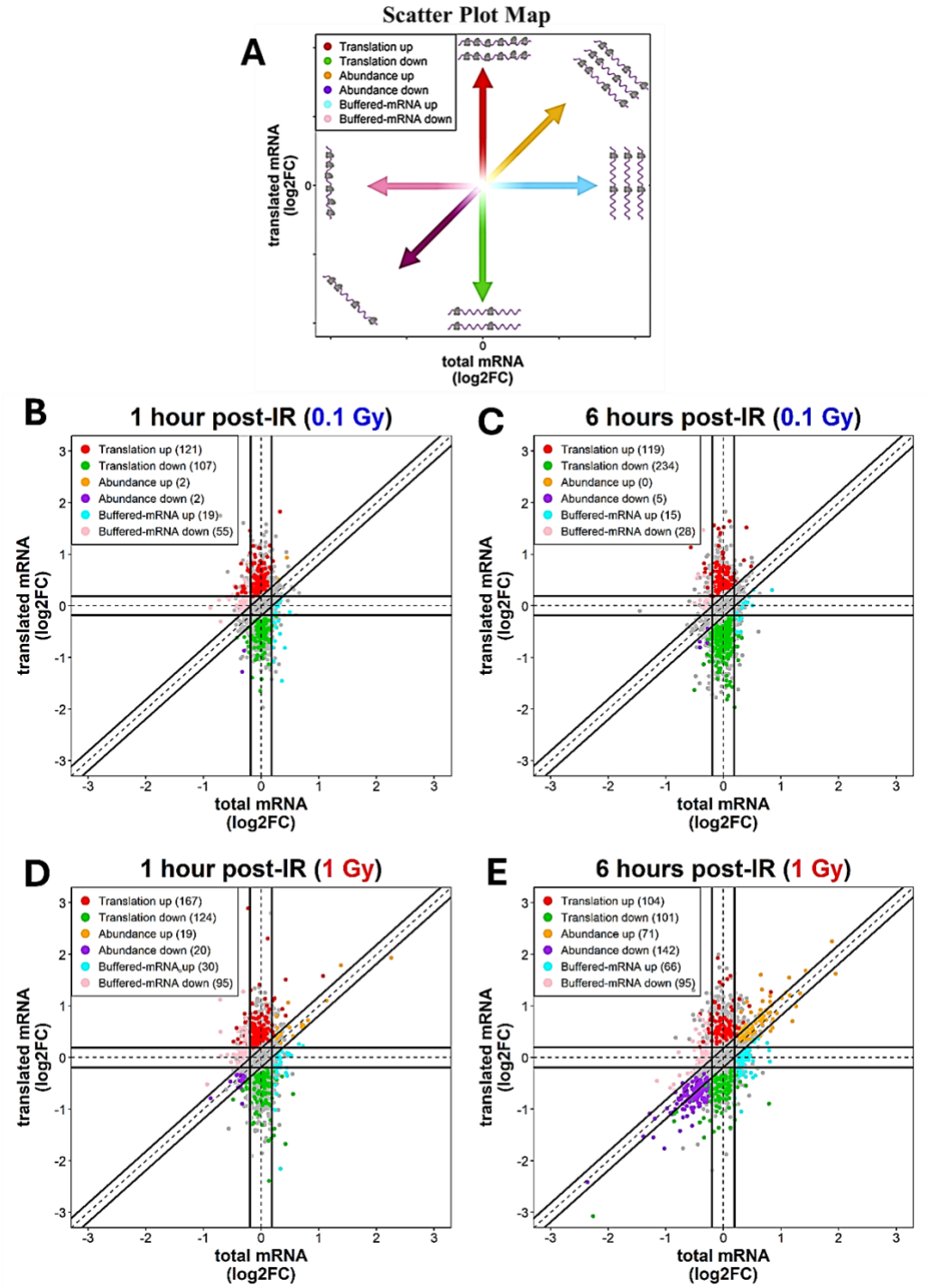

Figure 19) Low-dose γ-irradiation induces translation-specific gene regulation with minimal changes in mRNA abundance.

Schematic representation of different gene expression categories based on changes in total mRNA levels (x-axis, transcriptome) and translated mRNA levels (y-axis, translatome). Genes are classified into six groups:

- Translation up (red): Increased translation with no significant change in mRNA abundance.
- Translation down (green): Decreased translation with unchanged mRNA levels. Abundance up (yellow): Increased mRNA levels, likely due to transcriptional activation.
- Abundance down (Purple): Decreased mRNA levels, likely due to transcriptional repression.
- Buffered-mRNA up (Cyan): Increased mRNA levels without proportional translation, suggesting post-transcriptional buffering.
- Buffered-mRNA down (pink): Decreased mRNA levels without a corresponding reduction in translation, indicating compensatory translational regulation.

(B–E) Scatter plots comparing total mRNA (log_2 fold change, x-axis) and translated mRNA (log_2 fold change, y-axis) for genes 1 hour **(B)** or 6 hours **(C)** post-0.1 Gy radiation or 1hour (**D**) or 6 hours (**E**) post-1 Gy radiation. Each dot represents a gene, colored according to the classification in (**A**). Black diagonal lines indicate the threshold separating transcriptionally regulated genes from translationally regulated ones. A log_2 fold change threshold of 0.263 (corresponding to a 1.2-fold change) was applied to identify small but potentially relevant changes in gene expression. Data represent n = 3 independent biological replicates.

3.4 Magnitude of early transcriptional changes in response to γ-rays: Volcano plot analysis

To assess early transcriptional responses to γ-radiation, differential gene expression at 1 and 6 hours post-irradiation was analyzed using volcano plots. Cells were exposed to either 0.1 Gy or 1 Gy, and transcriptome-wide changes were evaluated based on $\log_2$ fold change and statistical significance. A significance threshold of $\log_2$ fold change $\geq |0.585|$ and $p < 0.02$ was used to identify differentially expressed genes. This threshold was chosen to balance sensitivity and specificity, since stricter corrections would likely exclude biologically meaningful but subtle transcriptional responses to low-dose IR.

Following 0.1 Gy exposure, relatively few genes were significantly upregulated or downregulated at either time point, suggesting that low-dose radiation induces only modest transcriptional changes **(Fig. 20 A, B).** In contrast, 1 Gy exposure led to a markedly broader transcriptional response, particularly at 6 hours post-irradiation, where many transcripts were differentially expressed **(Fig. 20 C, D).**

This pattern demonstrates a clear dose- and time-dependent effect, in which higher radiation doses trigger a more robust and widespread transcriptional activation or repression. In contrast, low-dose IR appears to induce a limited or possibly delayed transcriptomic response.

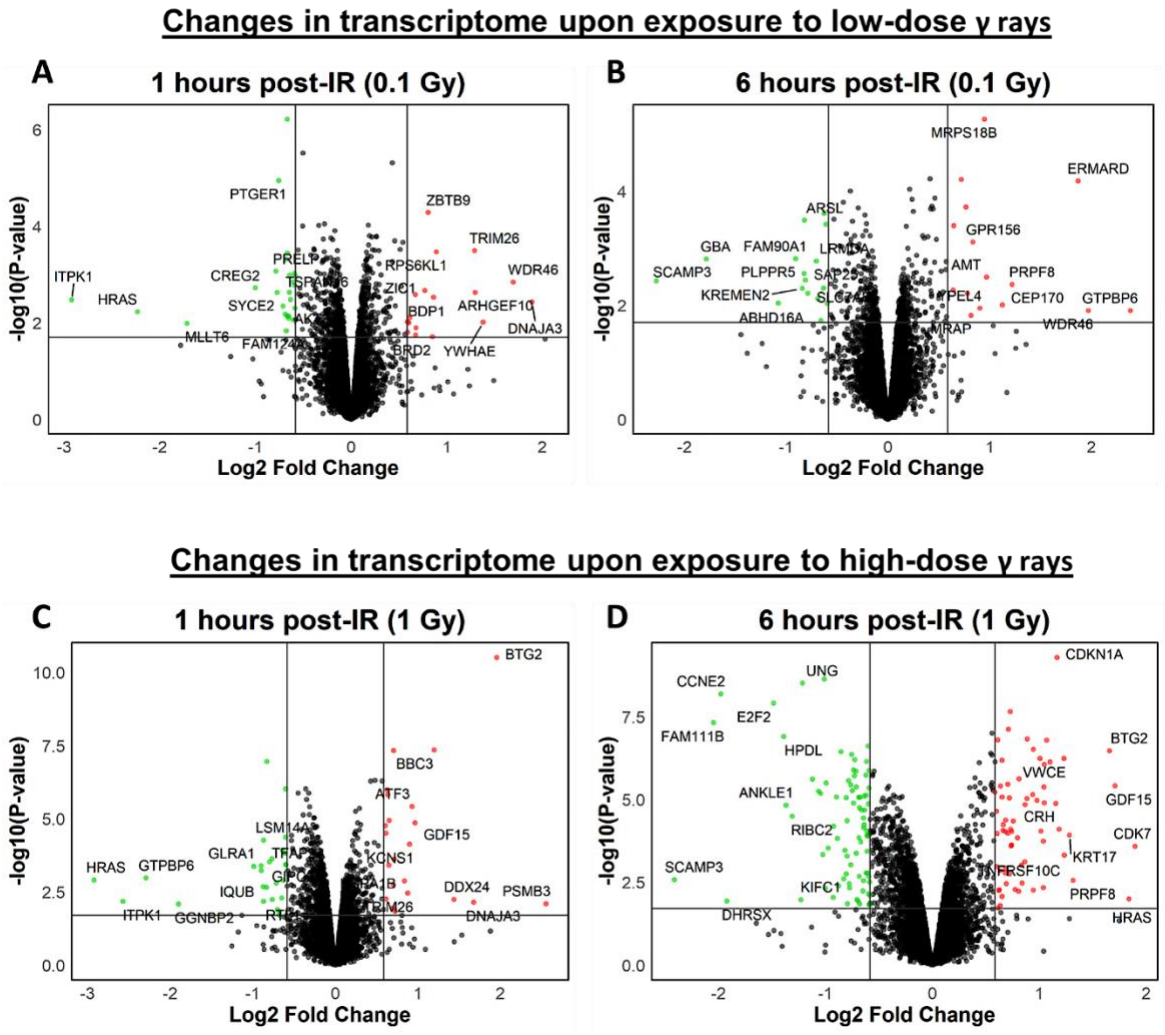

Figure 20) Magnitude of transcriptomic changes visualized by volcano plots

(A-D) Volcano plots show differential gene expression, at the transcriptional in response to 0.1 Gy and 1 Gy post-irradiation at 1- and 6-hours post-irradiation compared to unirradiated cells. Each plot displays log2 fold changes (x-axis) against -log10 (p-value) (y-axis) for individual transcripts. Statistically significant upregulated transcripts are marked in red, while downregulated transcripts are in green. Non-significant transcripts are indicated in black. **A, B)** Transcriptome, 0.1 Gy, 1 hour & 6 hours post-IR. **C, D)** Transcriptome, 1 Gy, 1 hour & 6 hours post-IR. A significance threshold of a $\log_2$ fold change of 0.585, corresponding to a 1.5-fold change, and $p < 0.02$ were applied. Data represent n = 3 independent biological replicates.

3.5 Gene Ontology (GO) enrichment analysis reveals biological processes affected at the transcriptome level by γ-irradiation

To investigate the functional significance of radiation-induced transcriptional changes, Gene Ontology (GO) enrichment analysis was conducted to identify biological processes (BPs) altered at 1 and 6 hours post-irradiation. At the low dose of 0.1 Gy, no significant GO term enrichment was detected, consistent with the minimal number of differentially expressed genes at this dose **(Fig. 21 A, Fig. 22 A)**. This suggests that low-dose γ-irradiation does not induce widespread transcriptional reprogramming at the biological process level within the early post-exposure window.

In contrast, at 1 hour post 1 Gy exposure, irradiation resulted in the enrichment of several stress-associated biological processes. Upregulated biological pathways included p-53-mediated signal transduction, apoptotic signaling, response to amino acid starvation, and positive regulation of cell death. These findings highlight an immediate activation of stress and survival pathways following high-dose IR exposure **(Fig. 21 B)**. However, genes associated with nucleosome assembly, epigenetic regulation, and humoral immune response were significantly downregulated at this time point, implying a rapid suppression of chromatin dynamics and immune signaling (**Fig. 22 B)**.

By 6 hours post-IR, the transcriptomic profile shifted toward processes supporting damage coordination, autophagy and cell cycle regulation. Upregulated pathways included G1/S transition, positive regulation of autophagy, and sustained activation of DNA damage response pathways, including continued enrichment of p53-mediated signaling **(Fig. 21 C).** Simultaneously, there was significant downregulation of genes involved in DNA

replication, recombination, repair, and chromosome organization **(Fig. 22 C).**, consistent with prolonged cell cycle arrest.

Together, these findings demonstrate a biphasic transcriptional response in HFL1 cells following γ-irradiation: an early phase characterized by stress signaling and apoptosis, followed by a later phase of adaptive responses involving autophagy and environmental stress signaling, along with persistent suppression of DNA replication machinery.

Table 10) Summary of GO enrichment of transcriptome-level biological processes altered by 1 Gy γ-irradiation

Dose	Timepoint	Direction	Key Biological Processes	Functional Category
1 Gy	1h	Upregulated	p53 signaling, amino acid starvation response, apoptosis, DNA damage signaling	Apoptosis & Stress Signaling
1 Gy	6h	Upregulated	Environmental stimulus response, cell death regulation, autophagy, viral response	Cell Death, Autophagy & Viral Defense
1 Gy	1h	Downregulated	Cell cycle regulation, mitotic checkpoint, DNA replication, spindle assembly	Cell Cycle & DNA Synthesis
1 Gy	6h	Downregulated	DNA replication, telomere maintenance, G1/S transition, chromatin assembly	Replication & Genome Stability

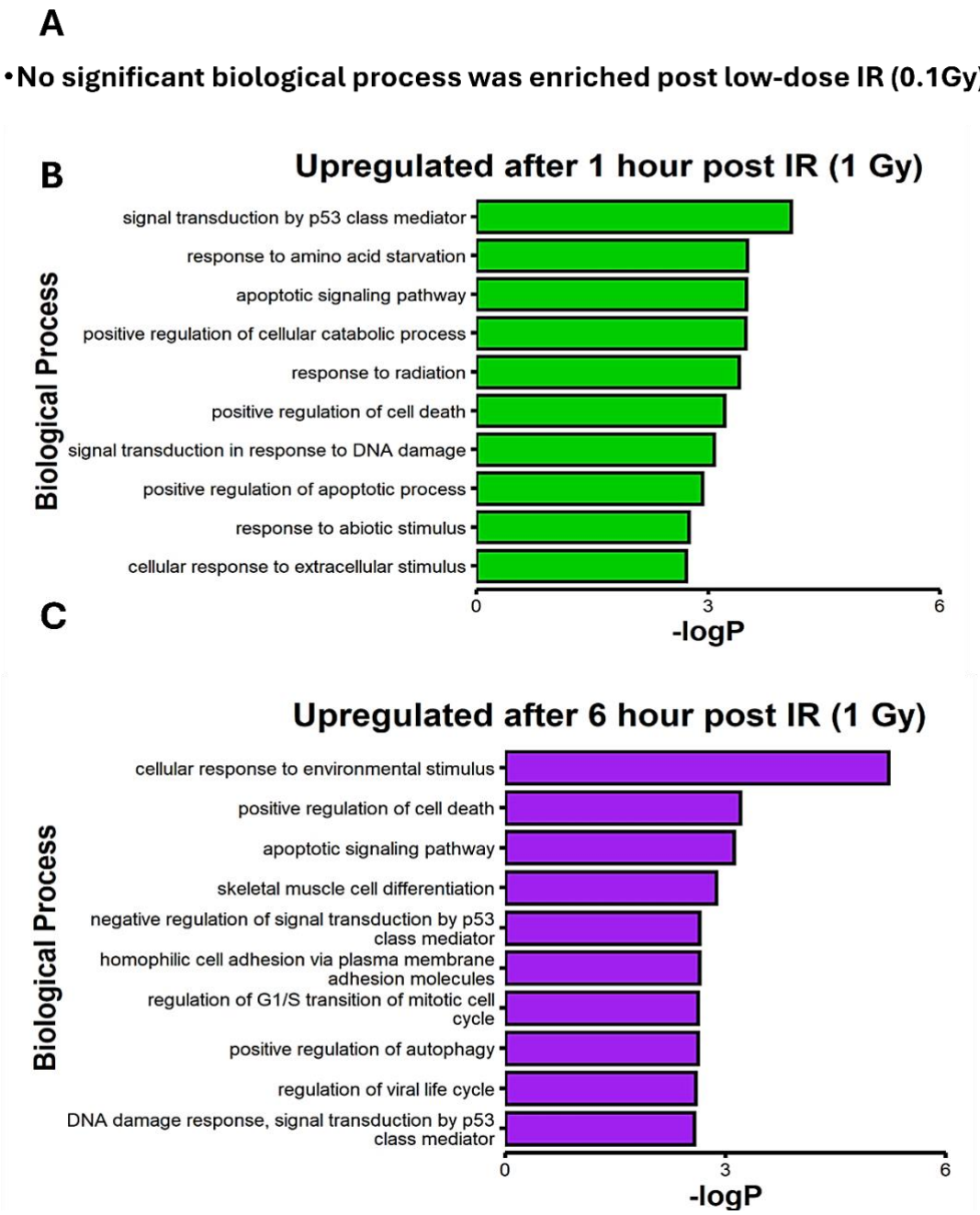

Figure 21) GO enrichment of upregulated biological processes following high-dose γ-irradiation (1 Gy).

B) Biological processes significantly enriched among upregulated genes at 1 hour post-IR. **C)** Biological processes significantly enriched among upregulated genes at 6 hours post-IR. Bar plots display the top enriched GO terms (Biological Process category) based on $-\log_{10}(p\text{-value})$. GO enrichment was performed on genes meeting the differential expression threshold ($\log_2 FC \geq |0.585|$ and $p < 0.02$; n = 3 biological replicates).

A

•No significant biological process was enriched post low-dose IR (0.1Gy).

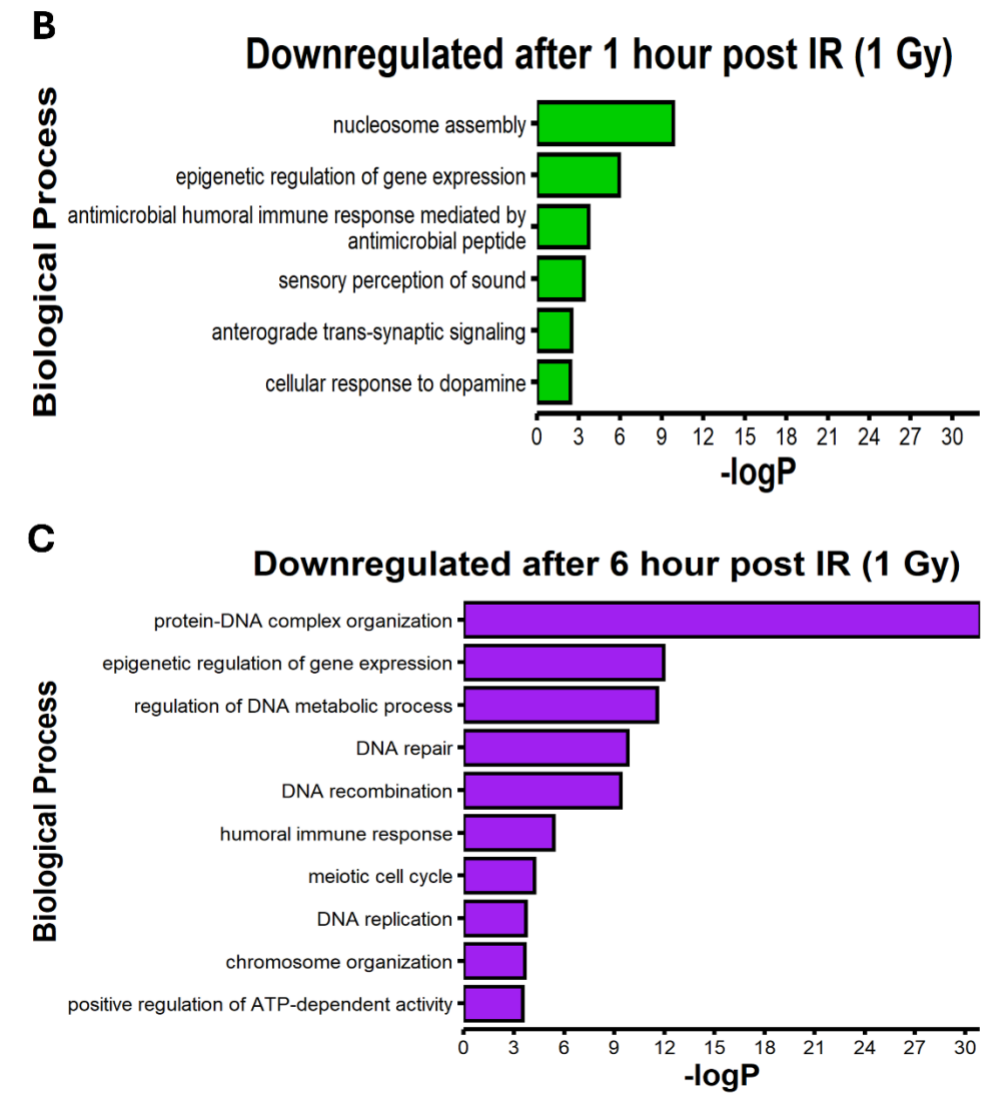

Figure 22) GO enrichment of downregulated biological processes following high-dose γ-irradiation (1 Gy).

B) Biological processes significantly enriched among downregulated genes at 1 hour post-IR. **C)** GO terms enriched among downregulated genes at 6 hours post-IR. organization, reflecting suppression of DNA metabolism and mitotic processes likely associated with radiation-induced cell cycle arrest. Bar plots show the top enriched GO Biological Processes based on $-\log_{10}(p\text{-value})$. Enrichment was conducted using genes differentially expressed at $\log_2 FC \geq |0.585|$ and $p < 0.02$ (n = 3 biological replicates).

3.6 Heatmap analysis reveals dose- and time- dependent transcriptional signatures.

To visualize gene-specific transcriptional responses to ionizing radiation, heatmaps were generated based on significantly differentially expressed genes across four conditions. The results illustrate clear dose- and time-dependent transcriptional shifts in response to γ-irradiation (**Fig. 23 A-B).** The red is upregulated, and green is downregulated.

At low-dose (0.1 Gy), transcriptional changes were modest and largely transient, most of these gene peak at 1 hour and then fade, with just a few lasting to 6 hours. A limited number of genes exhibited early upregulation. Time-dependent shifts were observed for genes like GTBPB6 and ZIC1, but overall, the expression magnitude remained low with only few genes overlap between the time points. These patterns suggest a subtle and short-lived transcriptional response (**Fig. 23 A**).

In contrast, high dose radiation (1 Gy) is a different story: it activates a broad panel of stress response genes like ATF3, GDF15, and CDKN1A, and keeps them elevated at 6 hours(**Fig. 23 B**).

In short, low dose induces a quick and contained signal in transcriptome, while high dose locks the transcriptome into sustained stress mode.

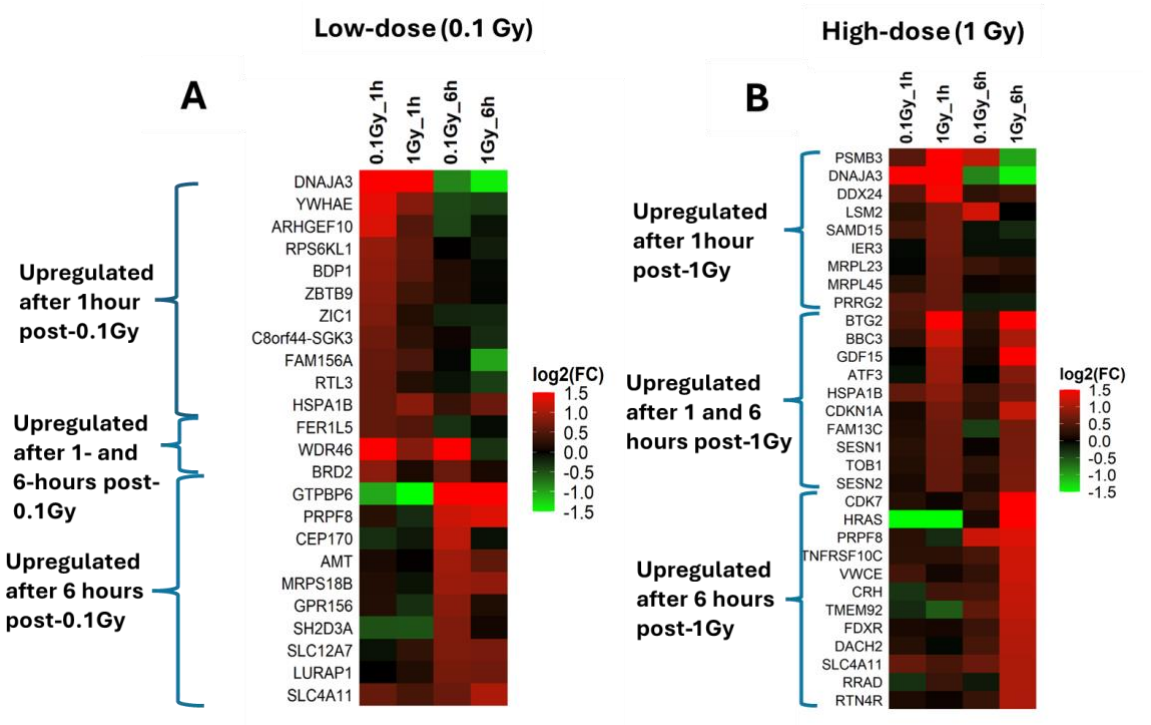

Figure 23) Transcriptomic heatmap of gene expression responses to low- and high-dose γ-irradiation

Heatmap of transcriptome-wide gene expression changes in HFL1 cells at 1 hour and 6 hours following 0.1 Gy (A) and 1 Gy (B) γ-irradiation. Color intensity reflects $\log_2$ fold change relative to non-irradiated controls, with red indicating upregulation and green indicating downregulation.

Table 11) Top 10 upregulated transcripts following γ-irradiation

Rank	Gene	log_2 Fold Change	P-value
1 hour post- 0.1 Gy			
1	**BTG2**	0.4301	4.91×10^{-6}
2	**ZBTB9**	0.8058	5.24×10^{-5}
3	**PIK3C2B**	0.2647	1.64×10^{-4}
4	**C11orf16**	0.2635	1.67×10^{-4}
5	**ZNF763**	0.4567	2.04×10^{-4}
6	**FAM83B**	0.5397	2.17×10^{-4}
7	**SERTAD4**	0.5136	3.06×10^{-4}
8	**TRIM26**	1.2891	3.23×10^{-4}
9	**ASTE1**	0.2906	3.23×10^{-4}
10	**RPS6KL1**	0.8918	3.43×10^{-4}
1 hour post- 1Gy			
1	**BTG2**	1.953	3.13×10^{-11}
2	**BBC3**	1.1949	4.49×10^{-8}
3	**CDKN1A**	0.7039	4.72×10^{-8}
4	**MDM2**	0.4783	4.96×10^{-7}
5	**PPM1D**	0.5685	5.21×10^{-7}
6	**GADD45A**	0.4286	5.33×10^{-7}
7	**MRPL45**	0.6264	1.03×10^{-6}
8	**SESN1**	0.632	1.52×10^{-6}
9	**ATF3**	0.928	3.87×10^{-6}
10	**AEN**	0.2912	4.42×10^{-6}
6 hours post- 0.1 Gy			
1	**MRPS18B**	0.9471	5.47×10^{-6}
2	**GABRE**	0.4122	6.12×10^{-5}
3	**LURAP1**	0.7214	6.22×10^{-5}
4	**ERMARD**	1.8678	6.60×10^{-5}
5	**PMF1-BGLAP**	0.4589	1.32×10^{-4}
6	**TMEM71**	0.4304	1.84×10^{-4}
7	**SLC12A7**	0.7641	1.91×10^{-4}
8	**BMP8A**	0.4417	2.04×10^{-4}
9	**DACH2**	0.4178	2.05×10^{-4}
10	**SLC4A11**	0.6453	4.03×10^{-4}
6 hours post- 1Gy			
1	**CDKN1A**	1.1635	5.15×10^{-10}
2	**ZMAT3**	0.7273	2.25×10^{-8}
3	**EPS8L2**	0.7096	7.70×10^{-8}
4	**TRIM22**	0.5558	1.01×10^{-7}
5	**MDM2**	0.8846	1.49×10^{-7}
6	**PPM1D**	0.61	1.61×10^{-7}
7	**DACH2**	1.069	1.62×10^{-7}
8	**ACER2**	0.9434	3.05×10^{-7}
9	**BTG2**	1.6546	3.42×10^{-7}
10	**PSTPIP2**	0.5455	4.01×10^{-7}

Table 12) Top 10 downregulated transcripts following γ-irradiation

Rank	Gene	log_2 Fold Change	P-value
1 hour post- 0.1 Gy			
1	**SLC25A18**	–0.6703	6.10×10^{-7}
2	**PPARGC1A**	–0.5032	3.09×10^{-6}
3	**PTGER1**	–0.7588	1.15×10^{-5}
4	**CLEC3B**	–0.2785	9.09×10^{-5}
5	**GRIK4**	–0.3395	9.76×10^{-5}
6	**ACCS**	–0.5070	9.93×10^{-5}
7	**KLF2**	–0.2922	1.87×10^{-4}
8	**C2orf81**	–0.3908	2.96×10^{-4}
9	**LMTK3**	–0.3851	3.12×10^{-4}
10	**SETBP1**	–0.5538	3.14×10^{-4}
1hour post- 1Gy			
1	**SLC25A18**	–0.832	1.13×10^{-7}
2	**NAV2**	–0.601	9.56×10^{-7}
3	**TROAP**	–0.360	9.57×10^{-7}
4	**GNB3**	–0.453	1.35×10^{-6}
5	**H3C12**	–0.323	1.36×10^{-6}
6	**H2BC17**	–0.349	2.25×10^{-6}
7	**H2BC11**	–0.311	3.92×10^{-6}
8	**SH3D21**	–0.315	7.35×10^{-6}
9	**PIF1**	–0.388	7.59×10^{-6}
10	**H1-3**	–0.271	1.63×10^{-5}
6 hours post- 0.1 Gy			
1	**PRXL2A**	–0.369	1.00×10^{-4}
2	**E2F2**	–0.439	1.57×10^{-4}
3	**ARHGEF4**	–0.292	1.96×10^{-4}
4	**ZNF664-RFLNA**	–0.628	2.47×10^{-4}
5	**FZD9**	–0.532	3.10×10^{-4}
6	**ARSL**	–0.821	3.25×10^{-4}
7	**EYS**	–0.350	3.38×10^{-4}
8	**MYLK4**	–0.611	3.81×10^{-4}
9	**GABRB3**	–0.411	5.60×10^{-4}
10	**FAM53A**	–0.329	6.12×10^{-4}
6hours post- 1Gy			
1	**CCNE2**	–1.981	6.57×10^{-9}
2	**FAM111B**	–2.049	4.76×10^{-8}
3	**UNG**	–1.216	3.08×10^{-9}
4	**E2F2**	–1.486	1.24×10^{-8}
5	**FAM156A**	–1.013	2.31×10^{-9}
6	**HPDL**	–1.391	1.26×10^{-7}
7	**WDR76**	–0.854	3.66×10^{-7}
8	**E2F8**	–0.757	4.41×10^{-7}
9	**CDCA7**	–0.729	6.36×10^{-7}
10	**TIPIN**	–0.618	7.13×10^{-7}

3.7 Volcano plot visualization of dose- and time-dependent translatome responses to γ-irradiation

To assess the translational impact of γ-irradiation, volcano plots were generated to visualize changes in the translatome at 1- and 6-hours following exposure to low (0.1 Gy) and high (1 Gy) radiation doses. Compared to transcriptional responses, the translatome showed more pronounced changes, particularly at the lower 0.1 Gy dose. By 6 hours post-irradiation, these translational changes became increasingly evident, suggesting a delayed yet significant response at the level of active translation **(Fig 24 A, B)**.

At 1 hour post-1 Gy exposure, a significant number of genes displayed both up- and downregulation in translational activity. These effects increased further by 6 hours, indicating a progressive remodeling of the translational landscape in response to radiation dose and exposure duration **(Fig 24 C, D)**.

These results propose that while transcriptional changes emerge gradually, translational regulation provides a more immediate and dynamic response to radiation exposure, emphasizing the important role of post-transcriptional mechanisms in radiation-induced gene expression.

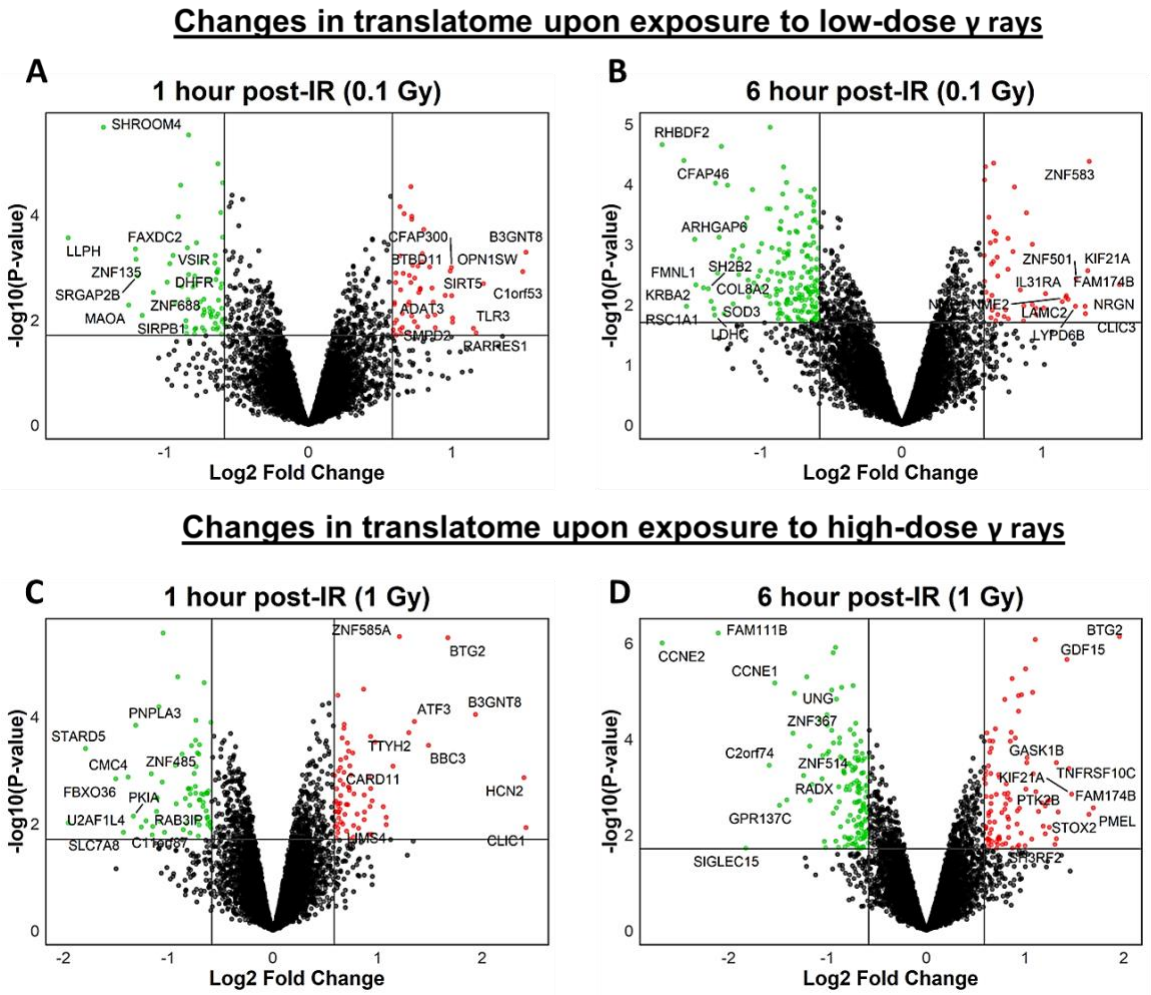

Figure 24) Magnitude of translatome changes visualized by volcano plots

(A-D) Volcano plots show differential gene expression, at the translational level in response to 0.1 Gy and 1 Gy post-irradiation at 1- and 6-hours post-irradiation compared to unirradiated cells. Each plot displays log2 fold changes (x-axis) against -log10 (p-value) (y-axis) for individual transcripts. Statistically significant upregulated translatome are marked in red, while downregulated translatome are in green. Non-significant translatome are indicated in black.

(A, B) Low-dose (0.1 Gy) translatome responses at 1- and 6-hours post-irradiation. **(C, D)** High-dose (1 Gy) translatome responses at 1- and 6- hours post-irradiation. A significance threshold of $\log_2$ fold change ≥ 0.585 (equivalent to a 1.5-fold change) and $p < 0.02$ was applied. Data represent n = 3 independent biological replicates.

3.8 GO enrichment analysis reveals biological processes affected at the translatome level by γ-irradiation

While exposure to 0.1 Gy showed no significant enrichment of biological processes at the transcriptome level, translatome analysis identified multiple enriched pathways, highlighting the role of post-transcriptional regulation in low-dose responses.

At 1 hour post-0.1 Gy radiation, early translational responses were mainly associated with immune regulation and ion transport processes, suggesting a role in maintaining cellular homeostasis. By 6 hours, enriched GO terms shifted toward metabolic and inflammatory signaling pathways such as glucose and carbohydrate transport, response to interleukin-1, and modulation of chemical synaptic transmission, indicating a dynamic and adaptive response over time **(Fig. 25 A, B).**

Under high-dose exposure (1 Gy), the translatome showed a more immediate activation of the DNA damage response pathway. At 1 hour, upregulated processes included mitotic G1/S checkpoint signaling, DNA damage response, and biosynthetic activity such as aminoglycan and carbohydrate biosynthesis. By 6 hours, the upregulated landscape expanded to include pathways associated with protein degradation and quality control, particularly ubiquitin-dependent and proteasome-related catabolic processes, reflecting a sustained cellular effort to manage proteotoxic stress and maintain proteostasis **(Fig. 26 A, B)**.

In contrast, downregulated biological processes at 1 hour post-0.1 Gy involved key immune functions, including leukocyte activation, interferon-gamma production, and leukocyte-mediated immunity. Interestingly, this contrasts with the simultaneous upregulation of complementary immune pathways, suggesting a fine-tuned, biphasic

immune modulation rather than a uniform suppression. By 6 hours, the downregulation profile shifted toward developmental regulation and transcriptional repression, including inhibition of DNA-binding transcription factor activity, indicating broader systemic shifts in gene regulation under low-dose stress **(Fig. 27 A, B)**.

Following 1 Gy exposure, the downregulation profile was more pronounced and targeted. At 1 hour, pathways involved in nucleosome assembly, chromatin remodeling, and telomere organization were suppressed, suggesting early cell cycle arrest and chromatin silencing. By 6 hours, these effects intensified, with enriched downregulation of processes related to DNA replication, meiotic progression, and cell cycle checkpoint signaling, consistent with a robust cellular shift toward proliferation arrest and genomic repair **(Fig. 28 A, B)**.

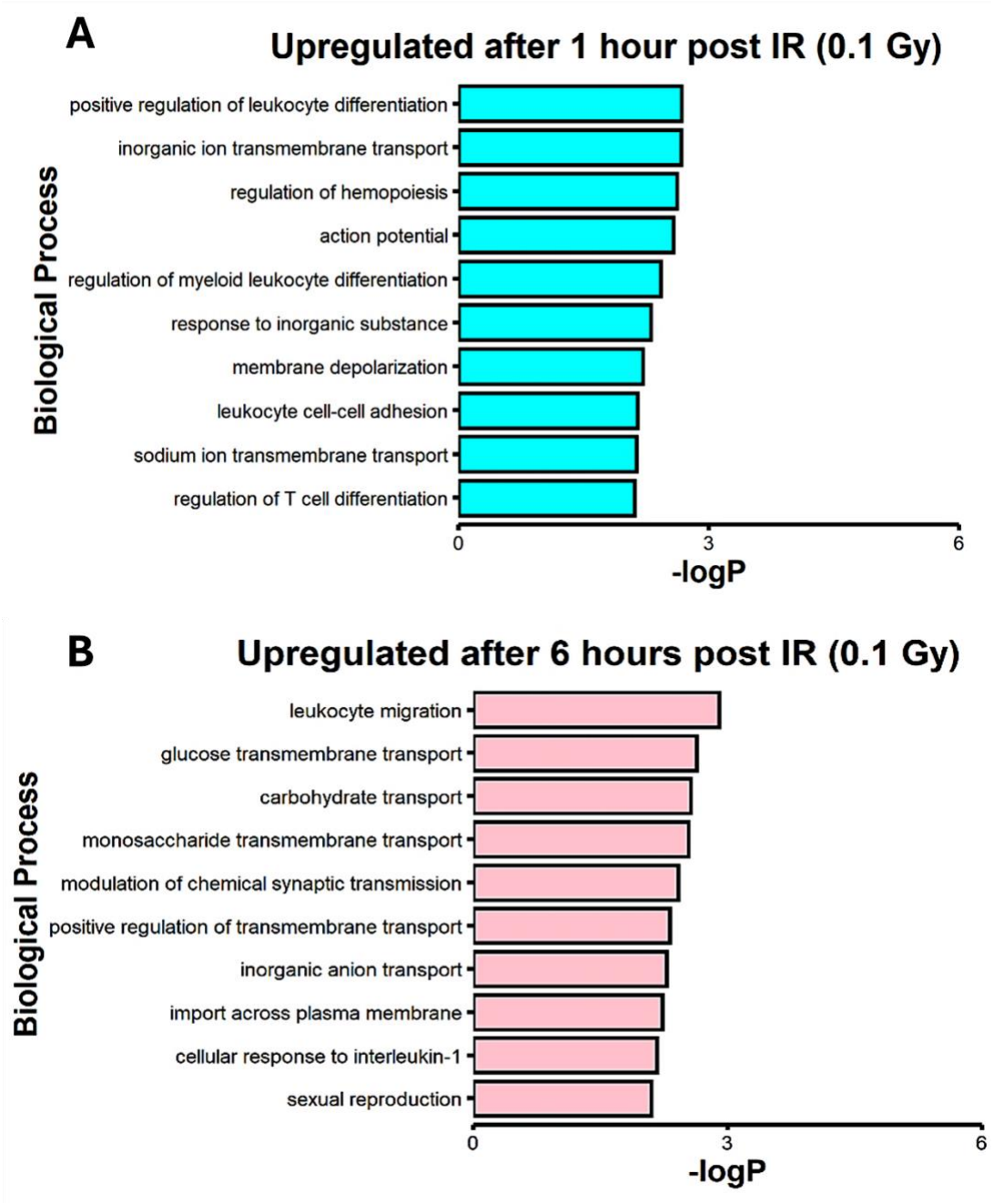

Figure 25) GO enrichment analysis of upregulated biological processes in the translatome following 0.1 Gy γ-irradiation

Bar plots show the top significantly enriched biological processes (GO terms) for upregulated translationally active genes. Enrichment is based on $-\log_{10}$(p-value), indicating the strength of association. **A)** Upregulated GO terms at 1 hour. **B)** Upregulated GO terms at 6 hours. Data represent n = 3 biological replicates, with significance threshold of adjusted $p < 0.02$.

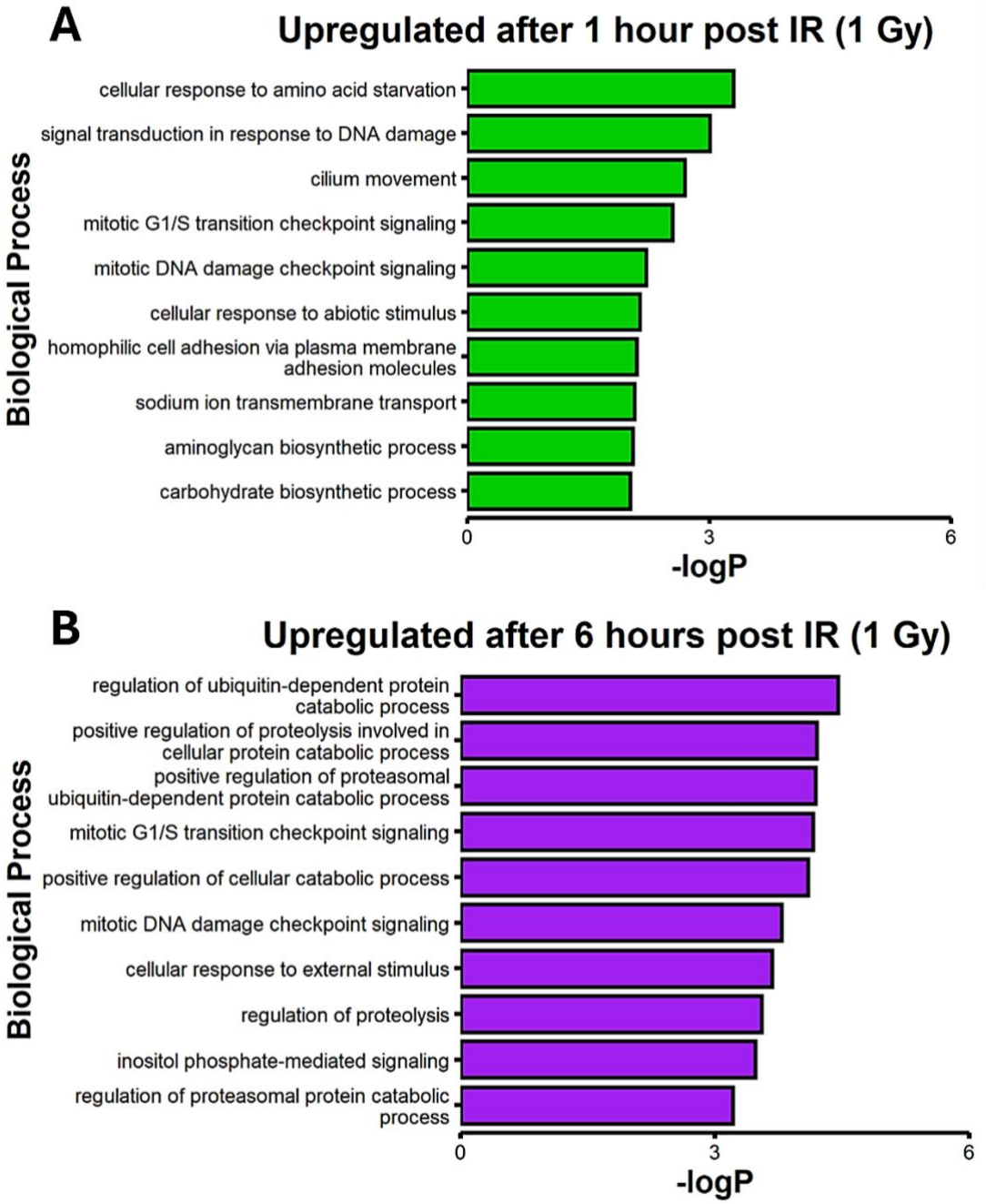

Figure 26) GO enrichment analysis of upregulated biological processes in the translatome following 1 Gy γ-irradiation

Bar plots show the top significantly enriched biological processes (GO terms) for upregulated translationally active genes. Enrichment is based on $-\log_{10}$(p-value), indicating the strength of association. A) Upregulated GO terms at 1 hour. B) Upregulated GO terms at 6 hours. Data represent n = 3 biological replicates, with significance threshold of adjusted $p < 0.02$.

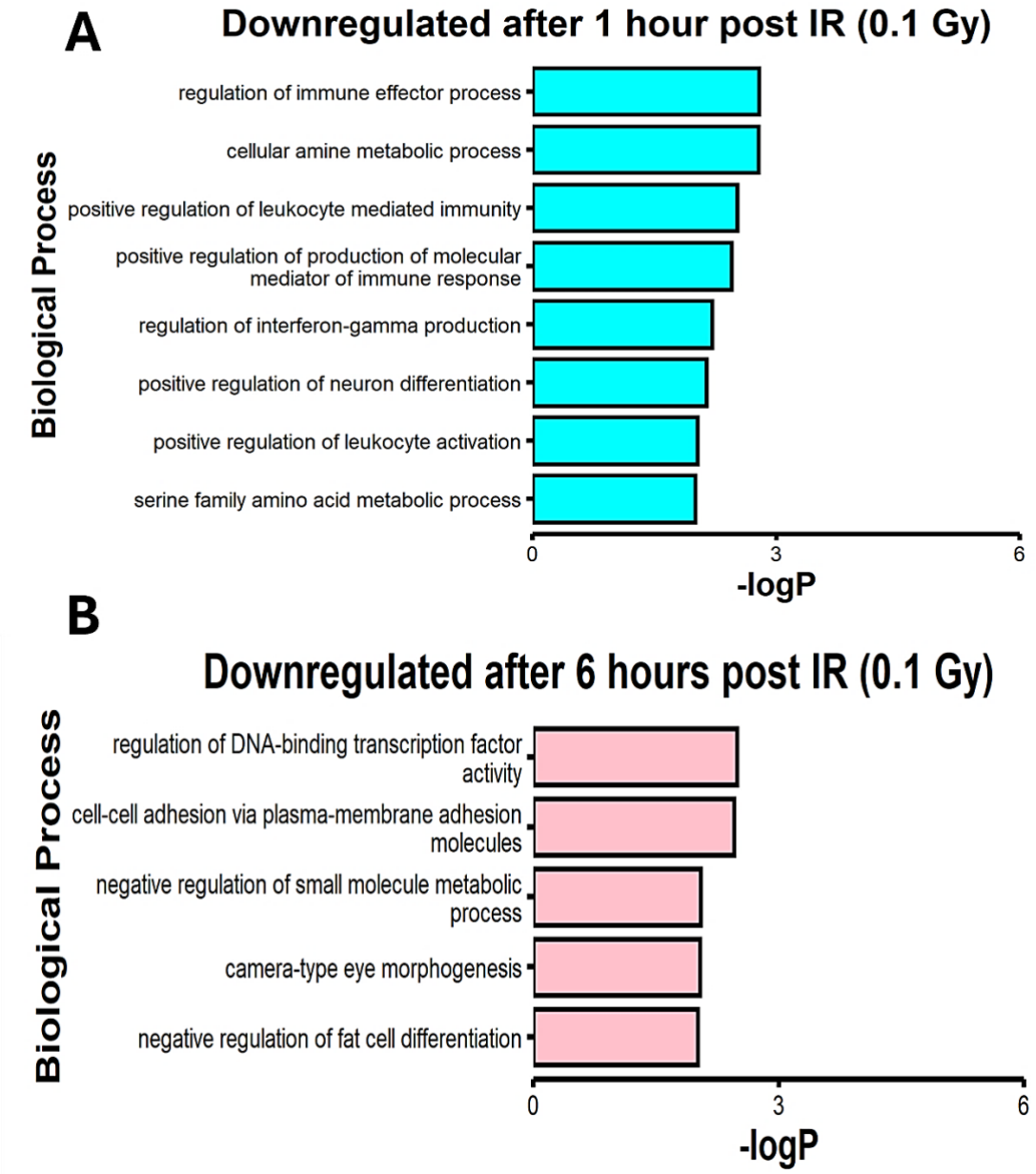

Figure 27) Gene Ontology (GO) enrichment analysis of downregulated biological processes in the translatome following 0.1 Gy γ-irradiation

Bar plots show the top significantly enriched biological processes (GO terms) for downregulated translationally active genes. Enrichment is based on $-\log_{10}$(p-value), indicating the strength of association. **A)** downregulated GO terms at 1 hour. **B)** downregulated GO terms at 6 hours. Data represent n = 3 biological replicates, with significance threshold of adjusted $p < 0.02$.

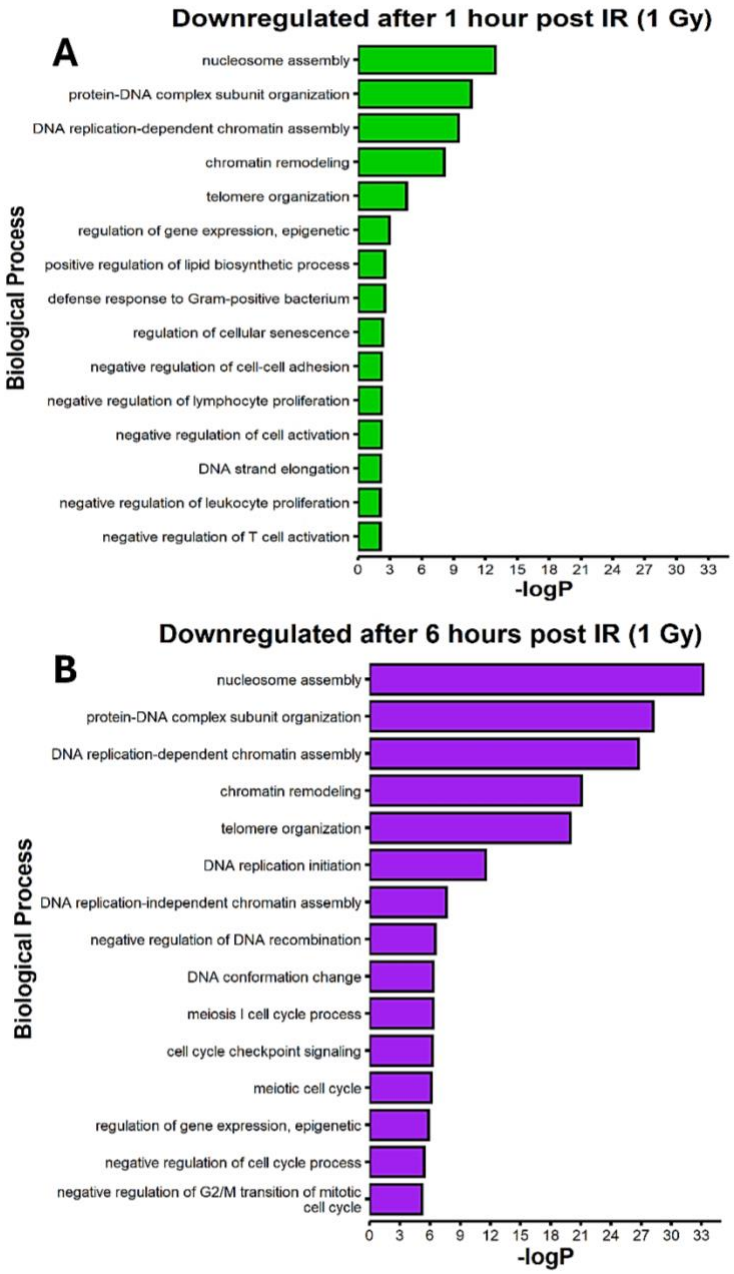

Figure 28) GO enrichment analysis of downregulated biological processes in the translatome following 1 Gy γ-irradiation

Bar plots show the top significantly enriched biological processes (GO terms) for downregulated translationally active genes. Enrichment is based on $-\log_{10}$(p-value), indicating the strength of association. **A)** downregulated GO terms at 1 hour. **B)** downregulated GO terms at 6 hours. Data represent n = 3 biological replicates, with significance threshold of adjusted $p < 0.02$.

Table 13) Summary of translationally regulated biological processes following γ-Irradiation

Dose	Timepoint	Direction	Key Biological Processes	Functional Category
0.1 Gy	1h	Upregulated	Leukocyte differentiation, ion transport, hemopoiesis, membrane depolarization	Immune & Ion Transport
0.1 Gy	6h	Upregulated	Glucose/carbohydrate transport, IL-1 response, synaptic transmission	Metabolic & Inflammatory Signaling
1 Gy	1h	Upregulated	DNA damage response, G1/S checkpoint, biosynthesis (aminoglycan, carbohydrate)	DNA Damage Response & Biosynthesis
1 Gy	6h	Upregulated	Protein degradation, ubiquitin-proteasome system, stress response	Proteostasis & Stress Adaptation
0.1 Gy	1h	Downregulated	Immune regulation (leukocyte activation, IFN-γ), neuron differentiation	Immune Suppression & Developmental Regulation
0.1 Gy	6h	Downregulated	Transcriptional repression, cell adhesion, eye morphogenesis	Transcriptional Repression & Morphogenesis
1 Gy	1h	Downregulated	Chromatin remodeling, nucleosome assembly, telomere organization	Chromatin Remodeling & Cell Cycle Arrest
1 Gy	6h	Downregulated	DNA replication, meiosis, cell cycle checkpoints	DNA Replication & Meiotic Regulation

3.9 Heatmap analysis reveals dose- and time-dependent gene expression signatures in translatome level

Heatmap analysis further demonstrated that the translatome response to low-dose irradiation (0.1 Gy) is highly time-dependent (Figure 3.9). Distinct groups of genes were upregulated at 1 h and 6 h, suggesting a stage-specific and selective adjustment rather than a broad, sustained response. In contrast, high-dose exposure (1 Gy) recruited a larger stress program, with more overlap in the transcriptional signatures observed at both timepoints, indicating continuity of response. On the downregulated side, the low-dose condition triggered selective and dynamic suppression, whereas the high-dose condition produced a more extensive and persistent repression, particularly in pathways related to cell cycle progression and DNA repair.

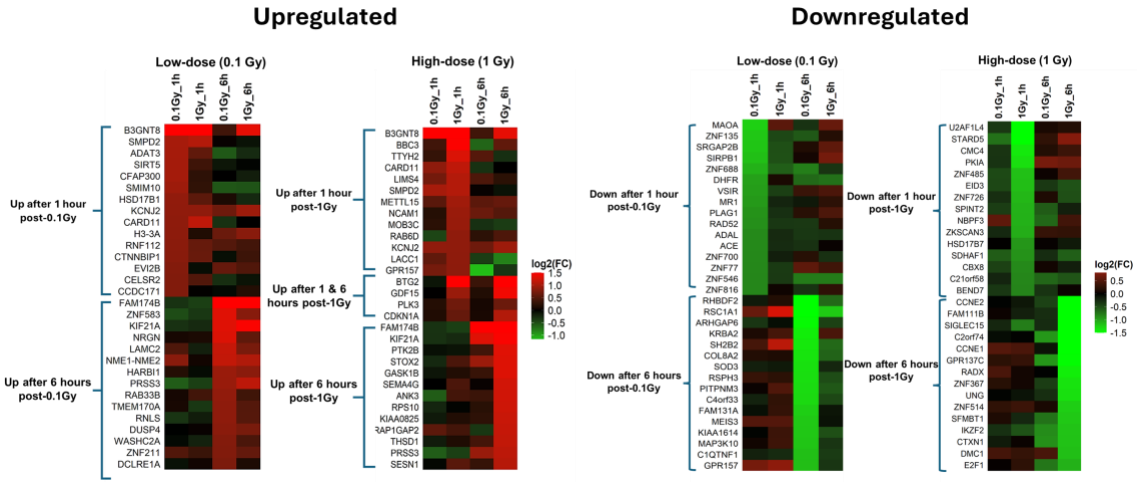

Figure 29) Heatmaps illustrating translational changes in upregulated and downregulated genes in HFL1 cells following IR

Heatmaps display dose- and time-dependent translational changes (log_2 fold change) in genes significantly affected following γ-irradiation. Color scale represents log_2 fold change (red = upregulated, green = downregulated). **A)** Upregulated genes after 0.1 Gy exposure. **B)** Upregulated genes after 1 Gy exposure. **C)** Downregulated genes after 0.1 Gy exposure. **D)** Downregulated genes after 1 Gy exposure. Data represent n = 3 independent biological replicates.

Table 14) Top 10 translationally upregulated transcripts following γ-irradiation

Rank	Gene	log_2 Fold Change	P-value
1 hour post- 0.1 Gy			
1	**B3GNT8**	1.5159	5.22×10^{-4}
2	**OPN1SW**	1.4941	1.22×10^{-3}
3	**CFAP300**	0.9972	1.02×10^{-3}
4	**SMPD2**	1.0054	1.12×10^{-2}
5	**ADAT3**	1.0041	9.38×10^{-3}
6	**CARD11**	0.8691	4.65×10^{-3}
7	**H3-3A**	0.8609	2.50×10^{-3}
8	**RNF112**	0.8449	9.91×10^{-4}
9	**EVI2B**	0.8032	1.92×10^{-4}
10	**MAP10**	0.7642	9.60×10^{-4}
1 hour post- 1Gy			
1	**ZNF585A**	1.2078	3.21E-06
2	**BTG2**	1.6708	3.39E-06
3	**GPR157**	0.8651	3.09E-05
4	**CDKN1A**	0.6189	4.06E-05
5	**ALDH3A2**	0.5354	5.72E-05
6	**ZBTB6**	0.4748	6.11E-05
7	**B3GNT8**	1.9344	9.19E-05
8	**SESN1**	0.5373	9.34E-05
9	**ATF3**	1.353	1.25E-04
10	**PAIP1**	0.3868	1.26E-04
6 hours post- 0.1 Gy			
1	**ZNF583**	1.3347	4.22E-05
2	**EMB**	0.6535	4.50E-05
3	**INTS9**	0.5945	5.13E-05
4	**ARNTL**	0.5899	8.57E-05
5	**WASHC2A**	0.8031	1.12E-04
6	**RAB33B**	0.8888	3.00E-04
7	**SLC45A1**	0.6199	3.55E-04
8	**ESM1**	0.6558	6.20E-04
9	**SORD**	0.6723	6.68E-04
10	**DNAJC25**	0.7565	8.01E-04
6 hours post- 1Gy			
1	**BTG2**	1.9539	7.32E-07
2	**SESN1**	1.1015	8.48E-07
3	**GDF15**	1.4225	2.22E-06
4	**MDM2**	1.0055	3.51E-06
5	**ZMAT3**	0.8691	5.56E-06
6	**CDKN1A**	1.0761	1.08E-05
7	**SLC45A1**	0.963	1.20E-05
8	**FRAS1**	0.9336	1.25E-05
9	**FAS**	0.7922	1.52E-05
10	**TRMT10B**	0.9335	2.66E-05

Table 15) Top 10 translationally downregulated transcripts following γ-irradiation

Rank	Gene	log_2 Fold Change	p-Value
1 hour post- 0.1 Gy			
1	**SHROOM4**	-1.4288	2.17E-06
2	**ZNF546**	-0.836	3.06E-06
3	**DENND1B**	-0.6311	1.08E-05
4	**IQCE**	-0.5975	2.48E-05
5	**RAD52**	-0.8905	2.76E-05
6	**MMD**	-0.5332	4.25E-05
7	**ZRANB3**	-0.4587	5.10E-05
8	**AASS**	-0.5395	5.87E-05
9	**PORCN**	-0.5513	7.07E-05
10	**IRX1**	-0.6111	9.17E-05
1hour post- 1Gy			
1	**CORO2A**	-1.0485	2.75E-06
2	**SDHAF1**	-0.9079	1.83E-05
3	**ABHD11**	-0.6557	2.35E-05
4	**SPINT2**	-1.0878	6.65E-05
5	**PCDH10**	-0.7352	1.18E-04
6	**DUSP22**	-0.5931	1.29E-04
7	**PNPLA3**	-1.3108	1.47E-04
8	**H3C11**	-0.4032	2.09E-04
9	**SMIM14**	-0.5651	2.35E-04
10	**TMEM80**	-0.7367	2.79E-04
6 hours post- 0.1 Gy			
1	**MTHFSD**	-0.9369	1.14E-05
2	**RHBDF2**	-1.7055	2.21E-05
3	**TMCO6**	-1.2847	2.36E-05
4	**CFAP46**	-1.5523	4.05E-05
5	**ZSCAN18**	-0.8419	5.21E-05
6	**PCDHGA9**	-0.8202	9.42E-05
7	**RSPH3**	-1.3253	9.69E-05
8	**FAM131A**	-1.2403	1.04E-04
9	**ZNF35**	-0.6228	1.23E-04
10	**ADCK2**	-1.0627	1.24E-04
6hours post- 1Gy			
1	**FAM111B**	-2.1076	6.18E-07
2	**CCNE2**	-2.6742	1.00E-06
3	**PRIM1**	-0.919	1.24E-06
4	**MCM10**	-0.9426	1.61E-06
5	**SFMBT1**	-1.2101	5.14E-06
6	**CCNE1**	-1.5341	6.90E-06
7	**SFI1**	-0.742	7.78E-06
8	**WDR76**	-0.8584	8.50E-06
9	**DTL**	-0.9589	9.57E-06
10	**UNG**	-1.3355	1.13E-05

3. 10 A subset of genes exhibits altered translation efficiency (TE) after γ-irradiation

Heatmaps were generated to visualize changes in TE at 1 and 6 hours following γ-irradiation with 0.1 Gy and 1 Gy, compared to non-irradiated controls **(Fig. 30, A-H).**

At 1 hour post-0.1 Gy, several transcripts indicated either enhanced or reduced translation efficiency. Interestingly, some genes with minimal changes at 1 hour showed increased translational activity by 6 hours, suggesting a delayed or sustained regulatory response. For example, RAB33B, a gene involved in vesicle trafficking and autophagy [186], showed a significant increase of TE at 6 hours post low-dose irradiation. Some transcripts showed a transient increase in TE at 1 hour post-0.1 Gy, followed by a decline at later timepoints or under high-dose conditions, indicating a tightly regulated, time-sensitive response.

Similarly, exposure to 1 Gy induced distinct, dose-specific and time-sensitive changes in TE as well. These included transcripts linked to apoptosis, DNA repair, and protein homeostasis, reflecting the more robust stress adaptation required under higher radiation burden.

These data provide the first detailed characterization of TE dynamics in HFL1 cells in response to both low- and high-dose γ-radiation, uncovering dose- and time-dependent post-transcriptional regulation within the translatome.

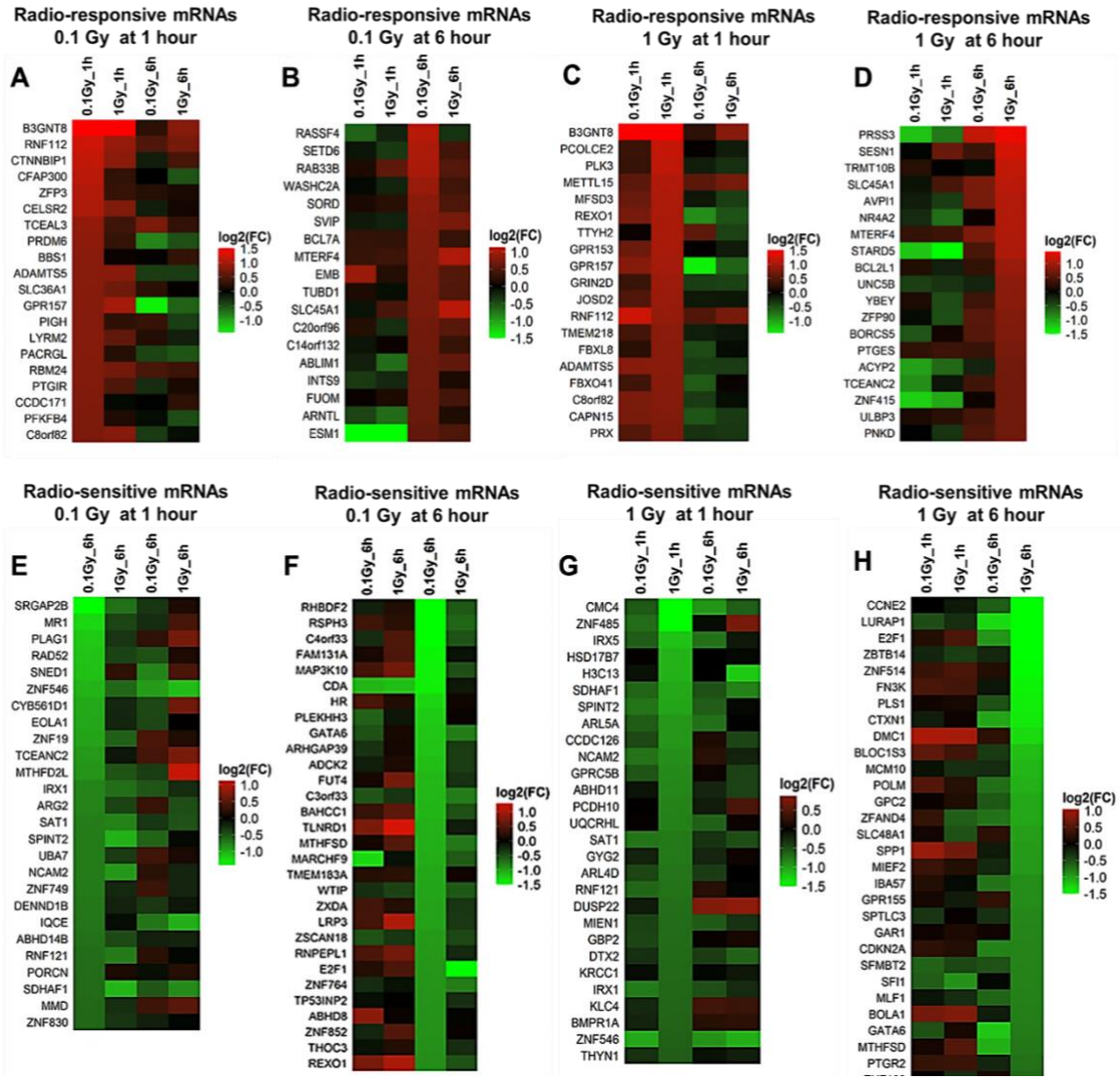

Figure 30) Heatmaps of transcript with altered TE following γ-irradiation

Heatmaps display $\log_2$ fold changes in TE for transcripts significantly affected by 0.1 Gy and 1 Gy γ-irradiation at 1- and 6-hours post-exposure, relative to non-irradiated controls. Increased TE is shown in red, decreased TE is shown in green, based on a $\log_2$ fold change and adjusted p-value < 0.02. **(A–D)** Transcripts with increased TE:

(A) 1 h post-0.1 Gy, **(B)** 6 h post-0.1 Gy, **(C)** 1 h post-1 Gy, **(D)** 6 h post-1 Gy. **(E–H)** Transcripts with decreased TE: **(E)** 1 h post-0.1 Gy, **(F)** 6 h post-0.1 Gy, **(G)** 1 h post-1 Gy, **(H)** 6 h post-1 Gy. Data represent n= 3 independent biological replicates.

Table 16) Top 10 transcripts with increased TE

Rank	Gene	log_2 Fold Change	p-value
1 hour post- 0.1 Gy			
2	**SLC36A1**	0.8236	0.001396
3	**RBM24**	0.7971	0.001738
4	**PIGH**	0.8103	0.001786
5	**COL15A1**	0.6366	0.002459
6	**ZFP3**	1.0723	0.002921
7	**PTER**	0.6727	0.00359
8	**LYRM2**	0.8093	0.003993
9	**GPD1L**	0.5861	0.004288
10	**GPR157**	0.8218	0.004561
1 hour post- 1Gy			
1	**TTYH2**	1.0249	0.000513
2	**ZNF585A**	1.4159	0.000753
3	**JOSD2**	0.931	0.000778
4	**RNF112**	0.9103	0.000932
5	**GRIN2D**	0.9491	0.001097
6	**PCOLCE2**	1.1854	0.001172
7	**PHYKPL**	0.7257	0.001338
8	**GPR157**	0.999	0.002071
9	**MFSD3**	1.0501	0.002171
10	**MARCHF4**	0.6412	0.002627
6 hours post- 0.1 Gy			
1	**EMB**	0.7521	0.001608
2	**WASHC2A**	0.9276	0.002222
3	**SLC29A3**	1.3127	0.00248
4	**INTS9**	0.6679	0.003279
5	**ARNTL**	0.6437	0.003289
6	**RAB33B**	1.0314	0.004295
7	**C20orf96**	0.6996	0.005334
8	**SLC45A1**	0.7413	0.006423
9	**ABLIM1**	0.6715	0.007567
10	**SVIP**	0.8058	0.008418
6hours post- 1Gy			
1	**STARD5**	1.0476	0.000491
2	**SLC45A1**	1.1237	0.001226
3	**TRMT10B**	1.1679	0.001309
4	**SESN1**	1.263	0.001315
5	**FRAS1**	0.9933	0.00165
6	**ZFP90**	0.7902	0.002293
7	**SLC29A3**	1.4314	0.002403
8	**NR4A2**	1.0735	0.004988
9	**MTERF4**	1.0604	0.00508
10	**ACYP2**	0.6973	0.006479

Table 17) Top 10 transcripts with decreased TE

Rank	Gene	log_2 Fold Change	p-value
1 hour post- 0.1 Gy			
1	**SHROOM4**	-1.646	0.00022
2	**ZNF546**	-1.0277	0.000242
3	**RAD52**	-1.1068	0.000876
4	**DENND1B**	-0.7017	0.001227
5	**MTHFD2L**	-0.8604	0.001313
6	**IQCE**	-0.6905	0.001376
7	**IRX1**	-0.7708	0.001494
8	**SPINT2**	-0.7271	0.001965
9	**MMD**	-0.6149	0.002354
10	**PORCN**	-0.6342	0.002388
1hour post- 1Gy			
1	**CORO2A**	-1.3443	3.87E-05
2	**SPINT2**	-1.0136	0.000376
3	**ABHD11**	-0.8359	0.000925
4	**SDHAF1**	-1.0316	0.001266
5	**NCAM2**	-0.8807	0.003009
6	**H3C13**	-1.0883	0.003582
7	**THYN1**	-0.5888	0.003708
8	**IRX1**	-0.6485	0.003721
9	**THAP9**	-0.5709	0.003764
10	**GYG2**	-0.7578	0.003897
6 hours post- 0.1 Gy			
1	**GATA6**	-1.1942	0.00015
2	**TMCO6**	-1.5649	0.00022
3	**RSPH3**	-1.5591	0.00029
4	**FUT4**	-1.1159	0.00046
5	**MTHFSD**	-1.0716	0.00055
6	**CFAP46**	-1.8691	0.00056
7	**WTIP**	-1.0166	0.00065
8	**RHBDF2**	-1.8867	0.00076
9	**ADCK2**	-1.1515	0.00102
10	**RNPEPL1**	-0.9429	0.00105
6hours post- 1Gy			
1	**PLS1**	-1.4108	0.00036
2	**LURAP1**	-2.4053	0.00134
3	**MCM10**	-1.11	0.00142
4	**ZBTB14**	-1.4985	0.00145
5	**SFI1**	-0.8117	0.00176
6	**GATA6**	-0.7774	0.00194
7	**FN3K**	-1.4356	0.00243
8	**GPR155**	-0.8755	0.00319
9	**GAR1**	-0.8276	0.00362
10	**PTGR2**	-0.7107	0.00374

3.11 Polysome profiling confirms stable global translation following γ-irradiation

While ribosome profiling technique offers high-resolution insights into translation dynamics, polysome profiling provides a complementary, classical approach to assess global translational activity. This method allows visualization of ribosome loading on mRNAs, offering a direct readout of translational engagement.

To validate the observed lack of change in global protein synthesis, polysome profiling was performed on irradiated HFL1 cell extracts collected 6 hours post-irradiation (**Fig. 31 A**). Cytoplasmic lysates from cells exposed to 0.1 Gy and 1 Gy doses were subjected to 10–50% sucrose gradient centrifugation, and ribosomal complexes were separated and analyzed by UV absorbance at 254 nm. Raw absorbance profiles were normalized by scaling the total area under the curve to a common value, allowing direct comparison of ribosome distribution across gradients and conditions.

Polysome profiles showed the expected distribution of ribosomal subunits (40S, 60S), monosomes (80S), and polysomes. While minor variations were noted between conditions, the overall monosome and polysome patterns remained comparable across irradiated samples (**Fig. 31 B**). These findings support our earlier observations of unchanged global protein synthesis rates, indicating that low-dose irradiation does not significantly perturb global translation in HFL1 cells under these experimental conditions.

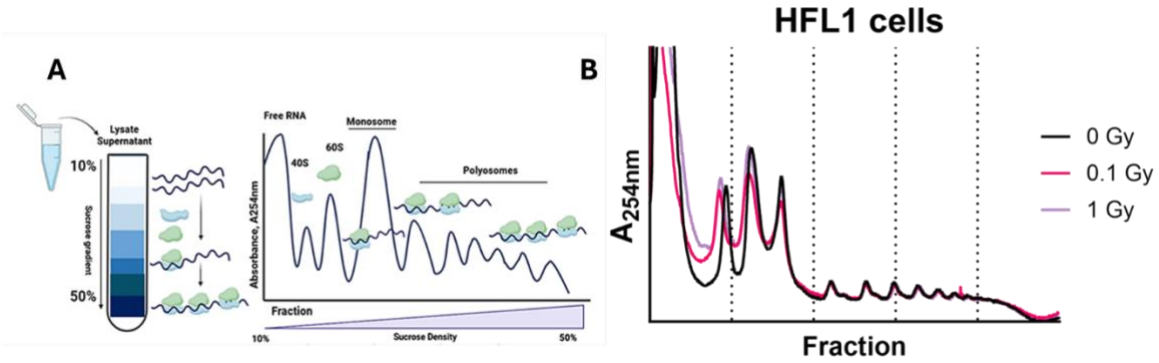

Figure 31) Polysome profiling of irradiated HFL1 cells at 6 hours post-irradiation

(A) Schematic representation of polysome profiling using 10–50% sucrose gradient centrifugation. Cytoplasmic extracts were layered onto the gradient and ultracentrifuged to separate free RNA, ribosomal subunits (40S and 60S), monosomes (80S), and polysomes. **(B)** Representative polysome profiles of HFL1 cells 6 hours after exposure to 0.1 Gy (magenta) and 1 Gy (purple) ionizing radiation. Absorbance at 254 nm was recorded across the gradient fractions. Polysome distribution patterns are similar between conditions, indicating no major shift in global translation activity. Absorbance profiles were normalized to total area under the curve to allow comparison of ribosome distribution across conditions.

3.12 RAB33B shows increased translation efficiency following low-dose γ-irradiation, independent of mRNA abundance

From the Ribo-Seq analysis, several candidate biomarkers were selected based on statistical significance (p-value), fold-change magnitude, and recurrence across datasets. Among these, RAB33B emerged as a top candidate, demonstrating significantly increased translation efficiency following low-dose γ-irradiation (fold change: 1.03; $p = 0.0043$ at 6 h post-0.1 Gy exposure). RAB33B was prioritized for further validation not only due to its robust translational upregulation but also because reliable commercial antibodies were available, making it a practical target for downstream protein-level confirmation by Western blot.

Following the initial polysome profiling analyses, the translational regulation of RAB33B in response to γ-irradiation was further examined. RT-qPCR was performed on sucrose gradient fractions obtained from HFL1 cells 6 hours post-irradiation with 0.1 Gy and 1 Gy. Luciferase RNA was spiked into each fraction to normalize technical variation.

The distribution of RAB33B mRNA showed a clear shift toward heavier polysome fractions (fractions with more polsyomes) in the low-dose (0.1 Gy) condition, indicating increased ribosome loading and enhanced translation (**Fig. 32 A**). In contrast, analysis of total RAB33B mRNA levels showed no significant difference between conditions (**Fig. 32 B**). Such observation suggests a change in TE rather than transcriptional activity. These results are consistent with the Ribo-Seq dataset, which identified RAB33B as a gene with significantly increased translation efficiency following low-dose γ-irradiation.

Together, these findings support the conclusion that exposure low-dose γ-rays induces selective translational reprogramming to facilitate early cellular adaptation.

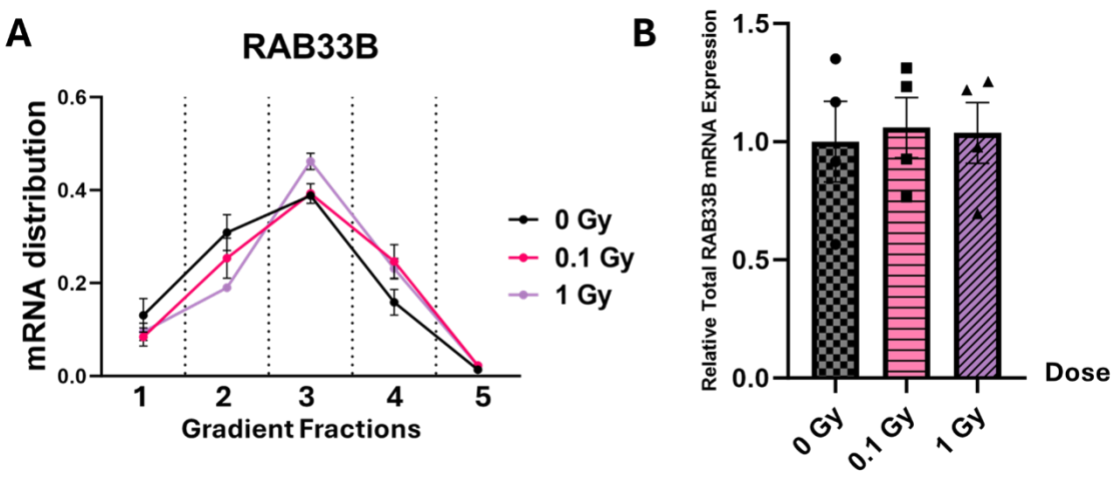

Figure 32) Analysis of RAB33B mRNA distribution and expression following γ-irradiation.

A) RAB33B mRNA distribution across gradient fractions was analyzed by RT-qPCR. Luciferase RNA, as an exogenous control, was spiked into each fraction to normalize recovery and technical variation. **B)** Total RAB33B mRNA levels were quantified from whole-cell lysates and normalized to GAPDH. Data are shown as mean ± SEM from three independent experiments using two-way ANOVA in panel A (mRNA distribution) and one-way ANOVA in panel B (total Total RAB33B mRNA), p=0.05.

3.13 RAB33B protein levels are selectively increased following ionizing radiation

To validate the enhanced translation of RAB33B suggested by polysome and Ribo-Seq data, RAB33B protein levels was examined by Western blot. Protein lysates were collected from HFL1 cells at 6 and 9 hours after exposure to 0, 0.1, or 1 Gy γ-irradiation. A modest increase was observed at 6 hours, but a clear and statistically significant upregulation of RAB33B protein was evident at 9 hours post-irradiation for both 0.1 and 1 Gy doses **(Fig. 33 A, B).**

To further explore the impact of dose and dose-rate, Western blot analysis was extended to include low-dose-rate (0.01, 0.05, and 0.1 Gy) and high-dose-rate (0.1, 0.5, 1, and 5 Gy) exposures. Protein lysates were collected at 6 and 9 hours post-irradiation. At 6 hours, no statistically significant increases in RAB33B protein were detected under low-dose-rate conditions. While high-dose-rate irradiation showed a trend toward increased RAB33B expression, statistical significance was only achieved at the highest dose of 5 Gy. Similarly, there was no significant increase in RAB33B expression under low-dose rate conditions at 9 hours, suggesting that dose-rate can be a confounder factor. These findings suggest that both total dose and dose rate influence induction of RAB33B protein.

These observations, along with the absence of corresponding changes in total mRNA levels and the observed increase in polysome association and protein abundance, support the conclusion that RAB33B is regulated primarily at the translational level in response to ionizing radiation.

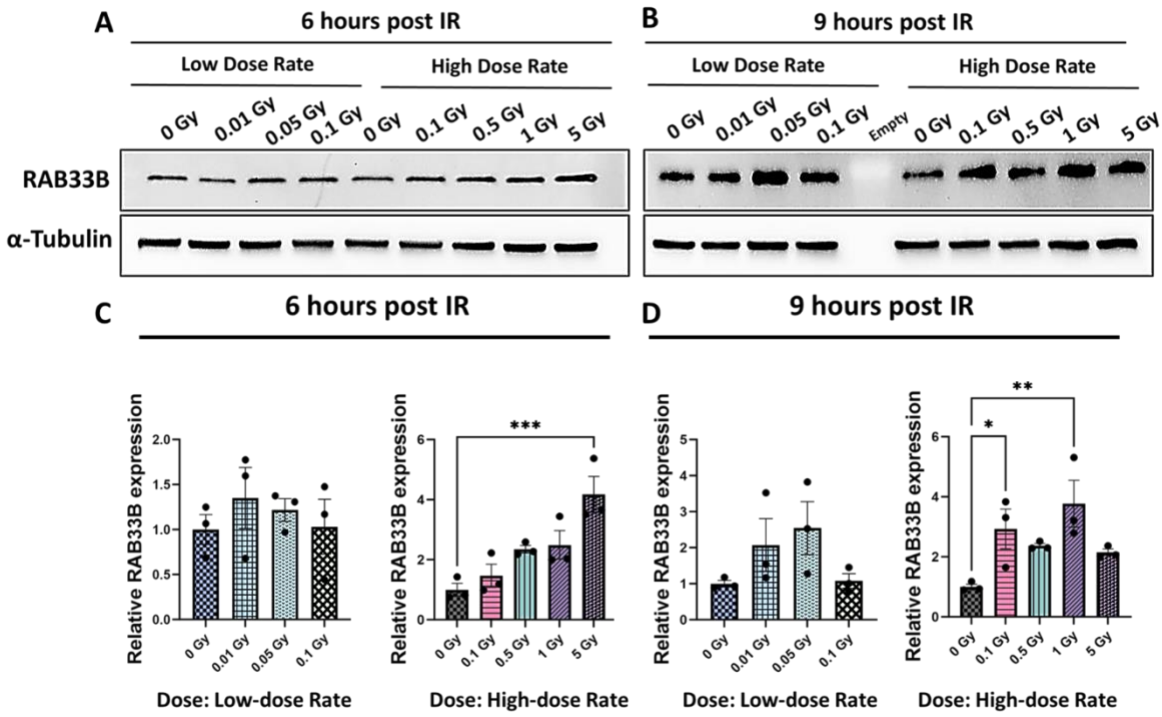

Figure 33) Western blot analysis of RAB33B expression post-IR

A-B) Representative Western blot images show RAB33B protein levels at different radiation doses and dose rates in two time points (6 hours and 9 hours). α-Tubulin was used as loading control to ensure equal protein loading. C-D) Quantification of relative RAB33B, normalized to tubulin and expressed relative to untreated controls. Bar graphs represent the mean ± SEM from at least three independent experiments ($n \geq 3$).

4: Discussion

Low-dose IR has been widely studied for its potential health effects, but the molecular mechanisms regulating the early cellular response remain poorly characterized. Recent advances in molecular biology have enabled high-resolution interrogation of gene expression at the level of translation, offering novel insights into cellular responses that may be missed by transcriptome-based approaches alone.

In this study, the effects of low-dose IR on the translatome of HFL1 human lung fibroblast cells were investigated using ribosome profiling, polysome fractionation, and complementary biochemical assays. The findings demonstrate that conventional transcriptome analysis alone does not fully capture the gene expression dynamics induced by low-dose IR. Instead, translational-level changes revealed a distinct layer of regulation, including selective ribosome engagement on specific mRNAs in the absence of corresponding changes in transcript abundance.

These findings highlight the importance of integrating translational profiling into radiation biology research, particularly at low doses, for a comprehensive evaluation of radiation-induced cellular responses. By focusing on translation efficiency and ribosome dynamics, this study provides new insights into the early molecular events triggered by low-dose IR and highlights the need to reevaluate current models of radiation-induced gene regulation.

4.1 Absence of global translation suppression suggests alternative regulatory mechanisms.

Despite the established role of cellular stress responses in suppressing global protein synthesis, no significant reduction in overall translation rates was observed following low-dose γ-irradiation in HFL1 cells. However, ribosome profiling at the transcript level revealed a nuanced yet significant reprogramming of the translational landscape in response to low-dose IR. These findings suggest that low-dose IR does not induce a broad shutdown of protein synthesis but rather promotes selective translation of specific mRNA subsets. In other words, only a specific subset of the mRNAs may be preferentially targeted by IR. How this may occur requires further investigation.

Mechanistically, this selective ribosome engagement raises important questions about the regulatory pathways involved. While ISR is a well-known regulator of translation under stress, no significant activation of the ISR was detected in this study. Similarly, key readouts of the mTORC1 pathway, a central regulator of growth and translation, remained unchanged following low-dose exposure.

One plausible explanation can be that ISR or mTORC1 activity may happen in a transient and low-amplitude manner, falling below the detection threshold of our experimental techniques and/or escaping the timepoints used in this study. Alternatively, low-dose IR may activate non-canonical or mRNA-specific mechanisms of translational control that bypass global pathway activation altogether.

These observations highlight the need for higher-resolution time-course experiments and broader pathway interrogation to fully shed light on the mechanisms driving this selective translational reprogramming.

4.2 Temporal dynamics of translational regulation and implications for biomarker discovery

The findings presented here suggest that the molecular response to IR is both time-dependent and dose-specific. As discussed in the introduction, while transcriptional induction and repression are slower and more long-lasting, post-transcriptional events, particularly translational regulation, happen within a few minutes [97]. For example, while the average transcription rate is two mRNA molecules per hour, the rate of protein synthesis can range from 180 to 1000 protein molecules per mRNA per hour [98]. Therefore, translational control operates on a time scale that is well-suited for managing the immediate adaptation or recovery phases following transient stress. In line with this, minimal changes were observed in the transcriptional response of HFL1 cells following 0.1 Gy exposure, yet several transcripts exhibited alterations in translational efficiency as early as one hour post-irradiation. These observations reinforce the concept that translation can function as a rapid-response regulatory mechanism, particularly under conditions where transcriptional modulation may be too slow to meet immediate cellular demands.

Importantly, cells must not only mount an effective stress response but also terminate it efficiently when no longer needed for maintaining maximal viability and reproductive fitness [97]. This requirement for tight temporal regulation makes the identification of IR-responsive biomarkers particularly challenging [173]. In this study, heatmap analysis showed that certain transcripts demonstrated early translational suppression followed by delayed upregulation, while others responded more immediately. This observation shows that the translation efficiency of these mRNAs is not only dose-dependent but also time-sensitive. It has been argued that the dose-time dynamics of

response have traditionally been ignored, leading to poor experimental reproducibility [187]. The findings presented here imply the need for precise temporal resolution in experimental design and biomarker discovery.

4.3 Gene-Pathway discrepancies highlight selective translational regulation

Pathway enrichment analysis indicated that low-dose γ-irradiation activated ion and carbohydrate transport processes (Fig. 25 A–B; Table 13). However, examining individual genes within these pathways showed that not all members follow the same trend.

For instance, SPINT2, a serine protease inhibitor important for epithelial sodium absorption [188], was translationally repressed (Fig. 30 E; Table 17), even though the broader ion transport pathway was enriched. Similarly, GATA6, a transcription factor that enhances glucose uptake via GLUT4 activation, was downregulated (Fig. 30 F; Table 17), despite the overall upregulation of carbohydrate/glucose transport pathways.[189].

These examples illustrate that one or two repressed genes cannot be taken as evidence against the pathway-level trend, since enrichment reflects the collective contribution of many transcripts. Instead, such discrepancies point to selective, transcript-specific regulation within otherwise activated pathways. It also poses challenges for functional validation, as phenotypic consequences may not be readily observed through single-gene knockouts or overexpression models, a limitation noted in previous studies [97]. This reinforces the value of genome-wide approaches like Ribo-seq, which can capture pathway-level complexity that would be missed if analysis focused only on a few genes [97].

4.3 Evidence of fine-tuned immune adaptation via translational control in response to low-dose γ-irradiation

While HFL1 cells showed minimal transcriptional changes in response to 0.1 Gy, translational regulation was substantially modified. Biological process enrichment analysis revealed an upregulation of immune response and ion transport pathways, possibly supporting cellular homeostasis. Although HFL1 fibroblasts are not immune cells, their role as lung-resident responders may explain their early stress response involving inflammatory signaling, cytokine secretion, and priming for tissue repair.

At 1 hour post-irradiation, translatome-level enrichment analysis suggested activation of immune-related pathways, including leukocyte differentiation, cell–cell adhesion, and T cell regulatory processes **(Fig. 25A)**. At the same time, certain pro-inflammatory pathways, such as interferon-gamma (IFN-γ) production, appeared downregulated **(Fig. 27A)**. This pattern may reflect a selective adjustment rather than a broad activation of immune functions. The observed suppression of IFN-γ translation alongside upregulation of other immune-associated processes could point to a post-transcriptional modulation where cells maintain readiness without fully engaging inflammatory programs. Similar patterns of immune "tuning" in response to low-dose γ-irradiation have been described previously [190, 191].

By 6 hours post low-dose γ-irradiation (0.1 Gy), translatome enrichment analysis showed a marked shift toward immune communication pathways. Specifically, leukocyte migration and interleukin-1 response were significantly upregulated, suggesting a role for fibroblasts in modulating the immune microenvironment. Leukocyte migration is a highly coordinated process governed by chemokines, adhesion molecules, and cytoskeletal

remodeling, and plays a key role in initiating immune surveillance and facilitating tissue repair [192]. The concurrent enhancement of interleukin-1 signaling implies that HFL1 fibroblasts, though not classified as immune cells, may function in a paracrine regulatory capacity, contributing to the early immune priming phase following stress. The autocrine or paracrine signaling of fibroblasts has been previously observed [193, 194]. This is particularly relevant in lung tissue, where fibroblasts serve as sentinel responders, capable of detecting damage and coordinating the recruitment of immune effectors such as macrophages and lymphocytes [194].

While these observations provide important insights into early stress responses in non-immune cells, further experimental validation is needed to confirm the functional relevance of these translational changes and to determine whether they translate into measurable effects on immune signaling, cytokine production, or cell-cell communication. Nevertheless, the results highlight translational regulation as a key control layer in low-dose radiation responses and suggest that immune tuning at the ribosomal level could be critical for balancing stress signaling and survival.

4.4. Translational control points toward metabolic adaptation under low-dose γ-irradiation

At 6 hours post-0.1 Gy, enrichment patterns suggested a shift from an immediate stress response toward a more sustained metabolic and immune adaptation phase. Specifically, pathways related to glucose and carbohydrate transport appeared upregulated. Low-dose radiation has been linked to metabolic reprogramming, where cells favor glycolysis over oxidative phosphorylation to maintain survival [49]. A possible

explanation is that although 0.1 Gy represents a low radiation dose, it can still induce mild oxidative stress through the generation of oxygen species (ROS), which are also byproducts of normal mitochondrial metabolism [81, 195]. Under such conditions, cells may adaptively shift toward glycolysis [196, 197]. In the heatmap data, increased translation efficiency was observed for several metabolism- and stress-associated genes, including SORD, B3GNT, RNF112, and MTERF4. These observations are consistent with the idea that metabolic adaptation may represent an important facet of the low-dose radiation response in fibroblasts. Interestingly, glycolysis is an ancient and evolutionarily conserved metabolic pathway, making it a reliable source of energy for organisms that evolved in the fluctuating environments of early Earth, where ionizing radiation levels were significantly higher [198].

4.5 Translational buffering may delay apoptosis and supports survival following high-dose irradiation

As expected, exposure to 1 Gy γ-irradiation was associated with rapid activation of transcriptional stress responses in HFL1 cells, including p53 signaling, DNA damage response, and apoptotic pathways **(Fig. 21 B)**. By 6 hours post-irradiation, these transcriptional changes intensified, with enriched processes related to cell death, autophagy, and cell cycle arrest, suggesting a progressive shift toward programmed cell death **(Fig. 21 C)**.

In contrast, the translatome showed a distinct and temporally regulated response. At 1 hour post-IR, translational enrichment was dominated by pathways involved in G1/S checkpoint control, DNA damage signaling, and amino acid starvation, which may reflect

an early emphasis on cell cycle arrest and metabolic conservation rather than immediate apoptosis **(Fig. 26 A)**. By 6 hours, the translational program appeared to shift toward proteostasis and protein quality control, including upregulation of ubiquitin-dependent protein catabolic processes, proteasomal degradation, and regulation of proteolysis **(Fig. 26 B)**. These observations are consistent with a cellular strategy of clearing damaged proteins and temporarily postponing commitment to apoptosis.

The divergence between transcriptomic and translatomic responses suggests that translational regulation serves as a buffering mechanism: by degrading misfolded or damaged proteins and channeling resources to repair processes, the cell can delay irreversible commitment to apoptosis and temporarily preserve viability. Similar transcriptome–translatome uncoupling after high-dose irradiation has been reported in previous studies [104, 106, 107]. Hence, our results support the idea that examining translational control at even higher radiation doses, as it provides valuable insights into the mechanisms regulating cellular radiosensitivity.

From a broader perspective, these findings raise the possibility that targeting early translational responses, such as protein quality control or amino acid stress pathways, to help extend cell survival following high-dose radiation exposure. By adjusting these early stress responses, it may be possible to develop treatments that protect tissues or to identify markers that predict delayed cell death. This could be especially useful in radiation therapy or emergency situations, where preserving healthy tissue in the early hours after exposure is critical.

Table 18) Summary Table: transcriptome vs. translatome response to 1 Gy γ-irradiation

Time-point	Direction	Translatome *Key Processes (Functional Category)*	Transcriptome *Key Processes (Functional Category)*	Overall Trend
1 h	**Up**	DNA-damage response, G1/S checkpoint, aminoglycan & carbohydrate biosynthesis *(DNA-Damage Response & Biosynthesis)*	p53 signalling, amino-acid-starvation response, apoptosis, DNA-damage signalling *(Apoptosis & Stress Signalling)*	Early activation of damage response and checkpoint signaling across both layers; transcription prioritizes apoptosis, while translation supports metabolic and checkpoint adjustments.
1 h	**Down**	Chromatin remodelling, nucleosome assembly, telomere organisation *(Chromatin Remodelling & Cell-Cycle Arrest)*	Cell-cycle regulation, mitotic checkpoint, DNA replication, spindle assembly *(Cell Cycle & DNA Synthesis)*	Coordinated repression of chromatin structure and cell cycle genes at both transcriptional and translational levels.
6 h	**Up**	Protein degradation, ubiquitin-proteasome system, general stress response *(Proteostasis & Stress Adaptation)*	Environmental-stimulus response, regulation of cell death, autophagy, antiviral response *(Cell Death, Autophagy*	Transition to late stress adaptation: translation enhances protein turnover; transcription promotes immune response and cell fate regulation.
6 h	**Down**	DNA replication, meiosis, cell-cycle checkpoints *(DNA Replication & Meiotic Regulation)*	DNA replication, telomere maintenance, G1/S transition, chromatin assembly *(Replication & Genome Stability)*	Persistent suppression of genome maintenance and replication functions, locking in long-term cell-cycle exit.

4.6 Dose rate influences translational outcomes

While many studies have focused on developing gene expression-based signatures in response to the absorbed radiation dose, the effects of dose rate are often overlooked [169, 199]. However, cellular protective mechanisms respond not only to dose but also to dose rate and the mode of delivery (acute stress or chronic stress) [13].

To investigate this, translation efficiency of RAB33B was assessed under low-dose conditions (0.01, 0.05, and 0.1 Gy) delivered at a low-dose-rate (0.0005 Gy/s) using Western blotting. By 9 hours post-irradiation, RAB33B protein expression remained unchanged across all tested doses under such condition.

These results propose that not only the total radiation dose but also the dose rate has the potential to significantly affect the translational outcomes, stressing the importance of incorporating both parameters when evaluating potential radiation-responsive and sensitive mRNAs. Therefore, taking dose rate into account is an important step in addressing the complexities of low-dose IR-induced responses.

4.7 RAB33B and autophagy: a potential adaptive axis in low-dose radiation response

Although no direct evidence currently links RAB33B regulation to IR exposure, it is well-established as a key player in autophagy and cellular stress resilience [186]. Autophagy is an important catabolic process by which cells digest and recycle damaged proteins and organelles, thereby generating energy and maintaining cellular homeostasis[200]. Since autophagy is a major mechanism of radiation survival [201], it is reasonable to hypothesize that RAB33B could play an adaptive and modulatory role during

the response to IR. also, heatmap data showed that RAB33B expression was upregulated alongside an enhancement in the translational efficiency of SVIP, a regulator of autophagy-related and endoplasmic reticulum (ER) stress pathways [202]. This co-expression may reflect a coordinated, fine-tuned adaptive response to low-dose radiation exposure.

4.8 Detection sensitivity and signal discrimination in low-dose IR studies

One limitation of the study is that low-dose radiation is inherently associated with responses close to detection thresholds, making it challenging to discern at the gene level which expression changes are truly driven by radiation and which reflect normal fluctuations (biological noise). Therefore, it is important to interpret with caution the genes classified as regulated by low-dose radiation, and future work will be necessary to refine the set of genes whose translation is genuinely responsive to it.

To distinguish biologically meaningful adaptive responses from passive fluctuations or background noise, future studies should adopt a multi-layered approach that integrates translational profiling with complementary temporal, proteomic, cellular, and functional analyses.

Time-course Ribo-seq would allow for the capture of transient or delayed translational events that may be missed in static snapshots. By including earlier (e.g., 30 min) and later (e.g., 12-24 h) time points in addition to the 1 h and 6 h profiles already examined, the temporal resolution of translational dynamics can be expanded. This would enable more precise classification of immediate-early, sustained, or secondary translational responses to low-dose irradiation.

Single-cell RNA-seq and translatomics (e.g., scRibo-seq or proximity ribosome profiling) could reveal heterogeneity in cellular responses that are masked in bulk analyses. This is particularly important under low-dose IR, where only a subset of cells may exhibit stress adaptation or damage signaling, and identifying these subpopulations could uncover key regulators of radiosensitivity.

Quantitative proteomics should be integrated to confirm that translational changes correspond to actual protein accumulation. Not all translated mRNAs produce stable or functional proteins; proteomic validation via mass spectrometry can establish which translation events lead to biologically meaningful outcomes.

Post-translational modifications (PTM) such as phosphorylation, ubiquitination, or acetylation often govern protein activation, localization, and degradation. PTM profiling, particularly phosphor-proteomics, would explain whether proteins induced translationally are also functionally activated.

Stress granule dynamics also offer insight into how translation is temporally regulated during stress [203]. Under irradiation, many transcripts are sequestered into stress granules, halting their translation temporarily. Some mRNAs may appear suppressed in Ribo-seq data simply because they are being stored rather than degraded. Profiling granule-associated RNAs or using imaging-based assays can help distinguish these cases from true repression.

Finally, for functional validation, tools such as luciferase reporter constructs and CRISPR-mediated gene perturbation (knockout, knockdown, or overexpression) can be directly tested to see whether candidate genes, such as RAB33B, contribute to adaptive outcomes like survival, autophagy, or delayed apoptosis.

Together, these approaches would provide a comprehensive framework to define true adaptive translational responses, refine radiation biomarkers, and uncover new targets for mitigating low-dose radiation effects. Nevertheless, in this study, the confirmation that RAB33B translation is modulated under low-dose conditions supports its classification as a genuine radiation-responsive target.

4.8 Model system limitations and future optimization

In this study, two-dimensional (2D) monolayer cultures of HFL1 cells were used as an *in vitro* model to assess radiation responses. This approach offers advantages such as low cost, simplicity, and high reproducibility. However, it also has limitations compared to *in vivo* models, including unnatural cell morphology, limited cell-to-cell communication, and uneven exposure of cells to nutrients or treatments [204].

To address these limitations, three-dimensional (3D) culture models such as organoids and organ-on-a-chip microfluidic (OCM) systems can be used for further Ribo-seq experiments. These advanced systems incorporate both cellular and non-cellular components, providing a better simulation of tissue architecture and the microenvironment [205]. Their ability to replicate key features of tissue structure and function, such as multicellular organization, extracellular matrix composition, and physiologically relevant gradients, allows for a more accurate representation of how human tissues respond to radiation. Consequently, they more closely mimic *in vivo* conditions while maintaining experimental control, enabling more reliable treatment response data and deeper insights into the biological consequences of low-dose radiation exposure [206, 207].

Several *in vivo* models have also been established to study radiation responses at the organismal level [208-210]. Murine models are the most widely used due to their genetic manipulability, well-characterized immune system, and availability of radiation-sensitive strains [211-213]. These models enable the evaluation of dose-rate effects, tissue-specific damage, and the role of systemic signaling in recovery or pathology. Zebrafish, with their optical transparency and rapid development, offer a high-throughput alternative for studying radiation-induced developmental and vascular defects, although their use in translational radiobiology remains more limited [214, 215]. For modeling human-specific responses, humanized mouse models engrafted with human hematopoietic or immune systems can simulate radiation effects on human-specific pathways, including immune suppression, cytokine storms, or bone marrow recovery [211, 216].

Together, these *in vivo* platforms provide a more comprehensive understanding of complex multicellular responses and play a pivotal role in validating *in vitro* findings and translating them into clinically meaningful applications.

4.9. Cell line-specific responses and the importance of model selection in radiobiology

It is well established that different cell lines and tissues exhibit varying responses and degrees of radiosensitivity [217-219]. Even among cells derived from the same histological type, considerable variability in radiation response can occur. Such differences may arise from variability in DNA repair capacity, cell cycle distribution, and microenvironmental context [220].

In this study, HFL1 cells, a human lung fibroblast line, were used to model pulmonary responses to low-dose IR. Fibroblasts play important roles in tissue repair, inflammation, and fibrosis; thus, understanding how they respond to low-dose IR has direct implications for both medical diagnosis and environmental exposure risk assessment. The human origin of the HFL1 cells enhances their relevance for modeling human-specific responses, making them widely used in toxicological studies [221-223]. However, their radiation response may not fully represent that of other lung-derived cell types. For instance, normal human bronchial epithelial cells exhibit less radiation-induced cell cycle arrest compared to HFL1 cells, likely due to their higher basal levels of p53 [224]. This stresses the importance of biologically relevant models in radiobiological research to ensure accurate prediction of radiation responses.

As a future direction, validating the translational responses identified in HFL1 cells using other lung-resident cell types, such as bronchial epithelial cells, alveolar macrophages, or endothelial cells, would help determine the cell-type specificity of observed effects. Incorporating co-culture systems or lung organoids may further recapitulate intercellular interactions and microenvironmental complexity. Additionally, applying single-cell RNA-seq or translatomic approaches could reveal heterogeneity in radiation responses within and across cell populations, enabling identification of rare but functionally important subpopulations involved in tissue adaptation, inflammation, or radiosensitivity.

4.10 Integrating multi-omics to uncover complex radiation responses

A comprehensive understanding of biological change requires investigation across multiple levels of organization, particularly focusing on how molecular alterations lead to

phenotypic outcomes that affect an organism's survival. A multiomics approach, which combines diverse data modalities such as gene expression, gene activation, and protein levels, offers a holistic view of molecular dynamics underlying cellular responses and disease mechanisms. These integrated datasets reveal genotype-to-phenotype links that single-omics studies often miss, illuminating novel biomarkers and targets that influence radiosensitivity in different cell lines and tissues [170, 225].

Extracting meaningful insights from such complex data demands advanced computational frameworks. Tools like Multi-Omics Factor Analysis (MOFA) capture shared and modality-specific sources of variation, aiding biological interpretation [226, 227]. Applying these integration strategies in future radiation-response studies promises more accurate characterization of dose- and dose-rate effects, ultimately improving risk assessment and therapeutic design.

4.11 Future directions: mechanisms of selective mRNA translation post low-dose IR

To better understand the mechanisms driving selective translation in response to low-dose γ-irradiation, future studies will focus on dissecting the regulatory features of translationally upregulated mRNAs through three complementary strategies.

4.11.1 Strategy 1: Cis-regulatory motif discovery and structural profiling

The first approach involves identifying conserved cis-regulatory elements and RNA structural motifs through in silico screening, using multiple sequence alignment and

motif discovery tools such as Clustal Omega and the MEME Suite. Particular attention will be given to elements such as AU-rich elements (AREs), which are known to regulate mRNA stability and degradation [228], and RNA G-quadruplexes, secondary structures that can modulate translation efficiency depending on their location and folding dynamics [229]. Pyrimidine-rich motifs, often enriched in stress-responsive transcripts, will also be analyzed within the 5′ and 3′ untranslated regions (UTRs) [230].

While RNA secondary structure will be predicted using the RNAfold platform, higher-resolution maps of RNA flexibility can be obtained using selective 2′-hydroxyl acylation analyzed by primer extension sequencing (SHAPE-seq) and dimethyl sulfate sequencing (DMS-seq), both of which provide nucleotide-resolution insights into RNA structural dynamics [231, 232].

Additional regulatory features, such as upstream open reading frames (uORFs), will be mapped using visualization tools like GWIPS-viz. The presence of internal ribosome entry sites (IRES elements) and G-quadruplexes within the 5′UTR will also be evaluated, given their roles in promoting cap-independent translation during stress [233]. In parallel, the influence of epitranscriptomic modifications, particularly m^6A, will be assessed due to their ability to alter mRNA structure, translation initiation, and ribosome recruitment. Many of these features are known to influence translation under stress conditions. For instance, uORFs are frequently used to mediate selective translation under stress conditions [107, 234], while m^6A modifications have been shown to promote cap-independent translation under oxidative or genotoxic stress [112]. Identifying the presence of these features in IR-responsive transcripts may uncover regulatory principles that allow specific

mRNAs to bypass global translational repression, supporting cell survival and adaptation following low-dose γ-irradiation.

4.11.2 Strategy 2: Trans-acting factor interrogation

To elucidate the trans-acting regulatory mechanisms influencing selective translation, RNA-binding protein (RBP) interaction profiling will be employed using high-resolution assays such as enhanced crosslinking and immunoprecipitation sequencing (eCLIP-seq) and RNA immunoprecipitation followed by sequencing (RIP-seq) [235, 236]. These methods enable transcriptome-wide identification of protein-RNA interactions, helping to uncover RBPs that associate with UTRs and influence mRNA fate.

In parallel, microRNA-mRNA interaction analyses will be performed using databases like TargetScan, miRDB, and miRTarBase to identify microRNAs that are predicted or experimentally confirmed to target the transcripts of interest [237-239].

CRISPR-Cas9 can be employed to evaluate the functional relevance of the identified trans-acting factors, for both loss-of-function and gain-of-function. Strategies will be used to selectively suppress or upregulate the expression of candidate RNA-binding proteins or microRNAs [240]. To determine whether post-transcriptional regulation is mediated through UTRs, luciferase reporter assays will be conducted using constructs harboring the 5′ and/or 3′ UTRs of these transcripts. This system enables quantification of translational effects conferred by specific UTR elements under controlled conditions [241]. Changes in reporter activity, either in the presence or absence of the regulatory factors or following exposure to low-dose IR, will help confirm whether the observed translational modulation is directly mediated via these UTRs and is sensitive to radiation-induced signaling pathways [242]. Such functional assays provide direct evidence linking molecular

interactions to phenotypic outcomes, reinforcing the mechanistic understanding of low-dose radiation responses at the translational level.

4.11.3 Strategy 3: Upstream signaling

To mechanistically dissect how upstream signaling pathways govern translational reprogramming following low-dose γ-irradiation, this strategy integrates quantitative phosphoproteomic profiling with pharmacological inhibition of key regulatory nodes.

Mass spectrometry-based phosphoproteomics will be employed to monitor dynamic phosphorylation changes in proteins involved in translation control, particularly within the mTORC1 and ISR pathways [243]. Parallel treatment with small-molecule inhibitors such as Torin1 (mTORC1 inhibitor) and ISRIB (ISR inhibitor) will enable functional interrogation of these pathways by identifying radiation-induced phosphorylation events that are sensitive to inhibition and correlate with changes in translational efficiency. This approach helps link specific signaling changes to selective translation of proteins, revealing how cells adjust protein production in response to low-dose stress.

Implementing these three strategies within an integrated multi-omics framework will generate a high-resolution map of the translational landscape under low-dose irradiation, clarify the hierarchy of regulatory events, and reveal actionable targets for radioprotection or radio-sensitization.

Table 19) Framework for dissecting mechanisms of translational regulation following low-dose γ-irradiation

Strategy	Focus Area	Methods & Tools	Key Targets	Purpose
1. Cis-regulatory motif discovery	Identification of RNA sequence/structural elements regulating translation	In silico analysis (Clustal Omega, MEME Suite) - RNAfold - SHAPE-seq, DMS-seq - GWIPS-viz - m⁶A prediction tools	AU-rich elements (AREs) - G-quadruplexes - Pyrimidine-rich motifs - uORFs, IRES elements - m⁶A sites	Discover RNA elements that enable selective translation despite global repression
2. Trans-acting factor interrogation	Mapping of protein–RNA and miRNA–mRNA interactions	eCLIP-seq, RIP-seq - TargetScan, miRDB, miRTarBase - CRISPR knockout/activation - Luciferase reporter assays	RBPs - microRNAs - UTR-dependent translation changes	Validate functional regulators that control translation of specific transcripts
3. Upstream signaling	Analysis of signaling pathways controlling translation	Phosphoproteomics (MS-based) - Drug inhibition (Torin1, ISRIB) - Ribo-seq correlation	mTORC1 - ISR (eIF2α pathway) - Phospho-sites on translation factors	Link signaling events to translational outputs

4.12 Conclusion

This study provides critical insight into the cellular adaptations that occur at the translational level in response to low-dose γ-irradiation. A central question emerging from these findings is why certain mRNAs exhibit enhanced translational efficiency despite minimal transcriptional changes. The selective activation of stress-responsive genes at the level of translation suggests an important layer of post-transcriptional regulation that may play a pivotal role in modulating cellular behavior under sub-lethal radiation exposure.

Understanding these mechanisms has broad and practical implications. In clinical settings, such as radiation therapy, improved knowledge of translation-level responses could enhance predictions of tissue sensitivity and support more precise radiation dosing strategies that minimize collateral damage to healthy tissue. In occupational health, where individuals such as nuclear medicine professionals, airline crew, or astronauts may face chronic low-dose radiation exposure, identifying translational biomarkers of early stress responses could inform personalized monitoring protocols or prophylactic interventions. Similarly, in environmental contexts where populations may be exposed to low-dose radiation from background sources or accidental releases, translational signatures could serve as sensitive early indicators of biological impact, even in the absence of overt symptoms or DNA damage.

Future studies should extend these findings by validating candidate mRNAs and proteins in more physiologically relevant models, including lung organoids, co-cultures with immune or epithelial cells, or whole-organism systems. These models will better recapitulate the complexity of the tissue microenvironment and intercellular signaling involved in real-world radiation responses. Ultimately, identifying universal versus tissue-

specific translational programs will deepen our understanding of radiation biology and guide the development of radioprotective countermeasures across therapeutic, occupational, and public health domains.

5: References

1. Mould, R.F., *The early history of x-ray diagnosis with emphasis on the contributions of physics 1895-1915.* Physics in Medicine & Biology, 1995. **40**(11): p. 1741.
2. Lee, B.Q., et al., *Atomic radiations in the decay of medical radioisotopes: a physics perspective.* Comput Math Methods Med, 2012. **2012**: p. 651475.
3. Fisher, D.R. and F.H. Fahey, *Appropriate Use of Effective Dose in Radiation Protection and Risk Assessment.* Health Phys, 2017. **113**(2): p. 102-109.
4. ICRP, *Use of dose quantities in radiological protection. ICRP Publication 147.* Ann ICRP, 2021. **50**(1): p. 1-82.
5. UNSCEAR-Annex, A., *Attributing health effects to ionizing radiation exposure and inferring risks.* Sources and effects of Ionizing Radiation: UNSCEAR, 2012: p. 1-92.
6. Rühm, W., D. Laurier, and R. Wakeford, *Cancer risk following low doses of ionising radiation–Current epidemiological evidence and implications for radiological protection.* Mutation Research/Genetic Toxicology and Environmental Mutagenesis, 2022. **873**: p. 503436.
7. Harrison, J.D., et al., *Low doses of ionising radiation: definitions and contexts.* Journal of Radiological Protection, 2024. **44**(4): p. 043003.
8. Gao, L. and A. Zhang, *Low-dose radiotherapy effects the progression of anti-tumor response.* Translational Oncology, 2023. **35**: p. 101710.
9. Dove, A.P.H., et al., *The Use of Low-Dose Radiation Therapy in Osteoarthritis: A Review.* International Journal of Radiation Oncology, Biology, Physics, 2022. **114**(2): p. 203-220.
10. Radiation, U.N.S.C.o.t.E.o.A. and C. Annex, *Biological mechanisms relevant for the inference of cancer risks from low-dose and low-dose-rate radiation.* Vienna: UNSCEAR, 2021.
11. Protection, R., *ICRP publication 103.* Ann ICRP, 2007. **37**(2.4): p. 2.
12. Hall, E.J., *Radiobiology for the radiologist*. 1973: Hagerstown, Md. : Medical Dept., Harper & Row, [1973] ©1973.
13. Brooks, A.L., D.G. Hoel, and R.J. Preston, *The role of dose rate in radiation cancer risk: evaluating the effect of dose rate at the molecular, cellular and tissue levels using key events in critical pathways following exposure to low LET radiation.* Int J Radiat Biol, 2016. **92**(8): p. 405-26.
14. Rühm, W., et al., *Dose and dose-rate effects of ionizing radiation: a discussion in the light of radiological protection.* Radiation and environmental biophysics, 2015. **54**: p. 379-401.
15. Blakely, E.A., *Biological Effects of Cosmic Radiation: Deterministic and Stochastic.* Health Physics, 2000. **79**(5).
16. Choudhary, S., *Deterministic and stochastic effects of radiation.* Cancer Therapy & Oncology International Journal, 2018. **12**(2): p. 31-32.
17. Fry, R.J.M., *DETERMINISTIC EFFECTS.* Health Physics, 2001. **80**(4).
18. Ainsbury, E.A., et al., *Ionizing radiation induced cataracts: Recent biological and mechanistic developments and perspectives for future research.* Mutation Research/Reviews in Mutation Research, 2016. **770**: p. 238-261.
19. Fornalski, K.W., L. Dobrzynski, and M.K. Janiak, *A Stochastic Markov Model of Cellular Response to Radiation.* Dose-Response, 2011. **9**(4): p. dose-response.11-003.Fornalski.

20. Kamiya, K., et al., *Long-term effects of radiation exposure on health.* The Lancet, 2015. **386**(9992): p. 469-478.
21. Baverstock, K. and A.V. Karotki, *Towards a unifying theory of late stochastic effects of ionizing radiation.* Mutation Research/Genetic Toxicology and Environmental Mutagenesis, 2011. **718**(1): p. 1-9.
22. Romanenko, A.Y., et al., *The Ukrainian-American study of leukemia and related disorders among Chornobyl cleanup workers from Ukraine: III. Radiation risks.* Radiation research, 2008. **170**(6): p. 711-720.
23. Radiation, U.N.S.C.o.t.E.o.A., *Sources, Effects and Risks of Ionizing Radiation – UNSCEAR 2020 Report*. 2022, United Nation: New York.
24. Boice Jr, J.D., *Radiation epidemiology: a perspective on Fukushima.* Journal of Radiological Protection, 2012. **32**(1): p. N33.
25. Satyamitra, M.M., et al., *Development of Biomarkers for Radiation Biodosimetry and Medical Countermeasures Research: Current Status, Utility, and Regulatory Pathways.* Radiat Res, 2022. **197**(5): p. 514-532.
26. Domina, E.A. and O.L. Kopylenko, *ROLE OF RADIOPROTECTORS IN MINIMIZATION OF STOCHASTIC EFFECTS OF RADIATION INCIDENTS.* Exp Oncol, 2022. **44**(3): p. 186-189.
27. Brenner, D.J., et al., *Cancer risks attributable to low doses of ionizing radiation: Assessing what we really know.* Proceedings of the National Academy of Sciences, 2003. **100**(24): p. 13761-13766.
28. Muller, H.J., *The Measurement of Gene Mutation Rate in Drosophila, Its High Variability, and Its Dependence upon Temperature.* Genetics, 1928. **13**(4): p. 279-357.
29. Preston, D.L., et al., *Solid cancer incidence in atomic bomb survivors: 1958-1998.* Radiat Res, 2007. **168**(1): p. 1-64.
30. Pearce, M.S., et al., *Radiation exposure from CT scans in childhood and subsequent risk of leukaemia and brain tumours: a retrospective cohort study.* Lancet, 2012. **380**(9840): p. 499-505.
31. Azzam, E.I., et al., *Is Ionizing Radiation Harmful at any Exposure? An Echo That Continues to Vibrate.* Health Physics, 2016. **110**(3): p. 249-251.
32. Doss, M., *Future of Radiation Protection Regulations.* Health Physics, 2016. **110**(3): p. 274-275.
33. Tubiana, M., et al., *The Linear No-Threshold Relationship Is Inconsistent with Radiation Biologic and Experimental Data.* Radiology, 2009. **251**(1): p. 13-22.
34. Tharmalingam, S., et al., *Re-evaluation of the linear no-threshold (LNT) model using new paradigms and modern molecular studies.* Chemico-Biological Interactions, 2019. **301**: p. 54-67.
35. Tanooka, H., *Threshold dose–response in radiation carcinogenesis: an approach from chronic β-irradiation experiments and a review of non-tumour doses.* International journal of radiation biology, 2001. **77**(5): p. 541-551.
36. Kathren, R.L., *Pathway to a paradigm: the linear nonthreshold dose-response model in historical context: the American Academy of Health Physics 1995 Radiology Centennial Hartman Oration.* Health Physics, 1996. **70**(5): p. 621-635.
37. Schaeffer, D.J., K.G. Janardan, and H.W. Kerster, *Threshold estimation from the linear dose-response model: Method and radiation data.* Environmental Management, 1981. **5**(6): p. 515-520.
38. Leblanc, J.E. and J.J. Burtt, *Radiation Biology and Its Role in the Canadian Radiation Protection Framework.* Health Physics, 2019. **117**(3): p. 319-329.

39. Scott, B.R., *Stochastic thresholds: a novel explanation of nonlinear dose-response relationships for stochastic radiobiological effects.* Dose Response, 2006. **3**(4): p. 547-67.
40. Osipov, A.N., et al., *In vivo γ-irradiation low dose threshold for suppression of DNA double strand breaks below the spontaneous level in mouse blood and spleen cells.* Mutation Research/Genetic Toxicology and Environmental Mutagenesis, 2013. **756**(1): p. 141-145.
41. Tubiana, M., et al., *Dose-effect relationships and the estimation of the carcinogenic effects of low doses of ionizing radiation.* Academy of Medicine (Paris) and Academy of Science (Paris) Joint Report, 2005(2).
42. Calabrese, V., et al., *Cellular stress responses, the hormesis paradigm, and vitagenes: novel targets for therapeutic intervention in neurodegenerative disorders.* Antioxid Redox Signal, 2010. **13**(11): p. 1763-811.
43. Yanagawa, T. and H. Fukunaga, *Random Threshold Model: A Low-Dose Radiation-Induced Risk Assessment Approach Considering Individual Susceptibility to Cancer.* Dose-Response, 2024. **22**(4): p. 15593258241298553.
44. Heidenreich, W.F., H.G. Paretzke, and P. Jacob, *No evidence for increased tumor rates below 200 mSv in the atomic bomb survivors data.* Radiation and environmental biophysics, 1997. **36**: p. 205-207.
45. Breckow, J., *Linear-no-threshold is a radiation-protection standard rather than a mechanistic effect model.* Radiation and environmental biophysics, 2006. **44**(4): p. 257-260.
46. Preston, D.L., et al., *Effect of recent changes in atomic bomb survivor dosimetry on cancer mortality risk estimates.* Radiation research, 2004. **162**(4): p. 377-389.
47. Olivieri, G., J. Bodycote, and S. Wolff, *Adaptive response of human lymphocytes to low concentrations of radioactive thymidine.* Science, 1984. **223**(4636): p. 594-597.
48. Youngblom, J.H., J.K. Wiencke, and S. Wolff, *Inhibition of the adaptive response of human lymphocytes to very low doses of ionizing radiation by the protein synthesis inhibitor cycloheximide.* Mutation Research Letters, 1989. **227**(4): p. 257-261.
49. Lall, R., et al., *Low-dose radiation exposure induces a HIF-1-mediated adaptive and protective metabolic response.* Cell Death & Differentiation, 2014. **21**(5): p. 836-844.
50. Kojima, S., et al., *Treatment of Cancer and Inflammation With Low-Dose Ionizing Radiation:Three Case Reports.* Dose-Response, 2017. **15**(1): p. 1559325817697531.
51. Schirrmacher, V., *Less Can Be More: The Hormesis Theory of Stress Adaptation in the Global Biosphere and Its Implications.* Biomedicines, 2021. **9**(3).
52. Tapio, S. and V. Jacob, *Radioadaptive response revisited.* Radiation and Environmental Biophysics, 2007. **46**(1): p. 1-12.
53. Thathamangalam Ananthanarayanan, A., et al., *Insights on the Radiation-Induced Adaptive Response at the Cellular Level and Its Implications in Cancer Therapy.* Cytogenetic and Genome Research, 2023. **163**(5-6): p. 257-273.
54. Nenoi, M., B. Wang, and G. Vares, *In vivo radioadaptive response: a review of studies relevant to radiation-induced cancer risk.* Hum Exp Toxicol, 2015. **34**(3): p. 272-83.
55. Wolff, S., et al., *Indications of repair of radon-induced chromosome damage in human lymphocytes: an adaptive response induced by low doses of X-rays.* Environmental Health Perspectives, 1993. **101**(suppl 3): p. 73-77.
56. Hyun, S.J., et al., *Enhancement of mitogen-stimulated proliferation of low dose radiation-adapted mouse splenocytes.* Anticancer research, 1997. **17**(1A): p. 225-229.

57. Otsuka, K., et al., *Activation of Antioxidative Enzymes Induced by Low-Dose-Rate Whole-Body γ Irradiation: Adaptive Response in Terms of Initial DNA Damage.* Radiation Research, 2006. **166**(3): p. 474-478.
58. Kryston, T.B., et al., *Role of oxidative stress and DNA damage in human carcinogenesis.* Mutat Res, 2011. **711**(1-2): p. 193-201.
59. Hanahan, D. and R.A. Weinberg, *The Hallmarks of Cancer.* Cell, 2000. **100**(1): p. 57-70.
60. Vasireddy, R.S., et al., *H2AX phosphorylation screen of cells from radiosensitive cancer patients reveals a novel DNA double-strand break repair cellular phenotype.* British Journal of Cancer, 2010. **102**(10): p. 1511-1518.
61. Noubissi, F.K., et al., *Detection and quantification of γ-H2AX using a dissociation enhanced lanthanide fluorescence immunoassay.* Scientific Reports, 2021. **11**(1): p. 8945.
62. Chang, H.H.Y., et al., *Non-homologous DNA end joining and alternative pathways to double-strand break repair.* Nature Reviews Molecular Cell Biology, 2017. **18**(8): p. 495-506.
63. Shibata, A. and P.A. Jeggo, *DNA Double-strand Break Repair in a Cellular Context.* Clinical Oncology, 2014. **26**(5): p. 243-249.
64. Nickoloff, J.A., et al., *Exploiting DNA repair pathways for tumor sensitization, mitigation of resistance, and normal tissue protection in radiotherapy.* Cancer Drug Resist, 2021. **4**(2): p. 244-263.
65. Belov, O., et al. *Dose-Dependent Shift in Relative Contribution of Homologous Recombination to DNA Repair after Low-LET Ionizing Radiation Exposure: Empirical Evidence and Numerical Simulation*. Current issues in molecular biology, 2023. **45**, 7352-7373 DOI: 10.3390/cimb45090465.
66. Boreham, D.R., et al., *The Adaptive Response and Protection against Heritable Mutations and Fetal Malformation.* Dose-Response, 2006. **4**(4): p. dose-response.06-104.Boreham.
67. Taylor, K., J.A. Lemon, and D.R. Boreham, *Radiation-induced DNA damage and the relative biological effectiveness of 18F-FDG in wild-type mice.* Mutagenesis, 2014. **29**(4): p. 279-287.
68. Pollycove, M. and L.E. Feinendegen, *Radiation-induced versus endogenous DNA damage: possible effect of inducible protective responses in mitigating endogenous damage.* Human & Experimental Toxicology, 2003. **22**(6): p. 290-306.
69. Feinendegen, L.E., M. Pollycove, and R.D. Neumann, *Whole-body responses to low-level radiation exposure: New concepts in mammalian radiobiology.* Experimental Hematology, 2007. **35**(4, Supplement): p. 37-46.
70. Pereira, S., et al., *Genotoxicity of acute and chronic gamma-irradiation on zebrafish cells and consequences for embryo development.* Environmental Toxicology and Chemistry, 2011. **30**(12): p. 2831-2837.
71. Simon, O., et al., *Investigating the embryo/larval toxic and genotoxic effects of γ irradiation on zebrafish eggs.* Journal of Environmental Radioactivity, 2011. **102**(11): p. 1039-1044.
72. Baudin, C., et al., *Biomarkers of Genotoxicity in Medical Workers Exposed to Low-Dose Ionizing Radiation: Systematic Review and Meta-Analyses.* Int J Mol Sci, 2021. **22**(14).
73. Blimkie, M.S., et al., *Repair of DNA double-strand breaks is not modulated by low-dose gamma radiation in C57BL/6J mice.* Radiat Res, 2014. **181**(5): p. 548-59.
74. Toprani, S.M., et al., *Suppressed DNA repair capacity in flight attendants after air travel.* Scientific Reports, 2025. **15**(1): p. 16513.

75. Toprani, S.M., C. Scheibler, and Z.D. Nagel, *Interplay between air travel, genome integrity, and COVID-19 risk vis-a-vis flight crew.* Frontiers in Public Health, 2020. **8**: p. 590412.
76. Heylmann, D., et al., *Comparison of DNA repair and radiosensitivity of different blood cell populations.* Scientific reports, 2021. **11**(1): p. 2478.
77. Averbeck, D., et al., *Establishing mechanisms affecting the individual response to ionizing radiation.* International Journal of Radiation Biology, 2020. **96**(3): p. 297-323.
78. Cologne, J., et al., *Chromosome aberrations among atomic-bomb survivors exposed in utero: updated analysis accounting for revised radiation doses and smoking.* Radiation and Environmental Biophysics, 2022. **61**(1): p. 59-72.
79. Bauchinger, M., *Quantification of low-level radiation exposure by conventional chromosome aberration analysis.* Mutation Research/Reviews in Genetic Toxicology, 1995. **339**(3): p. 177-189.
80. Kam, W.W.-Y. and R.B. Banati, *Effects of ionizing radiation on mitochondria.* Free Radical Biology and Medicine, 2013. **65**: p. 607-619.
81. Azzam, E.I., J.P. Jay-Gerin, and D. Pain, *Ionizing radiation-induced metabolic oxidative stress and prolonged cell injury.* Cancer Lett, 2012. **327**(1-2): p. 48-60.
82. Murphy, Michael P., et al., *Unraveling the Biological Roles of Reactive Oxygen Species.* Cell Metabolism, 2011. **13**(4): p. 361-366.
83. Jones, D.P., *Redefining oxidative stress.* Antioxidants & redox signaling, 2006. **8**(9-10): p. 1865-1879.
84. Ramana, C.V., et al., *Activation of apurinic/apyrimidinic endonuclease in human cells by reactive oxygen species and its correlation with their adaptive response to genotoxicity of free radicals.* Proceedings of the National Academy of Sciences, 1998. **95**(9): p. 5061-5066.
85. Feinendegen, L.E., et al., *Intracellular Stimulation of Biochemical Control Mechanisms by Low-dose, Low-let Irradiation.* Health Physics, 1987. **52**(5): p. 663-669.
86. Iyer, R. and B.E. Lehnert, *Low dose, low-LET ionizing radiation-induced radioadaptation and associated early responses in unirradiated cells.* Mutat Res, 2002. **503**(1-2): p. 1-9.
87. de Toledo, S.M., et al., *Adaptive responses to low-dose/low-dose-rate gamma rays in normal human fibroblasts: the role of growth architecture and oxidative metabolism.* Radiat Res, 2006. **166**(6): p. 849-57.
88. Einor, D., et al., *Ionizing radiation, antioxidant response and oxidative damage: A meta-analysis.* Science of The Total Environment, 2016. **548-549**: p. 463-471.
89. Menon, S.S., et al., *Radiation Metabolomics: Current Status and Future Directions.* Frontiers in Oncology, 2016. **Volume 6 - 2016**.
90. Chen, Z.D., et al., *Rapid and High-Throughput Detection and Quantitation of Radiation Biomarkers in Human and Nonhuman Primates by Differential Mobility Spectrometry-Mass Spectrometry.* Journal of the American Society for Mass Spectrometry, 2016. **27**(10): p. 1626-1636.
91. Guo, L., et al., *Long-term low-dose ionizing radiation induced chromosome-aberration-specific metabolic phenotype changes in radiation workers.* Journal of Pharmaceutical and Biomedical Analysis, 2022. **214**: p. 114718.
92. Jiang, C., et al., *Dynamic Human Environmental Exposome Revealed by Longitudinal Personal Monitoring.* Cell, 2018. **175**(1): p. 277-291.e31.
93. Laiakis, E.C., et al., *A Serum Small Molecule Biosignature of Radiation Exposure from Total Body Irradiated Patients.* Journal of Proteome Research, 2017. **16**(10): p. 3805-3815.

94. Gasch, A.P., et al., *Genomic expression programs in the response of yeast cells to environmental changes.* Mol Biol Cell, 2000. **11**(12): p. 4241-57.
95. Causton, H.C., et al., *Remodeling of yeast genome expression in response to environmental changes.* Mol Biol Cell, 2001. **12**(2): p. 323-37.
96. Zhong, Q., et al., *Protein posttranslational modifications in health and diseases: Functions, regulatory mechanisms, and therapeutic implications.* MedComm (2020), 2023. **4**(3): p. e261.
97. Hernández-Elvira, M. and P. Sunnerhagen, *Post-transcriptional regulation during stress.* FEMS Yeast Res, 2022. **22**(1).
98. Schwanhäusser, B., et al., *Global quantification of mammalian gene expression control.* Nature, 2011. **473**(7347): p. 337-342.
99. Chen, D., et al., *Global transcriptional responses of fission yeast to environmental stress.* Mol Biol Cell, 2003. **14**(1): p. 214-29.
100. Ruis, H. and F. Estruch, *The Saccharomyces cerevisiae zinc nger proteins Msn2p and Msn4p are required for transcriptional induction through the stress response element (STRE).* EMBO J, 1996. **15**: p. 22272235Peterbauer.
101. Brown, A.J.P., D.E. Larcombe, and A. Pradhan, *Thoughts on the evolution of Core Environmental Responses in yeasts.* Fungal Biology, 2020. **124**(5): p. 475-481.
102. Jorgensen, P., et al., *A dynamic transcriptional network communicates growth potential to ribosome synthesis and critical cell size.* Genes & development, 2004. **18**(20): p. 2491-2505.
103. Semchyshyn, H.M., *Hormetic Concentrations of Hydrogen Peroxide but Not Ethanol Induce Cross-Adaptation to Different Stresses in Budding Yeast.* International journal of microbiology, 2014. **2014**(1): p. 485792.
104. Birrell, G.W., et al., *Transcriptional response of Saccharomyces cerevisiae to DNA-damaging agents does not identify the genes that protect against these agents.* Proc Natl Acad Sci U S A, 2002. **99**(13): p. 8778-83.
105. Thorpe, G.W., et al., *Cells have distinct mechanisms to maintain protection against different reactive oxygen species: oxidative-stress-response genes.* Proceedings of the National Academy of Sciences, 2004. **101**(17): p. 6564-6569.
106. Lü, X., et al., *Radiation-Induced Changes in Gene Expression Involve Recruitment of Existing Messenger RNAs to and away from Polysomes.* Cancer Research, 2006. **66**(2): p. 1052-1061.
107. Hou, J., et al., *Ribosome profiling reveals dynamic translational landscape following X-ray irradiation.* Genomics, 2025. **117**(2): p. 110987.
108. Yang, H. and L. Lan, *Transcription-coupled DNA repair protects genome stability upon oxidative stress-derived DNA strand breaks.* FEBS Letters, 2025. **599**(2): p. 168-176.
109. Zhao, B.S., I.A. Roundtree, and C. He, *Post-transcriptional gene regulation by mRNA modifications.* Nature reviews Molecular cell biology, 2017. **18**(1): p. 31-42.
110. He, P.C. and C. He, *m6A RNA methylation: from mechanisms to therapeutic potential.* The EMBO journal, 2021. **40**(3): p. e105977.
111. Murakami, S., et al., *A alters ribosome dynamics to initiate mRNA degradation.* Cell.
112. Zhou, J., et al., *Dynamic m6A mRNA methylation directs translational control of heat shock response.* Nature, 2015. **526**(7574): p. 591-594.
113. Kumari, S., et al., *An RNA G-quadruplex in the 5′ UTR of the NRAS proto-oncogene modulates translation.* Nature chemical biology, 2007. **3**(4): p. 218-221.
114. Guo, J.U. and D.P. Bartel, *RNA G-quadruplexes are globally unfolded in eukaryotic cells and depleted in bacteria.* Science, 2016. **353**(6306): p. aaf5371.

115. Benhalevy, D., et al., *The human CCHC-type zinc finger nucleic acid-binding protein binds G-rich elements in target mRNA coding sequences and promotes translation.* Cell reports, 2017. **18**(12): p. 2979-2990.
116. Fleming, A.M., et al., *Rates of chemical cleavage of DNA and RNA oligomers containing guanine oxidation products.* Chemical research in toxicology, 2015. **28**(6): p. 1292-1300.
117. Stolc, V., et al., *RNA–DNA Differences: Mechanisms, Oxidative Stress, Transcriptional Fidelity, and Health Implications.* Antioxidants, 2025. **14**(5): p. 544.
118. Taylor, K.E., L.G. Miller, and L.M. Contreras, *RNA-binding proteins that preferentially interact with 8-oxoG-modified RNAs: our current understanding.* Biochemical Society Transactions, 2024. **52**(1): p. 111-122.
119. Simms, C.L., E.N. Thomas, and H.S. Zaher, *Ribosome-based quality control of mRNA and nascent peptides.* WIREs RNA, 2017. **8**(1): p. e1366.
120. Powers, K.T., J.-Y.A. Szeto, and C. Schaffitzel, *New insights into no-go, non-stop and nonsense-mediated mRNA decay complexes.* Current Opinion in Structural Biology, 2020. **65**: p. 110-118.
121. Tahmasebi, S., et al., *Translation deregulation in human disease.* Nat Rev Mol Cell Biol, 2018. **19**(12): p. 791-807.
122. Sonenberg, N. and A.G. Hinnebusch, *Regulation of translation initiation in eukaryotes: mechanisms and biological targets.* Cell, 2009. **136**(4): p. 731-45.
123. Buttgereit, F. and M.D. Brand, *A hierarchy of ATP-consuming processes in mammalian cells.* Biochem J, 1995. **312 (Pt 1)**(Pt 1): p. 163-7.
124. Hershey, J.W.B., N. Sonenberg, and M.B. Mathews, *Principles of Translational Control.* Cold Spring Harbor Perspectives in Biology, 2019. **11**(9): p. a032607.
125. Marcotrigiano, J., et al., *Cocrystal structure of the messenger RNA 5' cap-binding protein (eIF4E) bound to 7-methyl-GDP.* Cell, 1997. **89**(6): p. 951-961.
126. Sonenberg, N., et al., *Eukaryotic mRNA cap binding protein: purification by affinity chromatography on sepharose-coupled m7GDP.* Proceedings of the National Academy of Sciences, 1979. **76**(9): p. 4345-4349.
127. Gorgoni, B. and N.K. Gray, *The roles of cytoplasmic poly (A)-binding proteins in regulating gene expression: a developmental perspective.* Briefings in Functional Genomics, 2004. **3**(2): p. 125-141.
128. Sokabe, M. and C.S. Fraser, *Human eukaryotic initiation factor 2 (eIF2)-GTP-Met-tRNAi ternary complex and eIF3 stabilize the 43 S preinitiation complex.* Journal of Biological Chemistry, 2014. **289**(46): p. 31827-31836.
129. Majumdar, R., A. Bandyopadhyay, and U. Maitra, *Mammalian translation initiation factor eIF1 functions with eIF1A and eIF3 in the formation of a stable 40 S preinitiation complex.* Journal of Biological Chemistry, 2003. **278**(8): p. 6580-6587.
130. Gomez, E., S.S. Mohammad, and G.D. Pavitt, *Characterization of the minimal catalytic domain within eIF2B: the guanine-nucleotide exchange factor for translation initiation.* The EMBO journal, 2002.
131. Lamphear, B.J., et al., *Mapping of Functional Domains in Eukaryotic Protein Synthesis Initiation Factor 4G (eIF4G) with Picornaviral Proteases: IMPLICATIONS FOR CAP-DEPENDENT AND CAP-INDEPENDENT TRANSLATIONAL INITIATION (∗).* Journal of Biological Chemistry, 1995. **270**(37): p. 21975-21983.
132. Tsukumo, Y., et al., *Translation control during prolonged mTORC1 inhibition mediated by 4E-BP3.* Nature communications, 2016. **7**(1): p. 11776.
133. Alain, T., et al., *eIF4E/4E-BP ratio predicts the efficacy of mTOR targeted therapies.* Cancer research, 2012. **72**(24): p. 6468-6476.

134. Hayman, T.J., et al., *Translation initiation factor eIF4E is a target for tumor cell radiosensitization.* Cancer research, 2012. **72**(9): p. 2362-2372.
135. Merrick, W.C. and G.D. Pavitt, *Protein synthesis initiation in eukaryotic cells.* Cold Spring Harbor perspectives in biology, 2018. **10**(12): p. a033092.
136. Xu, B., L. Liu, and G. Song, *Functions and regulation of translation elongation factors.* Frontiers in molecular biosciences, 2022. **8**: p. 816398.
137. Lareau, L.F., et al., *Distinct stages of the translation elongation cycle revealed by sequencing ribosome-protected mRNA fragments.* elife, 2014. **3**: p. e01257.
138. Hellen, C.U., *Translation termination and ribosome recycling in eukaryotes.* Cold Spring Harbor perspectives in biology, 2018. **10**(10): p. a032656.
139. Salas-Marco, J. and D.M. Bedwell, *GTP hydrolysis by eRF3 facilitates stop codon decoding during eukaryotic translation termination.* Molecular and cellular biology, 2004. **24**(17): p. 7769-7778.
140. Schuller, A.P., et al., *eIF5A functions globally in translation elongation and termination.* Molecular cell, 2017. **66**(2): p. 194-205. e5.
141. Chaurasia, M., et al., *Radiation induces EIF2AK3/PERK and ERN1/IRE1 mediated pro-survival autophagy.* Autophagy, 2019. **15**(8): p. 1391-1406.
142. Yoshino, H., Y. Kumai, and I. Kashiwakura, *Effects of endoplasmic reticulum stress on apoptosis induction in radioresistant macrophages.* Mol Med Rep, 2017. **15**(5): p. 2867-2872.
143. Misra, J., et al., *Discordant regulation of eIF2 kinase GCN2 and mTORC1 during nutrient stress.* Nucleic Acids Research, 2021. **49**(10): p. 5726-5742.
144. Misra, J., et al., *Multiple mechanisms activate GCN2 eIF2 kinase in response to diverse stress conditions.* Nucleic Acids Res, 2024. **52**(4): p. 1830-1846.
145. Young, S.K. and R.C. Wek, *Upstream Open Reading Frames Differentially Regulate Gene-specific Translation in the Integrated Stress Response *.* Journal of Biological Chemistry, 2016. **291**(33): p. 16927-16935.
146. Hamanaka, R.B., et al., *PERK-dependent regulation of IAP translation during ER stress.* Oncogene, 2009. **28**(6): p. 910-20.
147. Saxton, R.A. and D.M. Sabatini, *mTOR Signaling in Growth, Metabolism, and Disease.* Cell, 2017. **168**(6): p. 960-976.
148. Hay, N. and N. Sonenberg, *Upstream and downstream of mTOR.* Genes Dev, 2004. **18**(16): p. 1926-45.
149. Gwinn, D.M., et al., *AMPK phosphorylation of raptor mediates a metabolic checkpoint.* Mol Cell, 2008. **30**(2): p. 214-26.
150. Jackson, R.J., C.U. Hellen, and T.V. Pestova, *The mechanism of eukaryotic translation initiation and principles of its regulation.* Nat Rev Mol Cell Biol, 2010. **11**(2): p. 113-27.
151. Holz, M.K., et al., *mTOR and S6K1 Mediate Assembly of the Translation Preinitiation Complex through Dynamic Protein Interchange and Ordered Phosphorylation Events.* Cell, 2005. **123**(4): p. 569-580.
152. Vladimirov, S.N., et al., *Characterization of the Human Small-Ribosomal-Subunit Proteins by N-Terminal and Internal Sequencing, and Mass Spectrometry.* European Journal of Biochemistry, 1996. **239**(1): p. 144-149.
153. Gressner, A.M. and I.G. Wool, *The Phosphorylation of Liver Ribosomal Proteins in Vivo: EVIDENCE THAT ONLY A SINGLE SMALL SUBUNIT PROTEIN (S6) IS PHOSPHORYLATED.* Journal of Biological Chemistry, 1974. **249**(21): p. 6917-6925.
154. Bohlen, J., M. Roiuk, and A.A. Teleman, *Phosphorylation of ribosomal protein S6 differentially affects mRNA translation based on ORF length.* Nucleic Acids Research, 2021. **49**(22): p. 13062-13074.

155. Yi, Y.W., et al., *Ribosomal Protein S6: A Potential Therapeutic Target against Cancer?* International Journal of Molecular Sciences, 2022. **23**(1): p. 48.
156. Gingras, A.C., et al., *Regulation of 4E-BP1 phosphorylation: a novel two-step mechanism.* Genes Dev, 1999. **13**(11): p. 1422-37.
157. Morita, M., et al., *mTORC1 Controls Mitochondrial Activity and Biogenesis through 4E-BP-Dependent Translational Regulation.* Cell Metabolism, 2013. **18**(5): p. 698-711.
158. Pause, A., et al., *Insulin-dependent stimulation of protein synthesis by phosphorylation of a regulator of 5'-cap function.* Nature, 1994. **371**(6500): p. 762-767.
159. Wu, C.-W. and K.B. Storey, *mTOR Signaling in Metabolic Stress Adaptation.* Biomolecules, 2021. **11**(5): p. 681.
160. Ingolia, N.T., et al., *Genome-Wide Analysis in Vivo of Translation with Nucleotide Resolution Using Ribosome Profiling.* Science, 2009. **324**(5924): p. 218-223.
161. Hoerth, K., S. Reitter, and J. Schott, *Normalized Ribo-Seq for Quantifying Absolute Global and Specific Changes in Translation.* Bio Protoc, 2022. **12**(4): p. e4323.
162. McGlincy, N.J. and N.T. Ingolia, *Transcriptome-wide measurement of translation by ribosome profiling.* Methods, 2017. **126**: p. 112-129.
163. Shaffer, T.M., C.M. Drain, and J. Grimm, *Optical Imaging of Ionizing Radiation from Clinical Sources.* Journal of Nuclear Medicine, 2016. **57**(11): p. 1661.
164. Youk, J., et al., *Quantitative and qualitative mutational impact of ionizing radiation on normal cells.* Cell Genom, 2024. **4**(2): p. 100499.
165. Yeager, M., et al., *Lack of transgenerational effects of ionizing radiation exposure from the Chernobyl accident.* Science, 2021. **372**(6543): p. 725-729.
166. Wang, S., D.H. Meyer, and B. Schumacher, *Inheritance of paternal DNA damage by histone-mediated repair restriction.* Nature, 2023. **613**(7943): p. 365-374.
167. Rose Li, Y., et al., *Mutational signatures in tumours induced by high and low energy radiation in Trp53 deficient mice.* Nat Commun, 2020. **11**(1): p. 394.
168. *Agency for Toxic Substances and Disease Registry (ATSDR) Toxicological Profiles*, in *Toxicological Profile for Ionizing Radiation*. 1999, Agency for Toxic Substances and Disease Registry (US): Atlanta (GA).
169. Ghandhi, S.A., et al., *Radiation dose-rate effects on gene expression for human biodosimetry.* BMC Medical Genomics, 2015. **8**(1): p. 22.
170. Maan, K., et al., *Metabolomics and transcriptomics based multi-omics integration reveals radiation-induced altered pathway networking and underlying mechanism.* npj Systems Biology and Applications, 2023. **9**(1): p. 42.
171. Rombouts, C., et al., *Transcriptomic profiling suggests a role for IGFBP5 in premature senescence of endothelial cells after chronic low dose rate irradiation.* International Journal of Radiation Biology, 2014. **90**(7): p. 560-574.
172. Lowe, D.J., et al., *Chronic irradiation of human cells reduces histone levels and deregulates gene expression.* Scientific Reports, 2020. **10**(1): p. 2200.
173. Liu, Z., et al., *Candidate biomarkers and persistent transcriptional responses after low and high dose ionizing radiation at high dose rate.* Int J Radiat Biol, 2023. **99**(12): p. 1853-1864.
174. Nosel, I., et al., *Characterization of gene expression profiles at low and very low doses of ionizing radiation.* DNA Repair, 2013. **12**(7): p. 508-517.
175. Zedan, M., et al., *Newly synthesized mRNA selectively escapes translational repression following acute stress.* bioRxiv, 2024: p. 2024.04.14.589419.
176. Braunstein, S., et al., *Regulation of Protein Synthesis by Ionizing Radiation.* Molecular and Cellular Biology, 2009. **29**(21): p. 5645-5656.

177. Trivigno, D., et al., *Regulation of protein translation initiation in response to ionizing radiation.* Radiation Oncology, 2013. **8**(1): p. 35.
178. Tamaddondoust, R.N., et al., *The highs and lows of ionizing radiation and its effects on protein synthesis.* Cellular Signalling, 2022. **89**: p. 110169.
179. Mito, M., Y. Mishima, and S. Iwasaki, *Protocol for Disome Profiling to Survey Ribosome Collision in Humans and Zebrafish.* STAR Protoc, 2020. **1**(3): p. 100168.
180. Gandin, V., et al., *Polysome fractionation and analysis of mammalian translatomes on a genome-wide scale.* J Vis Exp, 2014(87).
181. Zaharieva, E., et al., *Formation of DNA Damage Foci in Human and Mouse Primary Fibroblasts Chronically Exposed to Gamma Radiation at 0.1 mGy/min.* Radiation Research, 2021. **196**(1): p. 40-54.
182. Schmidt, E.K., et al., *SUnSET, a nonradioactive method to monitor protein synthesis.* Nature Methods, 2009. **6**(4): p. 275-277.
183. Kandala, D.T., et al., *Targeting Translation Activity at the Ribosome Interface with UV-Active Small Molecules.* ACS Omega, 2019. **4**(6): p. 10336-10345.
184. Aviner, R., *The science of puromycin: From studies of ribosome function to applications in biotechnology.* Computational and Structural Biotechnology Journal, 2020. **18**: p. 1074-1083.
185. Enam, S.U., et al., *Puromycin reactivity does not accurately localize translation at the subcellular level.* eLife, 2020. **9**: p. e60303.
186. Pantoom, S., et al., *RAB33B recruits the ATG16L1 complex to the phagophore via a noncanonical RAB binding protein.* Autophagy, 2021. **17**(9): p. 2290-2304.
187. Serra, A., et al., *TinderMIX: Time-dose integrated modelling of toxicogenomics data.* GigaScience, 2020. **9**(5).
188. Heinz-Erian, P., et al., *Mutations in SPINT2 Cause a Syndromic Form of Congenital Sodium Diarrhea.* The American Journal of Human Genetics, 2009. **84**(2): p. 188-196.
189. Yao, C.-X., et al., *Transcription Factor GATA-6 Recruits PPARα to Cooperatively Activate Glut4 Gene Expression.* Journal of Molecular Biology, 2012. **415**(1): p. 143-158.
190. Hussien, S.M. and E.R. Rashed, *Immune system modulation by low-dose ionizing radiation-induced adaptive response.* Int J Immunopathol Pharmacol, 2023. **37**: p. 3946320231172080.
191. Lumniczky, K., et al., *Low dose ionizing radiation effects on the immune system.* Environment International, 2021. **149**: p. 106212.
192. Nourshargh, S. and R. Alon, *Leukocyte Migration into Inflamed Tissues.* Immunity, 2014. **41**(5): p. 694-707.
193. Nishina, T., et al., *Interleukin-11-expressing fibroblasts have a unique gene signature correlated with poor prognosis of colorectal cancer.* Nature Communications, 2021. **12**(1): p. 2281.
194. Li, Y., et al., *Paracrine signaling in cancer-associated fibroblasts: central regulators of the tumor immune microenvironment.* Journal of Translational Medicine, 2025. **23**(1): p. 697.
195. Zorov, D.B., M. Juhaszova, and S.J. Sollott, *Mitochondrial reactive oxygen species (ROS) and ROS-induced ROS release.* Physiol Rev, 2014. **94**(3): p. 909-50.
196. Zheng, J., *Energy metabolism of cancer: Glycolysis versus oxidative phosphorylation (Review).* Oncol Lett, 2012. **4**(6): p. 1151-1157.
197. Kierans, S.J. and C.T. Taylor, *Glycolysis: A multifaceted metabolic pathway and signaling;hub.* Journal of Biological Chemistry, 2024. **300**(11).
198. Zagórski, Z.P. and E.M. Kornacka, *Ionizing radiation: friend or foe of the origins of life?* Orig Life Evol Biosph, 2012. **42**(5): p. 503-5.

199. Yamada, H., et al., *Radiation dose-rate is a neglected critical parameter in dose–response of insects.* Scientific Reports, 2022. **12**(1): p. 6242.
200. Tam, S.Y., V.W.C. Wu, and H.K.W. Law, *Influence of autophagy on the efficacy of radiotherapy.* Radiation Oncology, 2017. **12**(1): p. 57.
201. Roy, A., et al., *Role of autophagy in tumor response to radiation: Implications for improving radiotherapy.* Front Oncol, 2022. **12**: p. 957373.
202. Wang, Y., et al., *SVIP induces localization of p97/VCP to the plasma and lysosomal membranes and regulates autophagy.* PLoS One, 2011. **6**(8): p. e24478.
203. Marcelo, A., et al., *Stress granules, RNA-binding proteins and polyglutamine diseases: too much aggregation?* Cell Death & Disease, 2021. **12**(6): p. 592.
204. Raitanen, J., et al., *Comparison of Radiation Response between 2D and 3D Cell Culture Models of Different Human Cancer Cell Lines.* Cells, 2023. **12**(3).
205. Antonelli, F. *3D Cell Models in Radiobiology: Improving the Predictive Value of In Vitro Research*. International Journal of Molecular Sciences, 2023. **24**, DOI: 10.3390/ijms241310620.
206. Sercombe, L., K. Igawa, and K. Izumi, *Radiation evaluation assay using a human three-dimensional oral cancer model for clinical radiation therapy.* Talanta Open, 2024. **9**: p. 100297.
207. El-Ashmawy, M., et al., *Organotypic culture in three dimensions prevents radiation-induced transformation in human lung epithelial cells.* Scientific Reports, 2016. **6**(1): p. 31669.
208. Liu, M.-M., et al., *Multiple exposures to low-dose ionizing radiation induced the initiation and progression of pro-atherosclerotic phenotypes in mice and vascular endothelial cell damage.* Science Progress, 2024. **107**(1): p. 00368504241228668.
209. Ghandhi, S.A., et al., *Dose and dose-rate effects in a mouse model of internal exposure to 137Cs. Part 1: Global transcriptomic responses in blood.* Radiation research, 2021. **196**(5): p. 478-490.
210. Rios, C.I., et al., *Advanced Technologies in Radiation Research.* Radiation Research, 2024. **201**(4): p. 338-365.
211. Rongvaux, A., et al., *Human Hemato-Lymphoid System Mice: Current Use and Future Potential for Medicine.* Annual Review of Immunology, 2013. **31**(Volume 31, 2013): p. 635-674.
212. Down, J.D., et al., *Selecting the Most Relevant Mouse Strains for Evaluating Radiation-Induced Multiple Tissue Injury after Leg-Shielded Partial-Body Gamma Irradiation.* Radiat Res, 2024. **202**(3): p. 510-522.
213. Jackson, I.L., Z. Vujaskovic, and J.D. Down, *Revisiting strain-related differences in radiation sensitivity of the mouse lung: recognizing and avoiding the confounding effects of pleural effusions.* Radiat Res, 2010. **173**(1): p. 10-20.
214. Bladen, C.L., et al., *Quantification of ionizing radiation-induced cell death in situ in a vertebrate embryo.* Radiat Res, 2007. **168**(2): p. 149-57.
215. Bladen, C.L., et al., *DNA damage response and Ku80 function in the vertebrate embryo.* Nucleic Acids Res, 2005. **33**(9): p. 3002-10.
216. Chuprin, J., et al., *Humanized mouse models for immuno-oncology research.* Nature Reviews Clinical Oncology, 2023. **20**(3): p. 192-206.
217. Murray-Zmijewski, F., E.A. Slee, and X. Lu, *A complex barcode underlies the heterogeneous response of p53 to stress.* Nature Reviews Molecular Cell Biology, 2008. **9**(9): p. 702-712.
218. Moding, E.J., M.B. Kastan, and D.G. Kirsch, *Strategies for optimizing the response of cancer and normal tissues to radiation.* Nat Rev Drug Discov, 2013. **12**(7): p. 526-42.

219. Yu, H., et al., *Different responses of tumor and normal cells to low-dose radiation.* Contemp Oncol (Pozn), 2013. **17**(4): p. 356-62.
220. Flint, D.B., et al., *Cell lines of the same anatomic site and histologic type show large variability in intrinsic radiosensitivity and relative biological effectiveness to protons and carbon ions.* Med Phys, 2021. **48**(6): p. 3243-3261.
221. Barile, F.A. and M. Cardona, *Acute cytotoxicity testing with cultured human lung and dermal cells.* In Vitro Cellular & Developmental Biology - Animal, 1998. **34**(8): p. 631-635.
222. Park, E.-J., et al., *Lung fibroblasts may play an important role in clearing apoptotic bodies of bronchial epithelial cells generated by exposure to PHMG-P-containing solution.* Toxicology Letters, 2018. **286**: p. 108-119.
223. Zhang, X.Q., et al., *ZnO, TiO2, SiO2, and Al2O3 Nanoparticles-induced Toxic Effects on Human Fetal Lung Fibroblasts.* Biomedical and Environmental Sciences, 2011. **24**(6): p. 661-669.
224. Gadbois, D.M. and B.E. Lehnert, *Cell cycle response to DNA damage differs in bronchial epithelial cells and lung fibroblasts.* Cancer Res, 1997. **57**(15): p. 3174-9.
225. Lee, J., D.Y. Hyeon, and D. Hwang, *Single-cell multiomics: technologies and data analysis methods.* Experimental & Molecular Medicine, 2020. **52**(9): p. 1428-1442.
226. Canzler, S., et al., *Prospects and challenges of multi-omics data integration in toxicology.* Archives of Toxicology, 2020. **94**(2): p. 371-388.
227. Argelaguet, R., et al., *Multi-Omics Factor Analysis-a framework for unsupervised integration of multi-omics data sets.* Mol Syst Biol, 2018. **14**(6): p. e8124.
228. Barreau, C., L. Paillard, and H.B. Osborne, *AU-rich elements and associated factors: are there unifying principles?* Nucleic Acids Res, 2005. **33**(22): p. 7138-50.
229. Fay, M.M., S.M. Lyons, and P. Ivanov, *RNA G-Quadruplexes in Biology: Principles and Molecular Mechanisms.* J Mol Biol, 2017. **429**(14): p. 2127-2147.
230. Schuster, S.L. and A.C. Hsieh, *The Untranslated Regions of mRNAs in Cancer.* Trends Cancer, 2019. **5**(4): p. 245-262.
231. Lucks, J.B., et al., *Multiplexed RNA structure characterization with selective 2′-hydroxyl acylation analyzed by primer extension sequencing (SHAPE-Seq).* Proceedings of the National Academy of Sciences, 2011. **108**(27): p. 11063-11068.
232. Rouskin, S., et al., *Genome-wide probing of RNA structure reveals active unfolding of mRNA structures in vivo.* Nature, 2014. **505**(7485): p. 701-5.
233. Komar, A.A. and M. Hatzoglou, *Cellular IRES-mediated translation: the war of ITAFs in pathophysiological states.* Cell Cycle, 2011. **10**(2): p. 229-40.
234. Hoang, H.-D., et al., *Induction of an Alternative mRNA 5′ Leader Enhances Translation of the Ciliopathy Gene Inpp5e and Resistance to Oncolytic Virus Infection.* Cell Reports, 2019. **29**(12): p. 4010-4023.e5.
235. Van Nostrand, E.L., et al., *A large-scale binding and functional map of human RNA-binding proteins.* Nature, 2020. **583**(7818): p. 711-719.
236. Keene, J.D., J.M. Komisarow, and M.B. Friedersdorf, *RIP-Chip: the isolation and identification of mRNAs, microRNAs and protein components of ribonucleoprotein complexes from cell extracts.* Nature Protocols, 2006. **1**(1): p. 302-307.
237. Agarwal, V., et al., *Predicting effective microRNA target sites in mammalian mRNAs.* Elife, 2015. **4**.
238. Chen, Y. and X. Wang, *miRDB: an online database for prediction of functional microRNA targets.* Nucleic Acids Res, 2020. **48**(D1): p. D127-d131.
239. Huang, H.Y., et al., *miRTarBase 2020: updates to the experimentally validated microRNA-target interaction database.* Nucleic Acids Res, 2020. **48**(D1): p. D148-d154.

240. Shalem, O., et al., *Genome-scale CRISPR-Cas9 knockout screening in human cells.* Science, 2014. **343**(6166): p. 84-87.
241. Dhungel, P., et al., *In Vitro Transcribed RNA-based Luciferase Reporter Assay to Study Translation Regulation in Poxvirus-infected Cells.* J Vis Exp, 2019(147).
242. Spriggs, K.A., M. Bushell, and A.E. Willis, *Translational regulation of gene expression during conditions of cell stress.* Mol Cell, 2010. **40**(2): p. 228-37.
243. Olsen, J.V., et al., *Global, in vivo, and site-specific phosphorylation dynamics in signaling networks.* Cell, 2006. **127**(3): p. 635-48.